NUREG/CR-6717
ANL-00/27

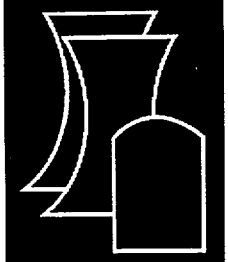

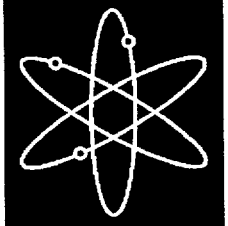

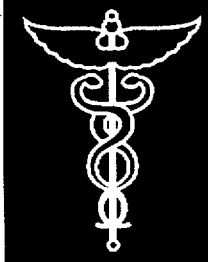

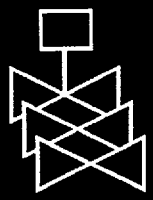

Environmental Effects on Fatigue Crack Initiation in Piping and Pressure Vessel Steels

Argonne National Laboratory

U.S. Nuclear Regulatory Commission
Office of Nuclear Regulatory Research
Washington, DC 20555-0001

AVAILABILITY OF REFERENCE MATERIALS IN NRC PUBLICATIONS

NRC Reference Material

As of November 1999, you may electronically access NUREG-series publications and other NRC records at NRC's Public Electronic Reading Room at www.nrc.gov/NRC/ADAMS/index.html. Publicly released records include, to name a few, NUREG-series publications; *Federal Register* notices; applicant, licensee, and vendor documents and correspondence; NRC correspondence and internal memoranda; bulletins and information notices; inspection and investigative reports; licensee event reports; and Commission papers and their attachments.

NRC publications in the NUREG series, NRC regulations, and *Title 10, Energy*, in the Code of *Federal Regulations* may also be purchased from one of these two sources.

1. The Superintendent of Documents
   U.S. Government Printing Office
   Mail Stop SSOP
   Washington, DC 20402–0001
   Internet: bookstore.gpo.gov
   Telephone: 202-512-1800
   Fax: 202-512-2250
2. The National Technical Information Service
   Springfield, VA 22161–0002
   www.ntis.gov
   1–800–553–6847 or, locally, 703–605–6000

A single copy of each NRC draft report for comment is available free, to the extent of supply, upon written request as follows:

Address: Office of the Chief Information Officer,
Reproduction and Distribution
Services Section
U.S. Nuclear Regulatory Commission
Washington, DC 20555-0001
E-mail: DISTRIBUTION@nrc.gov
Facsimile: 301–415–2289

Some publications in the NUREG series that are posted at NRC's Web site address www.nrc.gov/NRC/NUREGS/indexnum.html are updated periodically and may differ from the last printed version. Although references to material found on a Web site bear the date the material was accessed, the material available on the date cited may subsequently be removed from the site.

Non-NRC Reference Material

Documents available from public and special technical libraries include all open literature items, such as books, journal articles, and transactions, *Federal Register* notices, Federal and State legislation, and congressional reports. Such documents as theses, dissertations, foreign reports and translations, and non-NRC conference proceedings may be purchased from their sponsoring organization.

Copies of industry codes and standards used in a substantive manner in the NRC regulatory process are maintained at—

The NRC Technical Library
Two White Flint North
11545 Rockville Pike
Rockville, MD 20852–2738

These standards are available in the library for reference use by the public. Codes and standards are usually copyrighted and may be purchased from the originating organization or, if they are American National Standards, from—

American National Standards Institute
11 West 42nd Street
New York, NY 10036–8002
www.ansi.org
212–642–4900

Legally binding regulatory requirements are stated only in laws; NRC regulations; licenses, including technical specifications; or orders, not in NUREG-series publications. The views expressed in contractor-prepared publications in this series are not necessarily those of the NRC.

The NUREG series comprises (1) technical and administrative reports and books prepared by the staff (NUREG–XXXX) or agency contractors (NUREG/CR–XXXX), (2) proceedings of conferences (NUREG/CP–XXXX), (3) reports resulting from international agreements (NUREG/IA–XXXX), (4) brochures (NUREG/BR–XXXX), and (5) compilations of legal decisions and orders of the Commission and Atomic and Safety Licensing Boards and of Directors' decisions under Section 2.206 of NRC's regulations (NUREG–0750).

NUREG/CR-6717
ANL-00/27

Environmental Effects on Fatigue Crack Initiation in Piping and Pressure Vessel Steels

Manuscript Completed: October 2000
Date Published: May 2001

Prepared by
O. K. Chopra, W. J. Shack

Argonne National Laboratory
9700 South Cass Avenue
Argonne, IL 60439

J. Muscara, NRC Task Manager

Prepared for
Division of Engineering Technology
Office of Nuclear Regulatory Research
U.S. Nuclear Regulatory Commission
Washington, DC 20555-0001
NRC Job Code W6610

NUREG/CR-6717 has been reproduced from the best available copy.

Environmental Effects on Fatigue Crack Initiation in Piping and Pressure Vessel Steels

by

O. K. Chopra and W. J. Shack

Abstract

The ASME Boiler and Pressure Vessel Code provides rules for the construction of nuclear power plant components. Appendix I to Section III of the Code specifies fatigue design curves for structural materials. However, the effects of light water reactor (LWR) coolant environments are not explicitly addressed by the Code design curves. Test data illustrate potentially significant effects of LWR environments on the fatigue resistance of carbon and low–alloy steels and austenitic stainless steels. This report summarizes the work performed at Argonne National Laboratory on the fatigue of piping and pressure vessel steels in LWR coolant environments. The existing fatigue S–N data have been evaluated to establish the effects of various material and loading variables, such as steel type, strain range, strain rate, temperature, and dissolved–oxygen level in water, on the fatigue lives of these steels. Statistical models are presented for estimating the fatigue S–N curves for carbon and low–alloy steels and austenitic stainless steels as a function of material, loading, and environmental variables. The influence of reactor environments on the mechanism of fatigue crack initiation are discussed. Decreased fatigue lives of carbon and low–alloy steels and austenitic stainless steels in water are caused primarily by the effects of environment on the growth of short cracks. The results suggest that for carbon and low–alloy steels, the growth of these small cracks in high–purity oxygenated water occurs by a slip oxidation/dissolution process. A fracture mechanics approach has been used to evaluate the effects of environment on fatigue crack initiation in carbon and low–alloy steels. Environmentally assisted reduction in fatigue life of austenitic stainless steels is most likely caused by other mechanisms such as hydrogen–enhanced crack growth. Two methods for incorporating environmental effects into the ASME Code fatigue evaluations are discussed. Differences between the methods and their impact on the design fatigue curves are also discussed.

Contents

Figures

Tables

Executive Summary

Section III, Subsection NB of the ASME Boiler and Pressure Vessel Code contains rules for the design of Class 1 components of nuclear power plants. Figures I–9.1 through I–9.6 of Appendix I to Section III specify the Code design fatigue curves for applicable structural materials. However, Section III, Subsection NB–3121 of the Code states that effects of the coolant environment on fatigue resistance of a material were not intended to be addressed in these design curves. Therefore, the effects of environment on fatigue resistance of materials used in operating pressurized water reactor (PWR) and boiling water reactor (BWR) plants, whose primary–coolant–pressure–boundary components were designed in accordance with the Code are uncertain.

The current Section–III design fatigue curves of the ASME Code were based primarily on strain–controlled fatigue tests of small polished specimens at room temperature in air. Best–fit curves to the experimental test data, were first adjusted to account for the effects of mean stress and then lowered by a factor of 2 on stress and 20 on cycles, whichever was more conservative, to obtain the design fatigue curves. These factors are not safety margins but rather adjustment factors that must be applied to experimental data to obtain estimates of the lives of components. They were not intended to address the effects of the coolant environment on fatigue life. Recent fatigue–strain–vs.–life (S–N) data obtained in the U.S. and Japan demonstrate that light water reactor (LWR) environments can have potentially significant effects on the fatigue resistance of materials. Specimen lives obtained from tests in simulated LWR environments can be much shorter than those obtained from corresponding tests in air.

This report summarizes work performed at Argonne National Laboratory on fatigue of carbon and low–alloy steels and wrought and cast austenitic stainless steels (SSs) in simulated LWR environments. The existing fatigue S–N data, foreign and domestic, have been evaluated to establish the effects of various material and loading variables, such as steel type, strain range, strain rate, temperature, and dissolved–oxygen (DO) level in water, on the fatigue lives of these steels. Statistical models are presented for estimating the fatigue S–N curves for carbon and low–alloy steels and austenitic SSs as a function of material, loading, and environmental variables. Two methods for incorporating the effects of LWR coolant environments into the ASME Code fatigue evaluations are presented.

Mechanism of Fatigue Crack Initiation

The fatigue life of a material is defined as the number of cycles necessary to form an "engineering" crack, i.e., a 3–mm–deep crack. During cyclic loading, surface cracks, 10 μm or more in length, form quite early in life, i.e., <10% of life, even at low strain amplitudes. The fatigue life may be considered to be composed entirely of the growth of these short cracks. The growth of surface cracks may be divided into two regimes; an initial period that involves growth of microstructurally small cracks in which the crack growth behavior is very sensitive to microstructure and is characterized by decelerating crack growth, and a propagation period that involves growth of mechanically small cracks that can be predicted by fracture mechanics methodology and is characterized by accelerating crack growth.

Tests have been conducted to characterize the formation and growth of short cracks in carbon and low–alloy steels and austenitic SSs in LWR environments. The results indicate that

the decrease in fatigue life of these steels in LWR environments is primarily caused by the effects of environment on the growth of cracks <500 μm deep. For carbon and low–alloy steels in high–DO water, the growth rates of cracks <100 μm in size are nearly two orders of magnitude higher than those in air. In high–DO water, surface cracks in carbon and low–alloy steels grow entirely as tensile cracks normal to the stress axis; in air and low–DO water, surface cracks grow initially as shear cracks at ≈45° to the stress axis, and then as tensile cracks normal to the stress axis when slip is no longer confined to planes at 45° to the stress axis. The results indicate that in LWR environments, the growth of short fatigue cracks in carbon and low–alloy steels occurs by a slip oxidation/dissolution mechanism.

Environmental effects on the mechanism of fatigue crack initiation in austenitic SSs is not well understood. For SSs, fatigue lives are lower in low–DO water than in high–DO water; such results are difficult to reconcile in terms of the slip oxidation/dissolution mechanism. Also, SS specimens tested in water show well–defined fatigue striations. The results suggest that environmentally assisted reduction in fatigue life of austenitic SSs is most likely caused by mechanisms other than slip oxidation/dissolution, such as hydrogen–enhanced crack growth.

Overview of Fatigue S–N Data

In air, the fatigue life of carbon and low–alloy steels depends on steel type, temperature, orientation, and strain rate. The fatigue life of carbon steels is a factor of ≈1.5 lower than that of low–alloy steels. For both steels, fatigue life decreases with increase in temperature. Some heats of carbon and low–alloy steels exhibit effects of strain rate and orientation. For these heats, fatigue life decreases with decreasing strain rate. Also, based on the distribution and morphology of sulfides, the fatigue properties in transverse orientation may be inferior to those in the rolling orientation. The data indicate significant heat–to–heat variation; at 288°C, fatigue life of carbon and low–alloy steels may vary by up to a factor of 3 above or below the mean value. The results also indicate that in room-temperature air, the ASME mean curve for low–alloy steels is still in good agreement with the available experimental data and that for carbon steels is somewhat conservative.

The fatigue lives of both carbon and low–alloy steels are decreased in LWR environments; the reduction depends on temperature, strain rate, DO level in water, and S content of the steel. The fatigue life is decreased significantly when four conditions are satisfied simultaneously, viz., the strain amplitude, temperature, and DO in water are above certain minimum levels, and the strain rate is below a threshold value. The S content in the steel is also important; its effect on life depends on the DO level in water.

Although the microstructures and cyclic–hardening behavior of carbon and low–alloy steels differ significantly, environmental degradation of the fatigue life of these steels is very similar. For both steels, only a moderate decrease in life (by a factor of <2) is observed when any one of the threshold conditions is not satisfied, e.g., low–DO PWR environment, or temperatures <150°C, or vibratory fatigue. The existing fatigue S–N data have been reviewed to establish the critical parameters that influence fatigue life and define their threshold and limiting values within which environmental effects are significant.

In air, the fatigue lives of Types 304 and 316 SS are comparable; those of Type 316NG are superior to those of Types 304 and 316 SS. The fatigue S–N behavior of cast CF–8 and CF–8M SSs is similar to that of wrought austenitic SSs. The fatigue life of all steels is independent of

temperature in the range from room temperature to 427°C; at temperatures above 260°C, it may decrease with decreasing strain rate. The ASME mean curve for austenitic SSs is nonconservative with respect to the existing fatigue S–N data; at strain amplitudes <0.5%, the mean curve predicts significantly longer fatigue lives than those observed experimentally.

The existing fatigue S–N data have been reviewed to establish the critical parameters that influence fatigue life and define their threshold and limiting values within which environmental effects are significant. The fatigue lives of cast and wrought austenitic SSs are decreased in LWR environments. The reduction in life depends on strain rate, DO level in water, and temperature. The effects of LWR environments on fatigue life of wrought materials are comparable for Types 304, 316, and 316NG SSs. However, unlike ferritic steels, where environmental effects are greater in high–DO environments, environmental effects on fatigue life of SSs are more pronounced in low– than in high–DO water. In high–DO water when conductivity is maintained at <0.1 μS/cm and electrochemical potential of the steel has reached a stable value, environmental effects are moderate (less than a factor of 2 decrease in life). Although the fatigue lives of cast SSs are relatively insensitive to changes in ferrite content in the range of 12–28%, the effects of loading and environmental parameters on the fatigue life of cast SSs differ somewhat. The fatigue lives of cast SSs are approximately the same in both high– and low–DO water and are comparable to those observed for wrought SSs in low–DO water.

Incorporating Environmental Effects into ASME Code Fatigue Evaluations

Statistical models have been developed to predict fatigue lives of small smooth specimens of carbon and low–alloy steels and wrought and cast austenitic SSs as a function of material, loading, and environmental parameters. The functional form and bounding values of these parameters were based on experimental observations and data trends. The statistical models were obtained by minimizing the squared Cartesian distances from the data point to the predicted curve instead of minimizing the sum of the square of the residual errors for either strain amplitude or fatigue life. The models are applicable for predicted fatigue lives $\leq 10^6$ cycles. The results indicate that the ASME mean curve for SSs is not consistent with the experimental data at strain amplitudes <0.5% or stress amplitudes <975 MPa (<141 ksi); the ASME mean curve is nonconservative.

The design fatigue curves for these steels in LWR environments were obtained by the procedure that has been used to develop the current ASME Code design fatigue curves, i.e., by adjusting the best–fit experimental curve for the effect of mean stress and setting margins of 20 on cycles and 2 on strain to account for the uncertainties in life that are associated with material and loading conditions. However, for austenitic SSs, the margin on strain for the current ASME Code design fatigue curve is closer to 1.5 than 2.

The use of a fatigue life correction factor F_{en} to incorporate the effects of environment into the ASME Code fatigue evaluations is also discussed. In the F_{en} method, environmental effects on life are estimated from the statistical models but the correction is applied to fatigue lives estimated from the current Code design curves. Therefore, estimates of fatigue lives that are based on the two methods, i.e., F_{en} method and environmentally adjusted design curves, may differ because of differences between the ASME mean curves used to develop the current design curves and the best–fit curves to the existing data used to develop the environmentally adjusted curves. However, although estimates of fatigue lives based on the two methods may

differ, either of these methods provides an acceptable approach to account for environmental effects. Data available in the literature have been reviewed to evaluate the conservatism in the existing Code fatigue design curves.

Acknowledgments

The authors thank T. M. Galvin, J. Tezak, R. W. Clark, and D. R. Perkins for their contributions to the experimental effort. This work is sponsored by the Office of Nuclear Regulatory Research, U.S. Nuclear Regulatory Commission, under Job Code W6610; Task Manager: J. Muscara; Program Manager: M. B. McNeil.

1 Introduction

Cyclic loadings on a structural component occur because of changes in mechanical and thermal loadings as the system goes from one load set (e.g., pressure, temperature, moment, and force loading) to any other load set. For each load set, an individual fatigue usage factor is determined by the ratio of the number of cycles anticipated during the lifetime of the component to the allowable cycles. Figures I–9.1 through I–9.6 of Appendix I to Section III of the ASME Boiler and Pressure Vessel Code specify design fatigue curves that define the allowable number of cycles as a function of applied stress amplitude. The cumulative usage factor (CUF) is the sum of the individual usage factors, and the ASME Code Section III requires that the CUF at each location must not exceed 1.

The ASME Code fatigue design curves, given in Appendix I of Section III, are based on strain–controlled tests of small polished specimens at room temperature in air. The fatigue design curves were developed from the best–fit curves of the experimental data by first adjusting for the effects of mean stress on fatigue life and then reducing the fatigue life at each point on the adjusted curve by a factor of 2 on strain or 20 on cycles, whichever was more conservative. As described in the Section III criteria document, these factors were intended to account for data scatter (heat–to–heat variability), effects of mean stress or loading history, and differences in surface condition and size between the test specimens and actual components. The factors of 2 and 20 are not safety margins but rather conversion factors that must be applied to the experimental data to obtain reasonable estimates of the lives of actual reactor components. However, because the mean fatigue curve used to develop the current Code design curve for austenitic SSs does not accurately represent the available experimental data,[1,2] the current Code design curve for stainless steels (SSs) includes a reduction of only ≈1.5 and 15 from the mean curve for the SS data, not the 2 and 20 originally intended.

As explicitly noted in Subsection NB–3121 of Section III of the Code, the data used to develop the design fatigue curves (Figs. I–9.1 through I–9.6 of Appendix I to Section III) did not include tests in the presence of corrosive environments that might accelerate fatigue failure. Article B–2131 in Appendix B to Section III states that the owner's design specifications should provide information about any reduction to design fatigue curves that has been necessitated by environmental conditions. Existing fatigue–strain–vs.–life (S–N) data illustrate potentially significant effects of light water reactor (LWR) coolant environments on the fatigue resistance of carbon steels (CSs) and low–alloy steels (LASs),[3–15] as well as of austenitic SSs,[2,15–25] (Fig. 1). Under certain environmental and loading conditions, fatigue lives of CSs can be a factor of 70 lower in the environment than in air.[4,12] Therefore, the margins in the ASME Code may be less conservative than originally intended.

Two approaches have been proposed for incorporating the effects of LWR environments into ASME Section III fatigue evaluations: (a) develop new design fatigue curves for LWR applications, and (b) use a fatigue life correction factor to account for environmental effects. Both approaches are based on the existing fatigue S–N data in LWR environments, i.e., the best–fit curves to the experimental fatigue S–N data in LWR environments are used to obtain the design curves or fatigue life correction factor. As and when more data became available, the best–fit curves have been modified and updated to include the effects of various material, loading, and environmental parameters on fatigue life. Interim design fatigue curves that address environmental effects on fatigue life of carbon and low–alloy steels and austenitic SSs

were first proposed by Majumdar et al.[26] Design fatigue curves based on a rigorous statistical analysis of the fatigue S–N data in LWR environments were developed by Keisler et al.[27,28] Results of the statistical analysis have also been used to estimate the probability of fatigue cracking in reactor components. The Idaho National Engineering Laboratory assessed the significance of the interim fatigue design curves by performing fatigue evaluations of a sample of components in the reactor coolant pressure boundary.[29] In all, components from six locations at facilities designed by each of the four U.S. nuclear steam supply system vendors were evaluated. Selected components from older vintage plants designed under the B31.1 Code were also included in the evaluation. The design curves and statistical models for estimating fatigue lives in LWR environments have recently been updated for carbon and low-alloy steels[12–15] and austenitic SSs.[2,15,25]

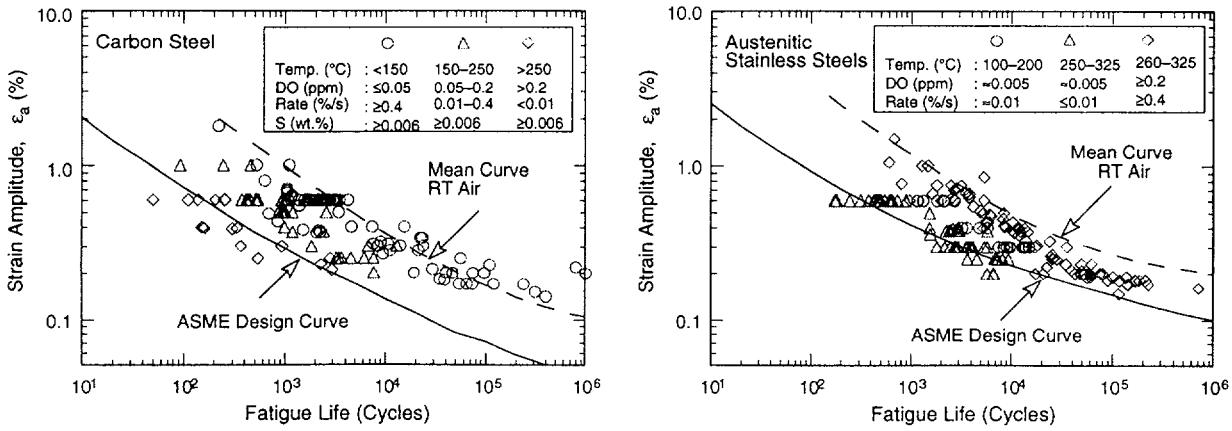

Figure 1. S–N data for (a) carbon steels and (b) austenitic stainless steels in water; RT = room temperature

The alternative approach, proposed initially by Higuchi and Iida,[4] considers the effects of reactor coolant environments on fatigue life in terms of a fatigue life correction factor F_{en}, which is the ratio of the life in air to that in water. To incorporate environmental effects into the ASME Code fatigue evaluations, a fatigue usage for a specific load set, based on the current Code design curves, is multiplied by the correction factor. Specific expressions for F_{en}, based on the statistical models[2,12–15,30,31] and on the correlations developed by the Environmental Fatigue Data Committee of Thermal and Nuclear Power Engineering Society of Japan,[32] have been proposed.

This report summarizes the data available on the effects of various material, loading, and environmental parameters on the fatigue lives of carbon and low-alloy steels and austenitic SSs. Effects of reactor coolant environment on the mechanism of fatigue crack initiation are discussed. The two methods for incorporating the effects of LWR coolant environments into the ASME Code fatigue evaluations are presented. Although estimates of fatigue lives based on the two methods may vary because of differences between the ASME mean curves used to develop the current design curves and the best-fit curves to the existing data used to develop the environmentally adjusted curves, either of these methods provides an acceptable approach to account for environmental effects. The fatigue S–N behavior of carbon and low-alloy steels in air and LWR environments has also been examined by using a fracture mechanics approach and crack growth data. Fatigue life is considered to be composed of the growth of

microstructurally small cracks (MSCs) and mechanically small cracks. The growth of the latter has been characterized in terms of the J–integral range ΔJ and crack–growth–rate (CGR) data in air and LWR environments.

2 Mechanism of Fatigue Crack Initiation

The formation of surface cracks and their growth as shear (Stage I) and tensile (Stage II) cracks to an engineering size (3 mm deep) constitute the fatigue life of a material, which is represented by the fatigue S–N curves. The curves specify, for a given stress or strain amplitude, the number of cycles needed to form an engineering crack. During fatigue loading of smooth test specimens, surface cracks 10 μm or longer form quite early in life (i.e., <10% of life) at surface irregularities or discontinuities either already in existence or produced by slip bands, grain boundaries, second-phase particles, etc.[12,33–37] Consequently, fatigue life may be considered to be composed entirely of crack propagation.[38]

Growth of these surface cracks may be divided into two regimes; an initial period, which involves growth of MSCs, that is very sensitive to microstructure and is characterized by decelerating crack growth (Region AB in Fig. 2), and a propagation period that involves growth of mechanically small cracks that can be predicted by fracture mechanics methodology and is characterized by accelerating crack growth (Region BC in Fig. 2). Mechanically small cracks, which correspond to Stage II, or tensile, cracks are characterized by striated crack growth and a fracture surface normal to the maximum principal stress. Conventionally, the former has been defined as the initiation stage and is considered sensitive to stress or strain amplitude, and the latter has been defined as the propagation stage and is less sensitive to strain amplitude. The characterization and understanding of both the crack initiation and crack propagation stage are important for accurate estimates of the fatigue lives of structural materials.

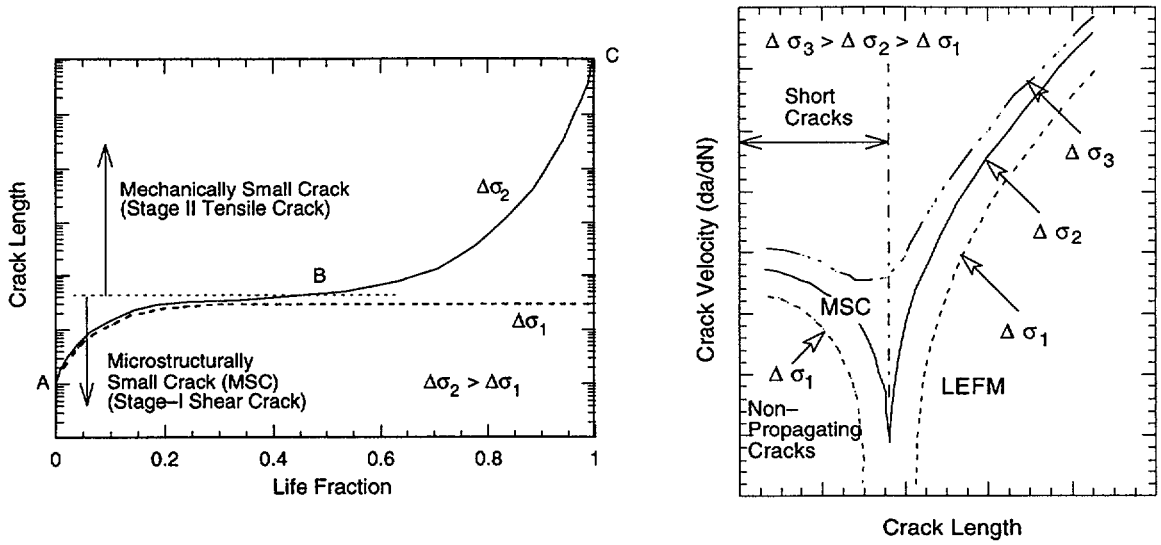

(a) (b)

Figure 2. Schematic illustration of (a) growth of short cracks in smooth specimens as a function of fatigue life fraction and (b) crack velocity as a function of crack length

2.1 Carbon and Low–Alloy Steels

Reduction of fatigue life in high–temperature water has often been attributed to easier crack initiation, because surface micropits that are formed in high–temperature water act as

stress raisers and provide preferred sites for the formation of fatigue cracks.[5] However, experimental data do not support this argument; the fatigue lives of carbon and low-alloy steel specimens that have been preoxidized at 288°C in high-dissolved-oxygen (DO) water and then tested in air are identical to those of unoxidized specimens (Fig. 3).[12] If the presence of micropits was responsible for the reduction in life, specimens preexposed to high-DO water and tested in air should show a decrease in life. Also, the fatigue limit of these steels should be lower in water than in air. Data obtained from specimens in high-DO water indicate that the fatigue limit is either the same as, or ≈20% higher, in water than in air.[12,13]

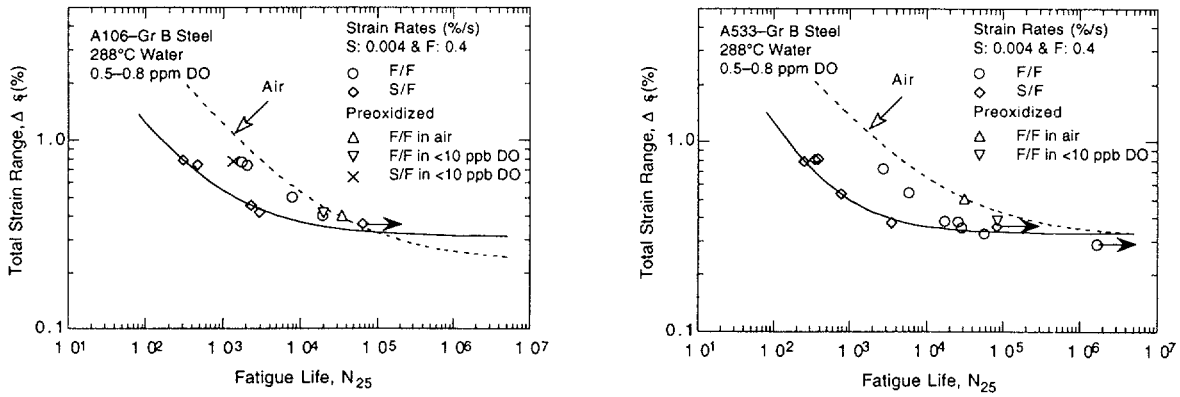

Figure 3. Effects of environment on formation of fatigue cracks in (a) carbon and (b) low-alloy steels. Preoxidized specimens were exposed at 288°C for 30–100 h in water with 0.6–0.8 ppm dissolved oxygen.

Furthermore, if reduction in life is caused by easier formation of cracks, the specimens tested in high-DO water should show more cracks. Figure 4 shows plots of the number of cracks >10 μm long, along longitudinal sections of the gauge length of A106-Gr B and A533-Gr B specimens as a function of strain range in air, simulated PWR environment, and high-DO water at two strain rates. The results show that, with the exception of the LAS tested in simulated pressurized water reactor (PWR) water, environment has no effect on the frequency (number per unit gauge length) of cracks. For similar loading conditions, the number of cracks in the specimens tested in air and high-DO water is identical, although fatigue life is lower by a factor of ≈8 in water. Detailed metallographic evaluation of the fatigue test specimens indicates that the water environment has little or no effect on the formation of surface microcracks. Irrespective of environment, cracks in carbon and low-alloy steels initiate along slip bands, carbide particles, or at the ferrite/pearlite phase boundaries.

The enhanced growth rates of long cracks in pressure vessel and piping steels in LWR environments have been attributed to either slip oxidation/dissolution[39] or hydrogen-induced cracking.[40] Both mechanisms depend on the rates of oxide rupture, passivation, and liquid diffusion. Therefore, it is often difficult to differentiate between the two processes or to establish their relative contributions to crack growth in LWR environments.

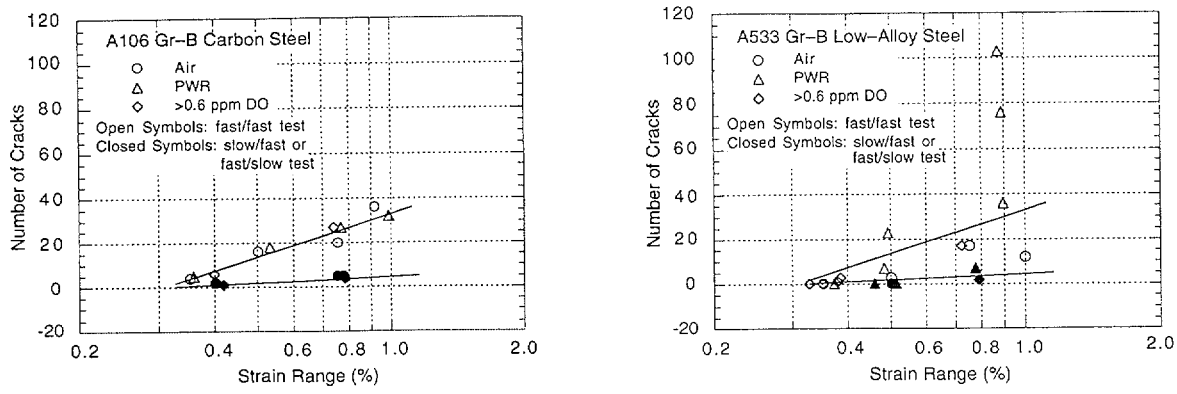

(a) (b)

Figure 4. Number of cracks >10 μm long along longitudinal section of fatigue specimens of (a) A106 Gr B carbon steel and (b) A533 Gr B low–alloy steel tested in LWR environments. Number of cracks represents the average value along a 7–mm gauge length.

Studies on crack initiation in smooth fatigue specimens[35] indicate that the decrease in fatigue life of CSs and LASs in LWR environments is caused primarily by the effects of environment on the growth of cracks <100 μm deep. When compared with CGRs in air, growth rates in high–DO water are nearly two orders of magnitude higher for cracks that are <100 μm deep and one order of magnitude higher for cracks that are >100 μm deep. Metallographic examination of test specimens indicates that in high–DO water, surface cracks <100 μm deep grow entirely as tensile cracks normal to the stress, whereas in air or simulated PWR environments, they are at an angle of 45° to the stress axis (Fig. 5).[35] Also, for CSs, cracks <100 μm deep propagate across both the soft ferrite and hard pearlite regions, whereas in air, they propagate along soft ferrite regions. The crack morphology on the specimen surface also differs in air and water environments (Fig. 6); surface cracks in high–DO water are always straight and normal to the stress axis, whereas in air or simulated PWR environments, they are mostly at 45° to the stress axis. The differing crack morphology, absence of Stage I crack

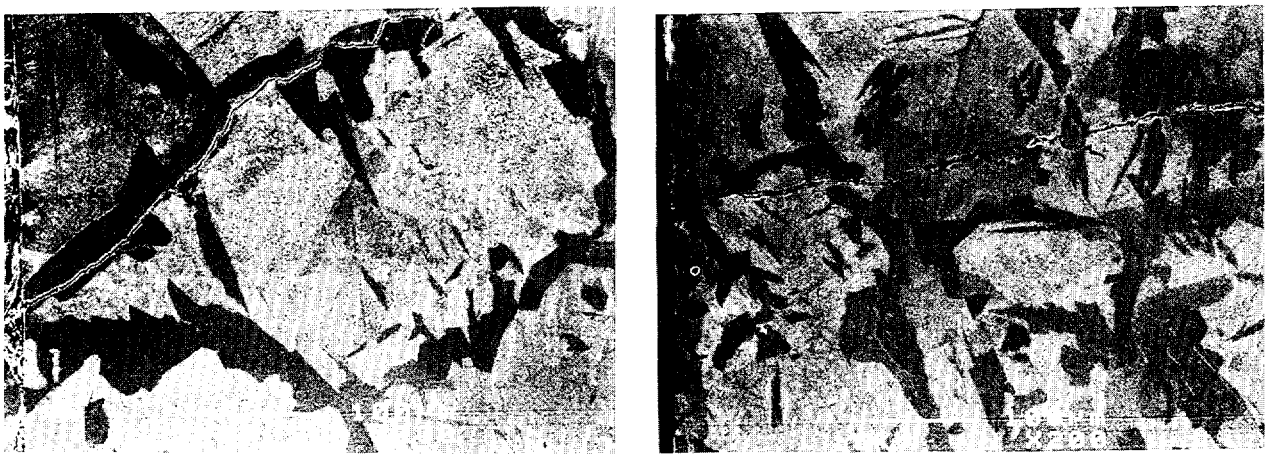

(a) (b)

Figure 5. Photomicrographs of fatigue cracks along gauge sections of A106–Gr B carbon steel in (a) air and (b) high–DO water at 288°C

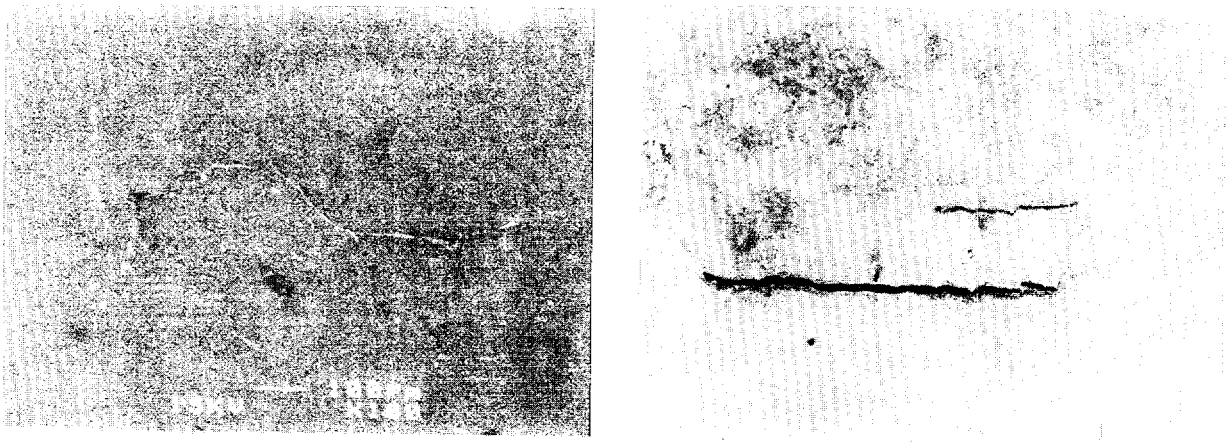

(a) (b)

Figure 6. Photomicrographs of fatigue cracks on gauge surfaces of A106–Gr B low–alloy steel in (a) air and (b) high–DO water at 288°C

growth, and propagation of near–surface cracks across pearlite regions indicate that in high-DO water, growth of MSCs occurs predominantly by the slip oxidation/dissolution process.

In high–DO water, crack initiation in CSs and LASs may be explained as follows: surface microcracks form quite early in fatigue life. During cyclic loading, the protective oxide film is ruptured at strains greater than the fracture strain of surface oxides, and the microcracks grow by anodic dissolution of the freshly exposed surface to crack lengths greater than the critical length of MSCs. These mechanically small cracks grow to engineering size, and their growth, which is characterized by accelerating rates, can be predicted by fracture mechanics methodology.

2.2 Austenitic Stainless Steels

Studies on crack initiation in austenitic SSs yield similar results; the decrease in fatigue life in LWR environments is caused primarily by the effects of environment on the growth of cracks that are <500 μm deep.[41] However, for SSs, fatigue lives are lower in low–DO water than in high–DO water; such results are difficult to reconcile in terms of the slip oxidation/dissolution mechanism.

Also, SS specimens tested in water show well–defined fatigue striations. Figure 7 shows photomicrographs of fracture surfaces of Type 304 and 316NG SS specimens, after chemical cleaning and at approximately the same crack length; specimens were tested at 288°C and ≈0.75% strain range in air, high–DO water, and a low–DO simulated PWR water. All of the specimens show fatigue striations; the spacing between striations is larger in low–DO water than in air. The presence of well–defined striations suggests that mechanical factors and not the slip dissolution/oxidation process are important.[25] The results indicate that environmentally assisted reduction in fatigue life of austenitic SSs is most likely caused by other mechanisms, such as hydrogen–enhanced crack growth.

Type 304 SS

Type 316NG SS

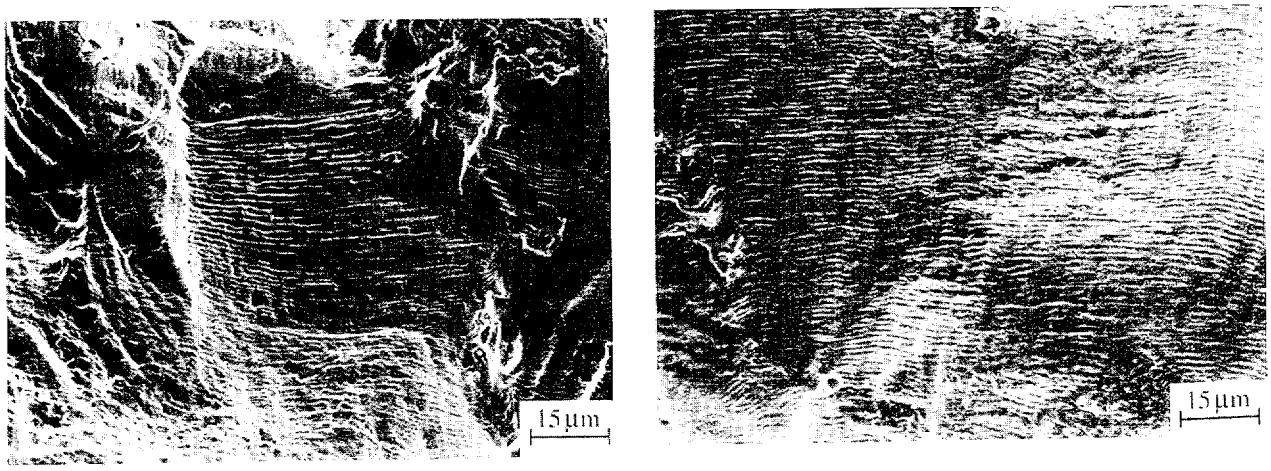

Air

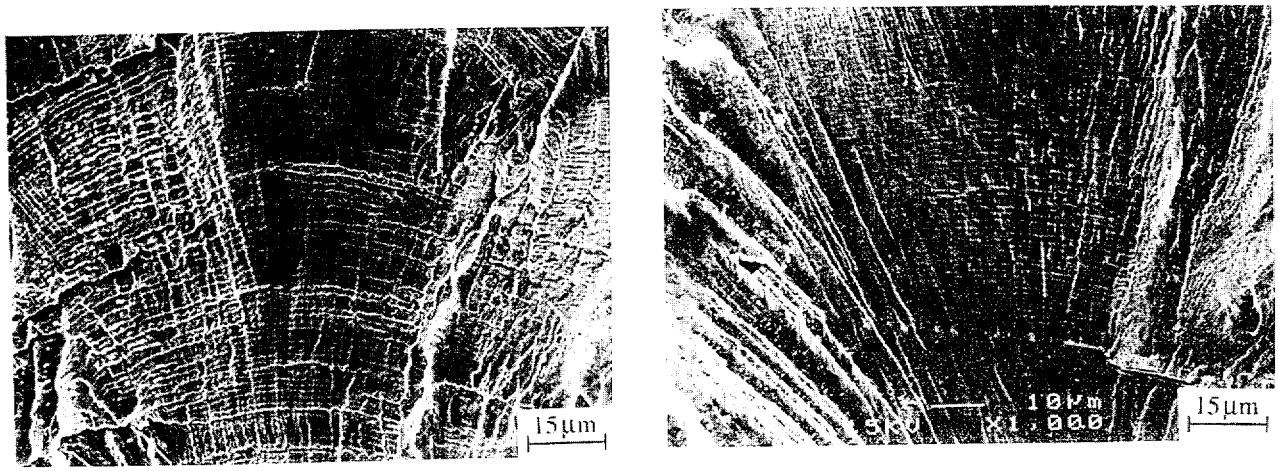

High–DO Water

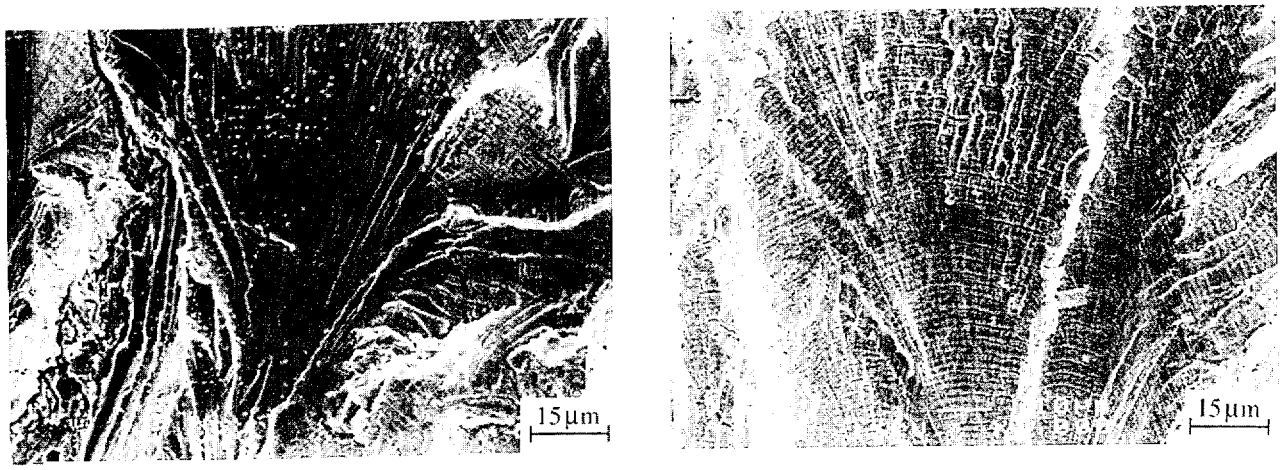

Low–DO PWR Water

Figure 7. Photomicrographs of fracture surfaces of Types 304 and 316NG SS specimens tested in air, high–DO water, and low–DO simulated PWR water

3 Overview of Fatigue S–N Data

3.1 Carbon and Low–Alloy Steels

The fatigue lives of both CSs and LASs are decreased in LWR environments; the reduction depends on temperature, strain rate, DO level in water, and S content of the steel. The fatigue S–N data obtained at ANL on carbon and low–alloy steels are summarized in Appendix A, Tables A1–A4. Fatigue life is decreased significantly when four conditions are satisfied simultaneously, viz., strain amplitude, temperature, and DO in water are above a minimum level, and strain rate is below a threshold value. The S content in the steel is also important; its effect on life depends on the DO level in water. Although the microstructures and cyclic–hardening behavior of CSs and LASs differ significantly, environmental degradation of fatigue lives of these steels is very similar. For both steels, only a moderate decrease in life (by a factor of <2) is observed when any one of the threshold conditions is not satisfied. The effects of the critical parameters on fatigue life and their threshold values are summarized below.

(a) *Strain:* A minimum threshold strain is required for environmentally assisted decrease in fatigue lives of CSs and LASs.[12–15] Limited data suggest that the threshold value is ≈20% higher than the fatigue limit for the steel. The results from fatigue tests conducted at constant strain range and from exploratory tests that have been conducted with waveforms in which the slow strain rate is applied during only a fraction of the tensile loading cycle (Fig. 8) yield similar values for threshold strain.[12] The data from exploratory tests indicate that loading histories with slow strain rate applied near maximum compressive strain produce no damage (line AD in Fig. 8) until the fraction of the strain is sufficiently large that slow strain rates are occurring for strain amplitudes greater than the threshold. The relative damage due to slow strain rate is independent of strain amplitude once the amplitude exceeds a threshold value. However, it is not known whether the threshold strain corresponds to the rupture strain of the surface oxide film.

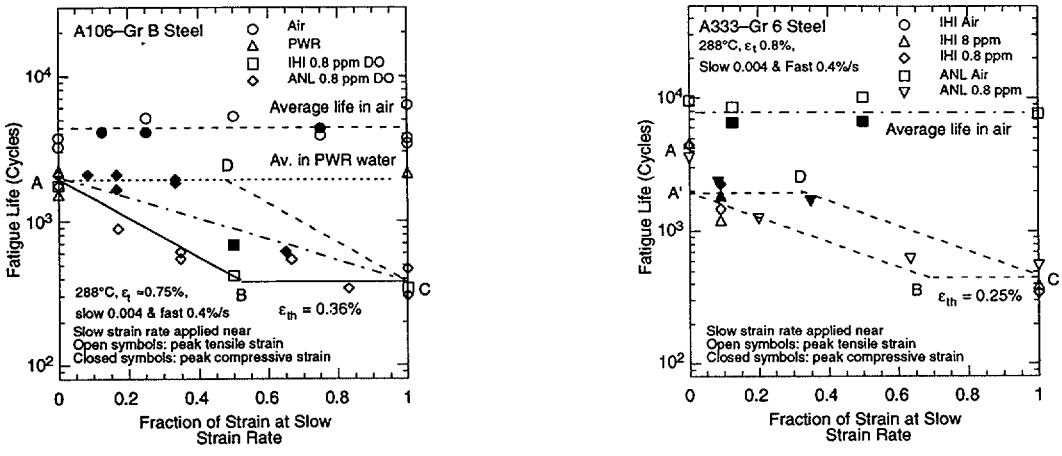

(a) (b)

Figure 8. Fatigue life of (a) A106–Gr B and (b) A333–Gr 6 carbon steels tested with loading waveforms where slow strain rate is applied during fraction of tensile loading cycle. IHI = Ishikawajima–Harima Heavy Industries Co., Japan.

(b) *Strain Rate*: Environmental effects on fatigue life occur primarily during the tensile–loading cycle, and at strain levels greater than the threshold value. When any one of the threshold conditions is not satisfied, e.g., DO <0.05 ppm or temperature <150°C, the effects of strain rate are consistent with those in air, i.e., only the heats that are sensitive to strain rate in air show a decrease in life in water. When all other threshold conditions are satisfied, fatigue life decreases logarithmically with decreasing strain rate below 1%/s;[4,8,42] the effect of environment on life saturates at ≈0.001%/s.[12–15] The dependence of fatigue life on strain rate for A106–Gr B CS and A533–Gr B LAS is shown in Fig. 9. For A533–Gr B steel, the fatigue life at a strain rate of 0.0004%/s in high–DO water (≈0.7 ppm DO) is lower by more than a factor of 40 than it is in air.

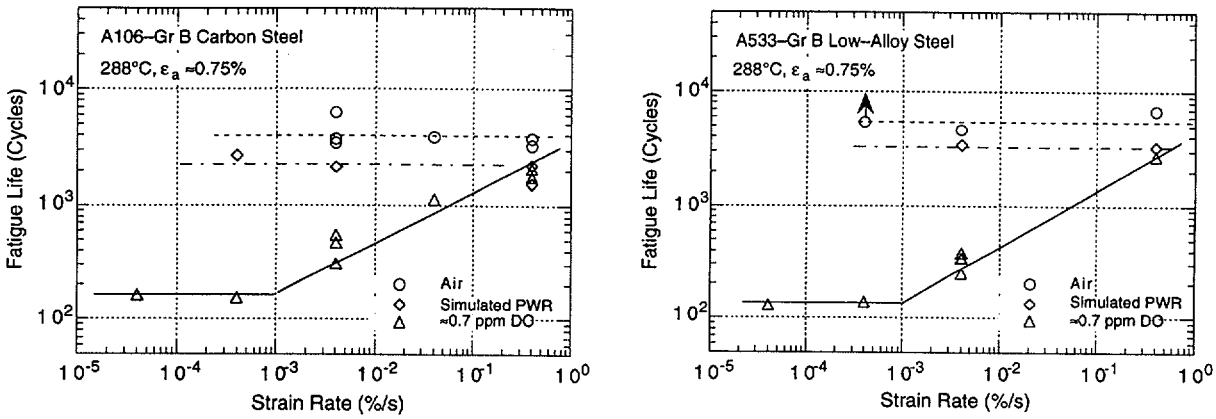

Figure 9. Dependence of fatigue lives of (a) carbon steels and (b) low–alloy steels on strain rate

(c) *Temperature*: When other threshold conditions are satisfied, fatigue life decreases linearly with temperature above 150°C and up to 320°C.[4,5,8] Fatigue life is insensitive to temperatures below 150°C or when any other threshold condition is not satisfied.

(d) *Dissolved Oxygen in Water*: When other threshold conditions are satisfied, fatigue life decreases logarithmically with DO above 0.05 ppm; the effect saturates at ≈0.5 ppm DO.[5,8] Fatigue life is insensitive to DO level below 0.05 ppm or when any other threshold condition is not satisfied.

(e) *S Content of Steel*: The effect of the S content of steel on fatigue life depends on the DO content in water. When the threshold conditions are satisfied and for DO contents ≤1.0 ppm, the fatigue life decreases with increasing S content. Limited data suggest that the effects of environment on life saturate at a S content of ≈0.015 wt.%.[12] At high DO levels, e.g., >1.0 ppm, fatigue life seems to be insensitive to S content in the range of 0.002–0.015 wt.%.[43] When any one of the threshold conditions is not satisfied, environmental effects on life are minimal and relatively insensitive to changes in S content.

(f) *Flow Rate*: It has long been recognized that the flow rate may have a strong effect on the fatigue life of materials because it may cause differences in the local environmental conditions at the crack tip. However, information about the effects of

flow rate has been very limited. Recent results indicate that under the environmental conditions typical of operating BWRs, e.g., high-purity water at 289°C with ≈0.2 ppm DO, environmental effects on the fatigue life of CSs and LASs are a factor of ≈2 lower at high flow rates than the environmental effects under semistagnant conditions or very low flow rates. Data on A333-Gr 6 CS indicate that at 289°C, relatively slow strain rate (0.01%/s), and under all DO conditions, a high flow rate has an appreciable effect on the fatigue life of the steel.[44] In high-DO water (i.e., 0.2 ppm or higher) at 289°C, environmental effects on the fatigue life are a factor of ≈2 lower at a flow rate of 7 m/s than at 0.3 m/s. The results also indicate that flow rate has little or no effect at high strain rates (0.4%/s). Similar effects have also been observed in another study at Kraftwerk Union (KWU) laboratories on A508 carbon steel pipe; environmental effects on fatigue life were a factor of ≈2 lower at a flow rate of 0.6 m/s than those at very low flow.[45]

3.2 Austenitic Stainless Steels

The fatigue lives of austenitic SSs are decreased in LWR environments; the reduction depends on strain rate, level of DO in water, and temperature.[15,19,23-25] The fatigue S-N data obtained at ANL on austenitic SSs and cast austenitic SSs are summarized in Appendix A, Tables A5-A7. The effects of LWR environments on fatigue life of wrought materials are comparable for Types 304, 316, and 316NG SSs. Although the fatigue lives of cast SSs are relatively insensitive to changes in ferrite content in the range of 12-28%,[19] the effects of loading and environmental parameters on the fatigue life of cast SSs differ somewhat. The significant results and threshold values of critical parameters are summarized below.

(a) *Dissolved Oxygen in Water*: For wrought austenitic SSs, environmental effects on fatigue life are more pronounced in low-DO, i.e., <0.01 ppm DO, than in high-DO, i.e., ≥0.1 ppm DO, water.[19,25] In high-DO water, environmental effects are moderate (less than a factor of 2 decrease in life) when conductivity is maintained at <0.1 μS/cm and electrochemical potential (ECP) of the steel has reached a stable value (Fig. 10). For fatigue tests in high-DO water, the SS specimens must be soaked for 5-6 days for the ECP of the steel to stabilize. Figure 10 shows that although fatigue life is decreased by a factor of ≈2 when conductivity of water is increased from ≈0.07 to 0.4 μS/cm, presoaking period appears to have a greater effect on life than does the conductivity of water. In low-DO water, the addition of lithium and boron, low conductivity, preexposing for ≈5 days prior to the test, or dissolved hydrogen have no effect on fatigue life of Type 304 SS (Table 1).

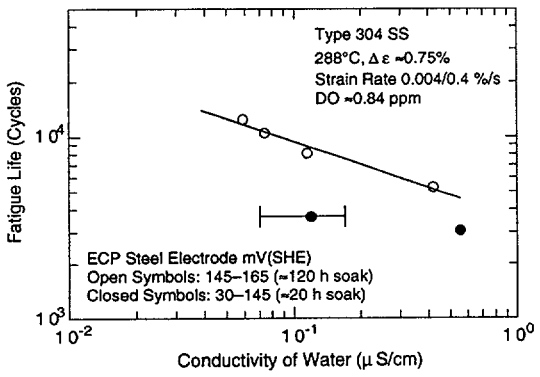

Figure 10.
Effects of conductivity of water and soak period on fatigue lives of Type 304 SS in high-DO water

Table 1. Fatigue test[a] results for Type 304 austenitic SS at 288°C

Test No.	Dis. Oxygen[b] (ppb)	Dis. Hydrogen (cc/kg)	Li (ppm)	Boron (ppm)	Pre-soak (days)	pH at RT	Conductivity[c] (μS/cm)	ECP SS[b] mV (SHE)	Ten. Rate (%/s)	Stress Range (MPa)	Strain Range (%)	Life N_{25} (Cycles)
1805	–	–				–	–	–	4.0E-3	467.9	0.76	14,410
1808	4	23	2	1000	1	6.4	18.87	–690	4.0E-3	468.3	0.77	2,850
1821	2	23	2	1000	1	6.5	22.22	–697	4.0E-3	474.3	0.76	2,420
1859	2	23	2	1000	1	6.5	18.69	–696	4.0E-3	471.7	0.77	2,420
1861	1	23	–	–	1	6.2	0.06	–614	4.0E-3	463.0	0.79	2,620
1862	2	23	–	–	5	6.2	0.06	–607	4.0E-3	466.1	0.78	2,450
1863	1	–	–	–	5	6.3	0.06	–540	4.0E-3	476.5	0.77	2,250
1871[d]	5	–	–	–	7	6.1	0.09	–609	4.0E-3	477.9	0.77	2,180

[a]Fully reversed axial fatigue tests at 288°C, ≈0.77% strain range, sawtooth waveform with 0.004/0.4%/s strain rates.
[b]DO and ECPs measured in effluent.
[c]Conductivity of water measured in feedwater supply tank.
[d]Test conducted with a 2 min hold period at zero strain.

(b) *Strain:* Nearly all of the existing fatigue S–N data have been obtained under loading histories with constant strain rate, temperature, and strain amplitude. Actual loading histories encountered during service of nuclear power plants are far more complex. Exploratory fatigue tests have been conducted with waveforms in which the slow strain rate is applied during only a fraction of the tensile loading cycle.[20] The results indicate that a minimum threshold strain is required for environmentally assisted decrease in fatigue lives of SSs (Fig. 11). Limited data suggest that the threshold strain range is between 0.32 and 0.36%.[20,25]

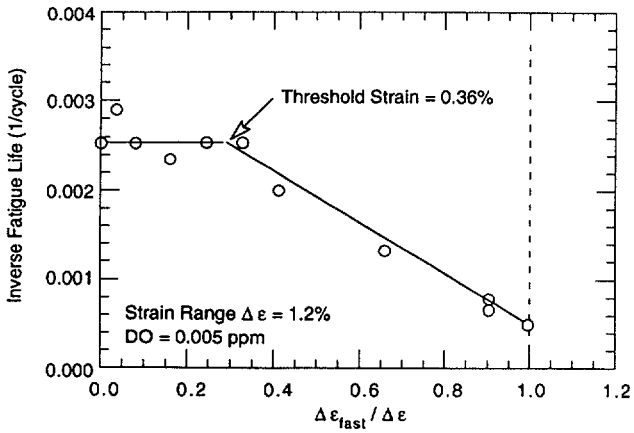

Figure 11.
Results of strain rate change tests on Type 316 SS in low–DO water at 325°C

During each fatigue cycle, relative damage due to slow strain rate is the same once the strain amplitude exceeds a threshold value. However, data also indicate that threshold strain does not correspond to rupture strain of the surface oxide film. The fatigue life of a fully–reversed (R = –1) axial fatigue test on Type 304 SS at 288°C in high-purity water with <3 ppb DO, 0.75% strain range, sawtooth waveform with 0.004%/s tensile strain rate, and a two–min hold period at zero strain during the tensile rise portion was identical to that of tests conducted under similar loading conditions but without the hold period (Table 1). If this threshold strain corresponds to the rupture strain of the surface oxide film, a hold period at the middle of each cycle should allow repassivation of the oxide film, and environmental effects on fatigue life should diminish.

(c) *Strain Rate*: In high–DO water (conductivity <0.1 μS/cm and stable ECP of the steel), fatigue life is insensitive to changes in strain rate. In low–DO water, fatigue life decreases logarithmically with decreasing strain rate below ≈0.4%/s; the effect of environment on life saturates at ≈0.0004%/s for wrought SSs.[20,25]

(d) *Temperature*: Existing data are also too sparse to establish the effects of temperature on fatigue life over the entire range from room temperature to reactor operating temperatures. Limited data indicate that environmental effects on fatigue life are minimal below 200°C and significant above 250°C;[20] life appears to be relatively insensitive to changes in temperature in the range of 250–330°C. The Pressure Vessel Research Council (PVRC) steering committee for cyclic life and environmental effects (CLEE) has proposed a ramp function to describe temperature effects on the fatigue lives of austenitic SSs; environmental effects are moderate at temperatures below 180°C, significant above 220°C, and increase linearly from 180 to 220°C.[46]

(e) *Flow Rate*: It is generally recognized that the flow rate most likely has a significant effect on the fatigue life of materials. However, fatigue S–N data that evaluate the effects of flow rate on the fatigue life of austenitic SSs are not available.

(f) *Cast Austenitic Stainless Steel*: The effects of loading and environmental parameters on the fatigue life of cast SSs differ somewhat from those for wrought SSs. For cast SSs, the fatigue lives are approximately the same in both high– or low–DO water and are comparable to those observed for wrought SSs in low–DO water.[25] Existing data are too sparse to define the saturation strain rate for cast SSs or to establish the dependence of temperature on the fatigue life in LWR environments; the effects of strain rate and temperature are assumed to be similar to those for wrought SSs.

4 Operating Experience in Nuclear Power Industry

Experience with operating nuclear power plants worldwide reveals that many failures may be attributed to fatigue; examples include piping components, nozzles, valves, and pumps.[47,48] In most cases, these failures have been associated with thermal loading due to thermal stratification and striping, or mechanical loading due to vibratory loading. Significant thermal loadings due to flow stratification were not included in the original design basis analysis. The effect of these loadings may also have been aggravated by corrosion effects due to a high-temperature aqueous environment. Fatigue cracks have been observed in pressurizer surge lines in PWRs,[49] and in feedwater lines connected to nozzles of pressure vessels in boiling water reactors (BWRs) and steam generators in PWRs.[50,51] A review of significant occurrences of corrosion fatigue damage and failures in various nuclear power plant systems has been presented in an Electric Power Research Institute report;[52] the results are summarized below.

4.1 Cracking in Feedwater Nozzle and Piping

Fatigue cracks have been observed in feedwater piping and nozzles of the pressure vessel in BWRs and steam generators in PWRs.[50,51,53] The mechanism of cracking has been attributed to corrosion fatigue[54,55] or strain-induced corrosion cracking (SICC).[56] Case histories and identification of conditions that lead to SICC of LASs in LWR systems have been summarized by Hickling and Blind.[57]

In BWR nozzle cracking, initiation has been attributed to high-cycle fatigue caused by the leakage of cold water around the junction area of the thermal sleeve, and crack propagation has been attributed to low-cycle fatigue due to plant transients such as startups/shutdowns and any feedwater on/off transients. The frequency of the high-cycle fatigue phenomenon due to leakage around the sleeve is ≈0.5–1 Hz; therefore, it is not expected to be influenced by the reactor coolant environment. Estimates of strain range and strain rates for typical transients associated with low-cycle fatigue are given in Table 2.[58] Under these loading and environmental conditions, significant reduction in fatigue life has been observed for carbon and low-alloy steels.[12,14]

In PWR feedwater systems, cracking has been attributed to a combination of thermal stratification and thermal striping.[52] Environmental factors, such as high DO in the feedwater, are believed to also have played a significant role in crack initiation. The thermal stratification is caused by the injection of low-flow, relatively cold feedwater during plant startup, hot standby, and variations below 20% of full power, whereas thermal striping is caused by rapid, localized fluctuations of the interface between hot and cold feedwater.

Table 2. Typical chemical and cyclic strain transients

Component	Operation	DO (ppb)	Temp. (°C)	Strain Range (%)	Strain Rate (%/s)
FW Nozzle	Startup	20/200	216/38	0.2-0.4	10^{-2}
FW Piping	Startup	20/200	216/38	0.2-0.5	10^{-3}–10^{-2}
FW Piping	Startup	20/200	288/38	0.07-0.1	4–8x10^{-6}
FW Piping	Turbine Roll	<200	288/80	0.4	3–6x10^{-3}
FW Piping	Hot Standby	<200	288/90	0.26	4x10^{-4}
FW Piping	Cool Down	<20	288/RT	0.2	6x10^{-4}
FW Piping	Stratifica-tion	200	250/50	0.2-0.7	10^{-4}–10^{-3}

Lenz et al.[56] showed that in feedwater lines, the strain rates are 10^{-3}–10^{-5}%/s due to thermal stratification and 10^{-1}%/s due to thermal shock and that thermal stratification is the primary cause of crack initiation due to SICC. Also, the results from small-size specimens, medium-size components (model vessels), and full-size thermal-shock experiments suggest an influence of oxygen content in pressurized water on crack initiation behavior.[53]

Several studies have been conducted at Electricité de France (EdF) to investigate the thermal and mechanical effects of stratification in pipes. Stephan and Masson[59] subjected a full-scale mock-up of the steam generator feedwater system to various regimes of stratification. After 4000 cycles of fatigue, destructive examination performed between two stable states of stratification revealed small cracks, 1.4–4.0 mm deep, in the weld region. The fatigue usage factors calculated with elastic and cyclic elastic-plastic computations gave values of 1.3–1.9. However, because the average DO level in water was ≈5 ppb, which corresponds to the maximum admissible value under normal operating conditions in French PWRs, environmental effects on life are expected to be minimal and environmental correction factors were not applied in the computations of the fatigue usage factor.

A detailed examination of cracking in a CS elbow adjacent to the steam generator nozzle weld[60] indicates crack morphologies that are identical to those observed in smooth specimens tested in high-DO water. For example, the deepest crack was straight, nonbranching, transgranular through both the ferrite and pearlite regions without any preference, and showed significant oxidation and some pitting at the crack origin. In fatigue test specimens, near-surface cracks grow entirely as tensile cracks normal to the stress and across both the soft ferrite and hard pearlite regions, whereas in air, cracks grow at an angle of 45° to the stress axis and only along the ferrite regions (see Fig. 5). The identical crack morphologies indicate that environment played a dominant role in crack initiation. Similar characteristics of transgranular crack propagation through both weld and base metal, without regard to microstructural features, have also been identified in German reactors.[57]

Tests have also been conducted on components to validate the calculation procedures and the applicability of the test results from specimen to actual reactor component. Tests on pipes, plates, and nozzles, under cyclic thermal loading in aqueous environment[47] indicate that crack initiation in simulated LWR environments may occur earlier than indicated by the values of the ASME Section III fatigue design curve; environmental effects are more pronounced in the ferritic steel than in the austenitic cladding. Tests performed at the reactor pressure vessel of the decommissioned HDR (Heissdampfreaktor)[61] have also shown good agreement between the fatigue lives applicable to specimens and components, e.g., first incipient crack on pipes appeared in 1200 cycles, compared with 1400 cycles for a test specimen made of the same material and tested under comparable conditions (8 ppm DO).

4.2 Steam Generator Girth Weld Cracking

Another instance of thermal-fatigue-induced cracking where environmental effects are believed to have played a role in crack initiation has been observed at the weld joint between the two shells of a steam generator.[62] The feedwater temperature in this region is nominally 204–227°C (440–440°F), compared with the steam generator temperature of 288°C (550°C). The primary mechanism of cracking has been considered corrosion fatigue, with possible slow crack growth due to stress corrosion cracking. A detailed analysis of girth-weld cracking

indicates that crack initiation was dominated by environmental influences, particularly under relatively high–DO content and/or oxidizing potential.[63]

4.3 PWR Primary System Leaks

Significant cracking has also occurred in unisolable pipe sections in the safety injection system piping connected to the PWR coolant system.[64,65] This phenomenon, which is similar to the nozzle cracking discussed above, is caused by thermal stratification. Also, regulatory evaluation has indicated that thermal stratification can occur in all PWR surge lines.[49] In PWRs, the pressurizer water is heated to ≈227°C (440°F). The hot water, flowing at a very slow rate from the pressurizer through the surge line to the hot–leg piping, rides on a cooler water layer. The thermal gradients between the upper and lower parts of the pipe can be as high as 149°C (300°F). Unisolable leaks due to thermal–stratification cycling have occurred in reactor coolant loop drain lines and excess letdown lines at Three Mile Island, Oconee, Mihama, and Loviisa plants.[66] Thermal fatigue has caused leakage in the CVCS (chemical and volume control system) pipe of the regenerative heat exchanger at Tsuruga 2,[67] and in the residual heat removal system of the Civaux 1 plant.[68]

Full–scale mock-up tests to generate thermal stratification in a pipe in a laboratory have confirmed the applicability of laboratory data to component behavior.[69] The material, loading, and environmental conditions were simulated on a 1:1 scale, using only thermohydraulic effects. Under the loading conditions, i.e., strain rate and strain range typical of thermal stratification in these piping systems, the coolant environment is known to have a significant effect on fatigue crack initiation.[14,19,20]

5 Incorporating Environmental Effects into Fatigue Evaluations

Two procedures are currently being proposed for incorporating the effects of LWR coolant environments into the ASME Section III fatigue evaluations: (a) develop a new set of environmentally adjusted design fatigue curves[2,12,14,15,25] or (b) use a fatigue life correction factor F_{en} to adjust the current ASME Code fatigue usage values for environmental effects.[2,14,15,30,31] For both approaches, the range and bounding values must be defined for key service parameters that influence fatigue life. It has been demonstrated that estimates of fatigue life based on the two methods may differ because of differences between the ASME mean curves used to develop the current design curves and the best-fit curves to the existing data that are used to develop the environmentally adjusted curves. However, either of these methods provides an acceptable approach to account for environmental effects.

5.1 Design Fatigue Curves

A set of environmentally adjusted design fatigue curves can be developed from the best-fit stress-vs.-life curves to the experimental data in LWR environments by using the same procedure that was used to develop the current ASME Code design fatigue curves. The stress-vs.-life curves are obtained from the S-N curves, e.g., stress amplitude is the product of strain amplitude and elastic modulus. The best-fit experimental curves are first adjusted for the effect of mean stress by using the modified Goodman relationship

$$S'_a = S_a\left(\frac{\sigma_u - \sigma_y}{\sigma_u - S_a}\right) \qquad \text{for } S_a < \sigma_y, \tag{1}$$

and

$$S'_a = S_a \qquad \text{for } S_a > \sigma_y, \tag{2}$$

where S'_a is the adjusted value of stress amplitude, and σ_y and σ_u are yield and ultimate strengths of the material, respectively. Equations 1 and 2 assume the maximum possible mean stress and typically give a conservative adjustment for mean stress, at least when environmental effects are not significant. The design fatigue curves are then obtained by lowering the adjusted best-fit curve by a factor of 2 on stress or 20 on cycles, whichever is more conservative, to account for differences and uncertainties in fatigue life that are associated with material and loading conditions.

Statistical models based on the existing fatigue S-N data have been developed for estimating the fatigue lives of pressure vessel and piping steels in air and LWR environments.[12,14,15,25] In room-temperature air, the fatigue life N of CSs is represented by

$$\ln(N) = 6.564 - 1.975 \ln(\varepsilon_a - 0.113) \tag{3}$$

and of LASs by

$$\ln(N) = 6.627 - 1.808 \ln(\varepsilon_a - 0.151), \tag{4}$$

where ε_a is applied strain amplitude (%). In LWR environments, the fatigue life of CSs is represented by

$$\ln(N) = 6.010 - 1.975 \ln(\varepsilon_a - 0.113) + 0.101\, S^*\, T^*\, O^*\, \dot{\varepsilon}^* \quad (5)$$

and of LASs, by

$$\ln(N) = 5.729 - 1.808 \ln(\varepsilon_a - 0.151) + 0.101\, S^*\, T^*\, O^*\, \dot{\varepsilon}^*, \quad (6)$$

where S^*, T^*, O^*, and $\dot{\varepsilon}^*$ are transformed S content, temperature, DO, and strain rate, respectively, defined as follows:

$$\begin{aligned} S^* &= 0.015 && (DO > 1.0 \text{ ppm}) \\ S^* &= S && (DO \leq 1.0 \text{ ppm and } 0 < S \leq 0.015 \text{ wt.\%}) \\ S^* &= 0.015 && (DO \leq 1.0 \text{ ppm and } S > 0.015 \text{ wt.\%}) \end{aligned} \quad (7)$$

$$\begin{aligned} T^* &= 0 && (T < 150°C) \\ T^* &= T - 150 && (T = 150\text{–}350°C) \end{aligned} \quad (8)$$

$$\begin{aligned} O^* &= 0 && (DO \leq 0.04 \text{ ppm}) \\ O^* &= \ln(DO/0.04) && (0.04 \text{ ppm} < DO \leq 0.5 \text{ ppm}) \\ O^* &= \ln(12.5) && (DO > 0.5 \text{ ppm}) \end{aligned} \quad (9)$$

$$\begin{aligned} \dot{\varepsilon}^* &= 0 && (\dot{\varepsilon} > 1\%/s) \\ \dot{\varepsilon}^* &= \ln(\dot{\varepsilon}) && (0.001 \leq \dot{\varepsilon} \leq 1\%/s) \\ \dot{\varepsilon}^* &= \ln(0.001) && (\dot{\varepsilon} < 0.001\%/s). \end{aligned} \quad (10)$$

In air at room temperature, the fatigue data for Types 304 and 316 SS are best represented by

$$\ln(N) = 6.703 - 2.030 \ln(\varepsilon_a - 0.126) \quad (11)$$

and for Type 316NG, by

$$\ln(N) = 7.422 - 1.671 \ln(\varepsilon_a - 0.126). \quad (12)$$

In LWR environments, fatigue data for Types 304 and 316 SS are best represented by

$$\ln(N) = 5.768 - 2.030 \ln(\varepsilon_a - 0.126) + T'\, \dot{\varepsilon}'\, O' \quad (13)$$

and for Type 316NG, by

$$\ln(N) = 6.913 - 1.671 \ln(\varepsilon_a - 0.126) + T'\, \dot{\varepsilon}'\, O', \quad (14)$$

where T', $\dot{\varepsilon}'$, and O' are transformed temperature, strain rate, and DO, respectively, defined as follows:

$$
\begin{aligned}
T' &= 0 && (T < 180°C) \\
T' &= (T - 180)/40 && (180 \le T < 220°C) \\
T' &= 1 && (T \ge 220°C)
\end{aligned} \tag{15}
$$

$$
\begin{aligned}
\dot{\varepsilon}' &= 0 && (\dot{\varepsilon} > 0.4\%/s) \\
\dot{\varepsilon}' &= \ln(\dot{\varepsilon}/0.4) && (0.0004 \le \dot{\varepsilon} \le 0.4\%/s) \\
\dot{\varepsilon}' &= \ln(0.0004/0.4) && (\dot{\varepsilon} < 0.0004\%/s)
\end{aligned} \tag{16}
$$

$$
\begin{aligned}
O' &= 0.260 && (DO < 0.05 \text{ ppm}) \\
O' &= 0 && (DO \ge 0.05 \text{ ppm}).
\end{aligned} \tag{17}
$$

The models are recommended for predicted fatigue lives $\le 10^6$ cycles. The design fatigue curves were obtained from the best-fit curves, represented by Eqs. 3–6 for CSs and LASs, and by Eqs. 11 and 13 for austenitic SSs. To be consistent with the current ASME Code philosophy, the best-fit curves were first adjusted for the effect of mean stress by using the modified Goodman relationship, and the mean-stress-adjusted curves were then decreased by a factor of 2 on stress and 20 on cycles to obtain the design fatigue curves.

The new design fatigue curves for CSs and LASs and austenitic SS in air are shown in Fig. 12, those in LWR coolant environments are shown in Figs. 13–16; only the portions of the environmentally adjusted curves that fall below the current ASME Code curve are shown in Figs. 13–16. Because the fatigue life of Type 316NG is superior to that of Types 304 or 316 SS,

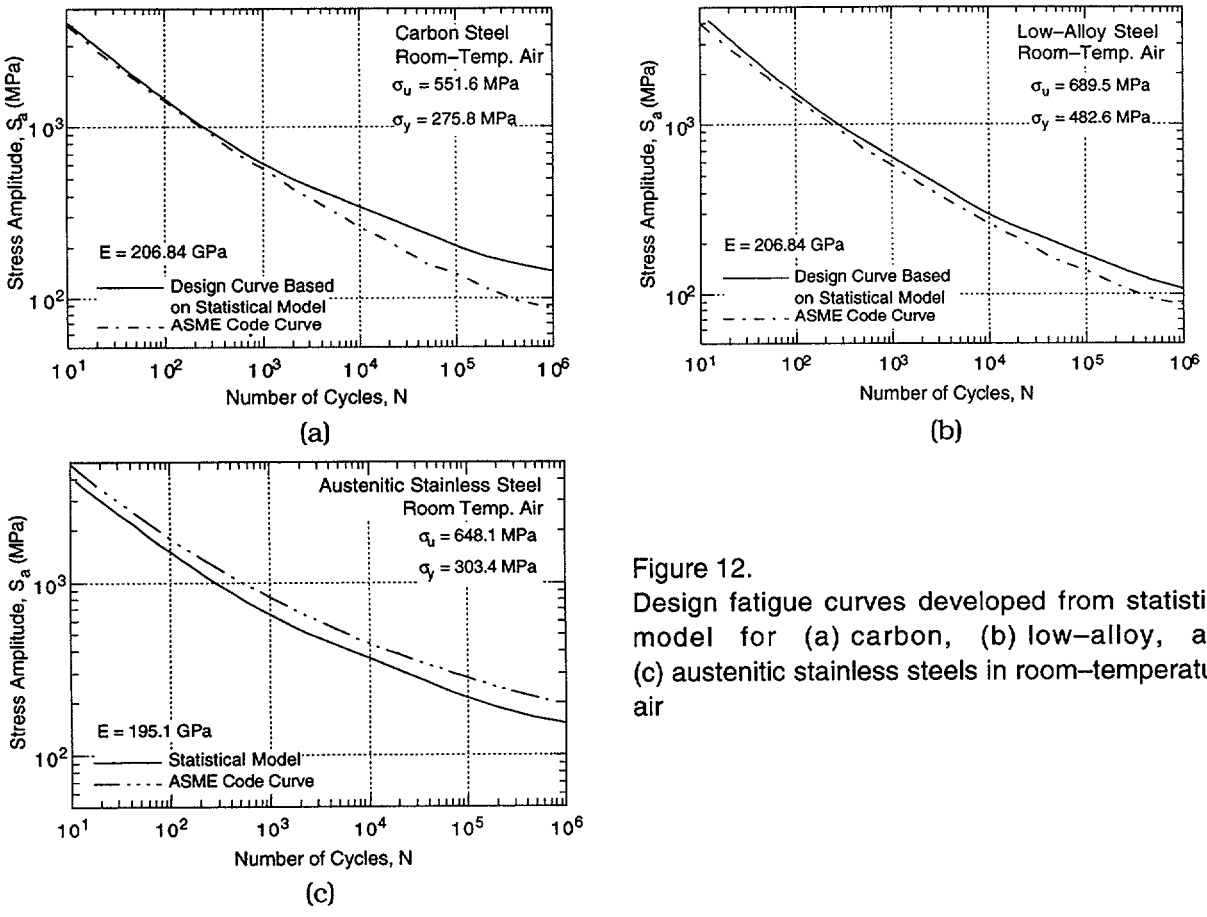

Figure 12.
Design fatigue curves developed from statistical model for (a) carbon, (b) low-alloy, and (c) austenitic stainless steels in room-temperature air

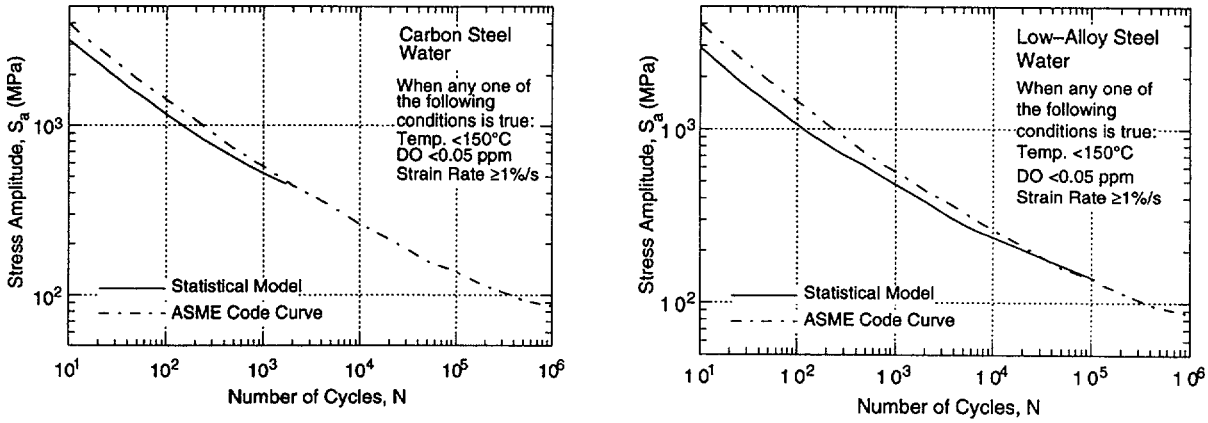

Figure 13. Design fatigue curves developed from statistical model for (a) carbon and (b) low–alloy steels under service conditions where one or more critical threshold values are not satisfied

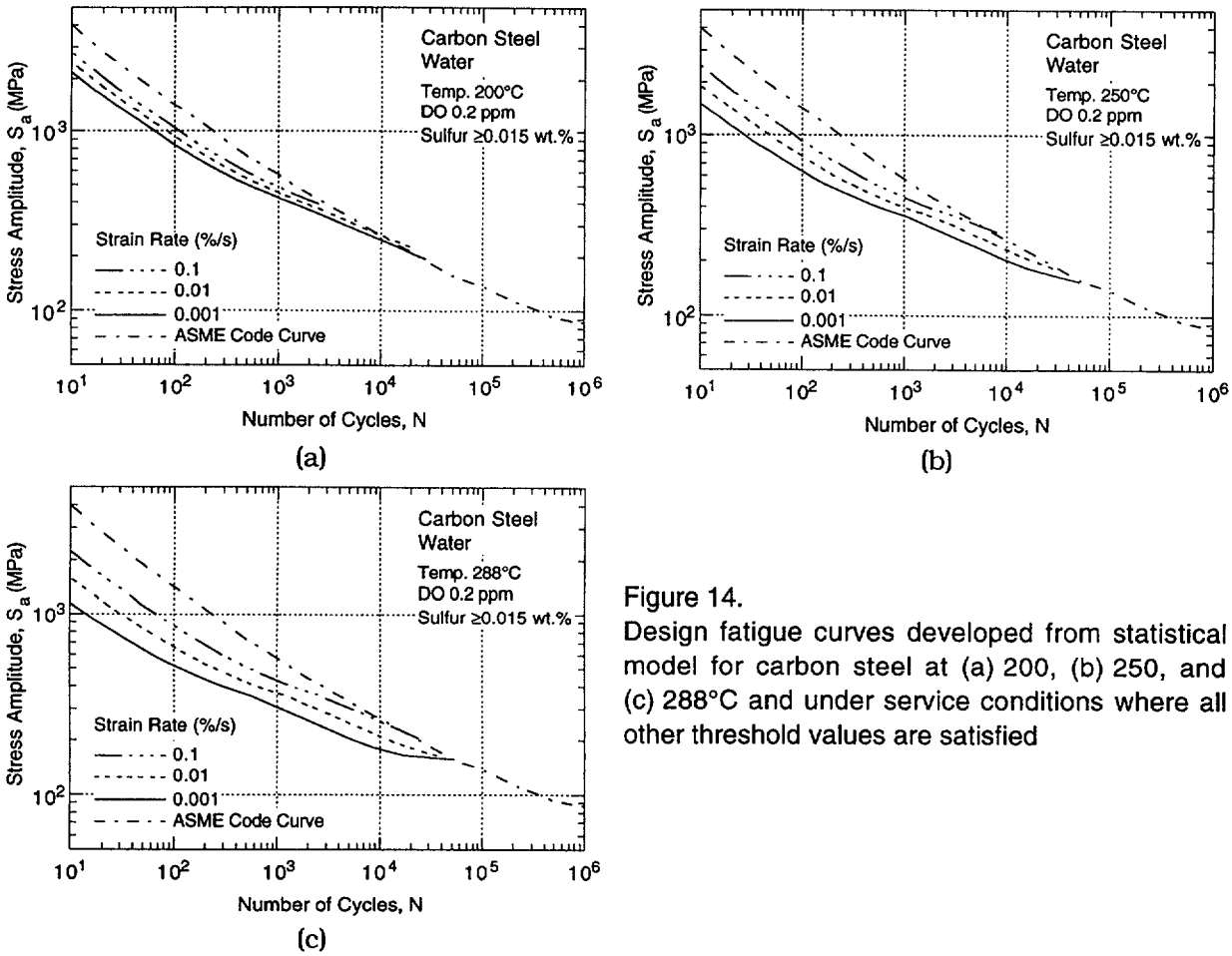

Figure 14.
Design fatigue curves developed from statistical model for carbon steel at (a) 200, (b) 250, and (c) 288°C and under service conditions where all other threshold values are satisfied

the design curves in Figs. 12 and 16 will be somewhat conservative for Type 316NG SS. For CSs and LASs, a set of design curves similar to those shown in Figs. 14 and 15 can be developed for low–S steels, i.e., steels with ≤0.007 wt.% S. The results indicate that in room–temperature air, the current ASME Code design curve for CSs and LASs is somewhat

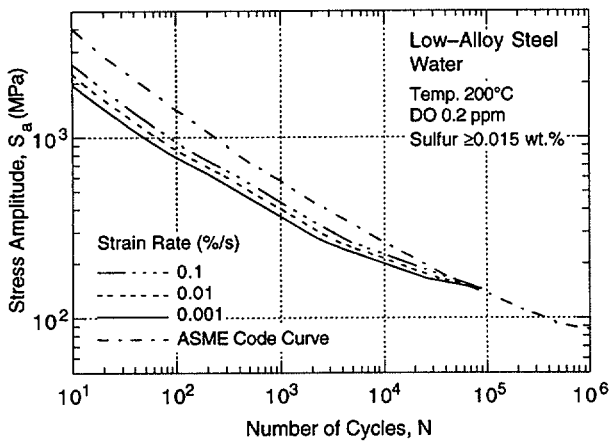

(a)

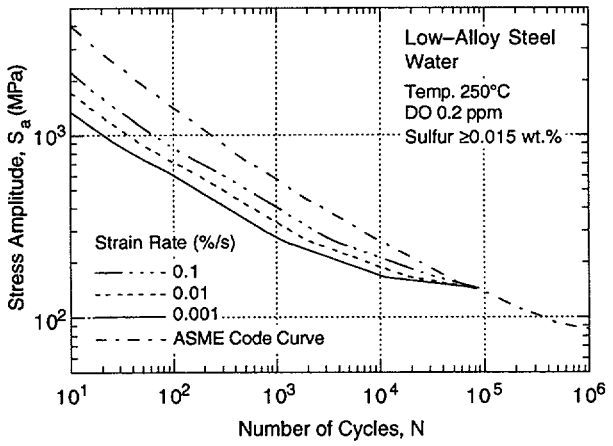

(b)

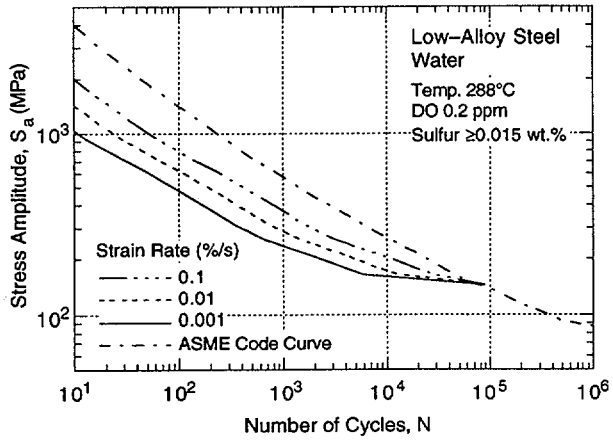

(c)

Figure 15.
Design fatigue curves developed from statistical model for low–alloy steel at (a) 200, (b) 250, and (c) 288°C and under service conditions where all other threshold values are satisfied

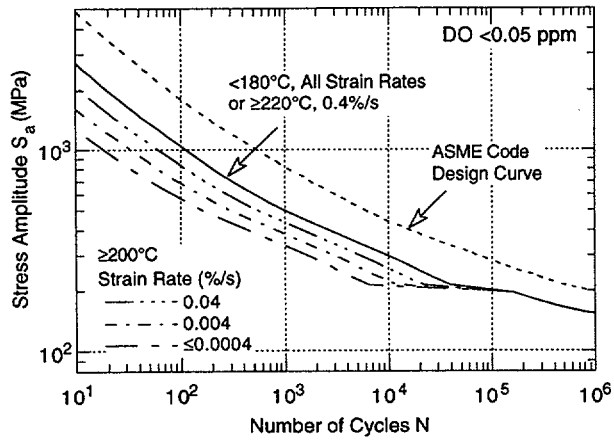

(a)

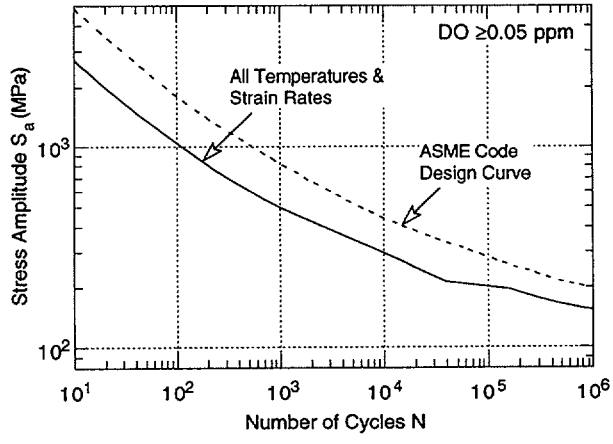

(b)

Figure 16. Design fatigue curves developed from statistical models for Types 304 and 316 SS in water with (a) <0.05 and (b) ≥0.05 ppm DO

conservative and that for austenitic SSs is nonconservative with respect to the design curves based on the statistical models. In other words, the margins between the current Code design curve and the best-fit of existing experimental data are greater than 2 on stress and 20 on

cycles for CSs and LASs, and less than 2 on stress and 20 on cycles for austenitic SSs. For SSs, actual margins are ≈1.5 on stress and 10–16 on cycles.

For environmentally adjusted design fatigue curves (Figs. 13–16), a minimum threshold strain is defined, below which environmental effects are modest. The threshold strain for CSs and LASs appears to be ≈20% higher than the fatigue limit of the steel. This translates into strain amplitudes of 0.140 and 0.185%, respectively, for CSs and LASs. These values must be adjusted for mean stress effects and variability due to material and experimental scatter. The threshold strain amplitudes are decreased by ≈15% for CSs and by ≈40% for LASs to account for the effects of mean stress, and by a factor of 1.7 on strain to provide 90% confidence for the variations in fatigue life associated with material variability and experimental scatter.[27] Thus, a threshold strain amplitude of 0.07% (or a stress amplitude of 145 MPa) is obtained for both CSs and LASs. The existing fatigue data indicate a threshold strain range of ≈0.32% for austenitic SSs. This value is decreased by ≈10% to account for mean stress effects and by a factor of 1.5 to account for uncertainties in fatigue life that are associated with material and loading variability. Thus, a threshold strain amplitude of 0.097% (stress amplitude of 189 MPa) is obtained for austenitic SSs. The PVRC steering committee for CLEE[46] has proposed a ramp for the threshold strain; a lower strain amplitude below which environmental effects are insignificant, a slightly higher strain amplitude above which environmental effects decrease fatigue life, and a ramp between the two values. The two strain amplitudes are 0.07 and 0.08% for carbon and low–alloy steels, and 0.10 and 0.11% for austenitic SSs (both wrought and cast SS). These threshold values have been used to develop Figs. 14–16.

5.2 Extension of Design Curves from 10^6 to 10^{11} Cycles (Carbon and Low–Alloy Steels)

The experimental fatigue S–N curves that were used to develop the current Code fatigue design curves were based on low–cycle fatigue data for fatigue lives of $< \approx 2 \times 10^5$ cycles. The design curves developed from more rigorous statistical models are based on a larger data base that includes fatigue lives up to 10^8 cycles. Both the ASME mean curves and statistical models use the modified Langer equation to express fatigue S–N curves and are not recommended for estimating lives beyond the range of the experimental data, i.e., in the high–cycle fatigue regime.

Manjoine and Johnson[70,71] have developed fatigue design curves up to 10^{11} cycles for carbon and low–alloy steels from inelastic and elastic strain relationships. The log–log plots of both inelastic and elastic strain amplitudes vs. fatigue life data for CSs and LASs are best represented by a bilinear curve. In the high–cycle regime, the slope of the inelastic–strain–vs.–life curve does not change significantly with either temperature or strain rate.[70,71] The high–cycle curve can be used to extend the fatigue design curves beyond 10^6 cycles; the design curve will exhibit a small negative slope instead of a fatigue limit predicted in the modified Langer equation.

For fatigue lives $>10^5$ cycles, the existing elastic–strain–vs.–life data at room temperature yield a fatigue life exponent <0.007 for both CSs and LASs. A value of 0.01, proposed by Manjoine and Johnson,[71] may be used conservatively. For fatigue lives up to 10^7 cycles, the fatigue design curves can be obtained from the statistical model (Eqs. 3 and 4), and from the elastic–strain–vs.–life correlation for lives between 10^7 and 10^{11} cycles. In the high–cycle regime, applied stress amplitude S_a is given by the relationship

$$S_a = E\varepsilon_a = CN^{-0.01}, \quad (18)$$

where ε_a is applied strain amplitude, E is the elastic modulus, N is the fatigue life, and C is a constant that is determined by pinning the lower end of the curve at the value of stress amplitude at 10^7 cycles obtained from either Eq. 3 or 4. The best-fit experimental curves, given by either Eqs. 3 and 18 or 4 and 18, are first adjusted for mean stress effects by using the modified Goodman relationship (Eqs. 1 and 2), and then lowered by factors of 20 on cycles and 2 on stress to account for the uncertainties in life associated with material and loading conditions. The design curves based on the statistical models and elastic-strain-vs.-life data for carbon and low-alloy steels in air are shown in Fig. 17. Because the high-cycle curve is below the threshold stress of 145 MPa, it is also applicable to LWR environments.

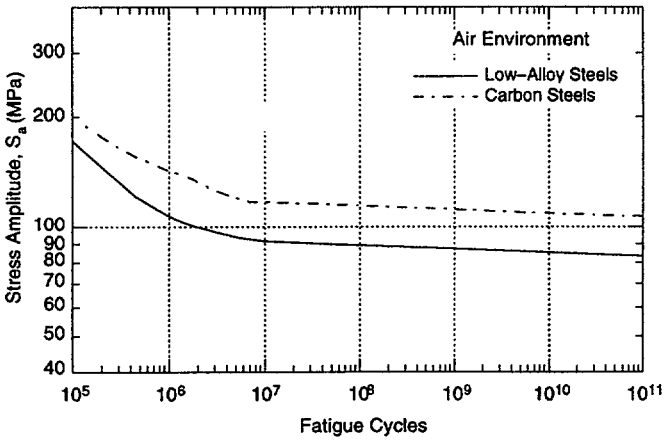

Figure 17.
Extension of fatigue design curves for carbon and low-alloy steels from 10^5 to 10^{11} cycles

5.3 Fatigue Life Correction Factor

The effects of reactor coolant environments on fatigue life have also been expressed in terms of a fatigue life correction factor F_{en}, which is the ratio of life in air at room temperature to that in water at the service temperature.[4] A fatigue life correction factor F_{en} can be obtained from the statistical model (Eqs. 3–17), where

$$\ln(F_{en}) = \ln(N_{RTair}) - \ln(N_{water}). \quad (19)$$

The fatigue life correction factor for CSs is given by

$$F_{en} = \exp(0.554 - 0.101\, S^*\, T^*\, O^*\, \dot{\varepsilon}^*), \quad (20)$$

for LASs, by

$$F_{en} = \exp(0.898 - 0.101\, S^*\, T^*\, O^*\, \dot{\varepsilon}^*), \quad (21)$$

and for austenitic SSs, by

$$F_{en} = \exp(0.935 - T'\, \dot{\varepsilon}'\, O'), \quad (22)$$

where the constants S^*, T^*, $\dot{\varepsilon}^*$, and O^* are defined in Eqs. 7–10, and T', $\dot{\varepsilon}'$, and O' are defined in Eqs. 15–17. A strain threshold is also defined, below which environmental effects are modest.

The strain threshold is represented by a ramp, i.e., a lower strain amplitude below which environmental effects are insignificant, a slightly higher strain amplitude above which environmental effects are significant, and a ramp between the two values. Thus, the negative terms in Eqs. 20–22 are scaled from zero to their actual values between the two strain thresholds. The two strain amplitudes are 0.07 and 0.08% for CSs and LASs, and 0.10 and 0.11% for austenitic SSs (both wrought and cast SS). To incorporate environmental effects into the Section III fatigue evaluation, a fatigue usage for a specific stress cycle, based on the current Code design fatigue curve, is multiplied by the correction factor. The experimental data adjusted for environmental effects, i.e., the product of experimentally observed fatigue life in LWR environments and F_{en}, are presented with the best–fit S–N curve in room–temperature air in Fig. 18.

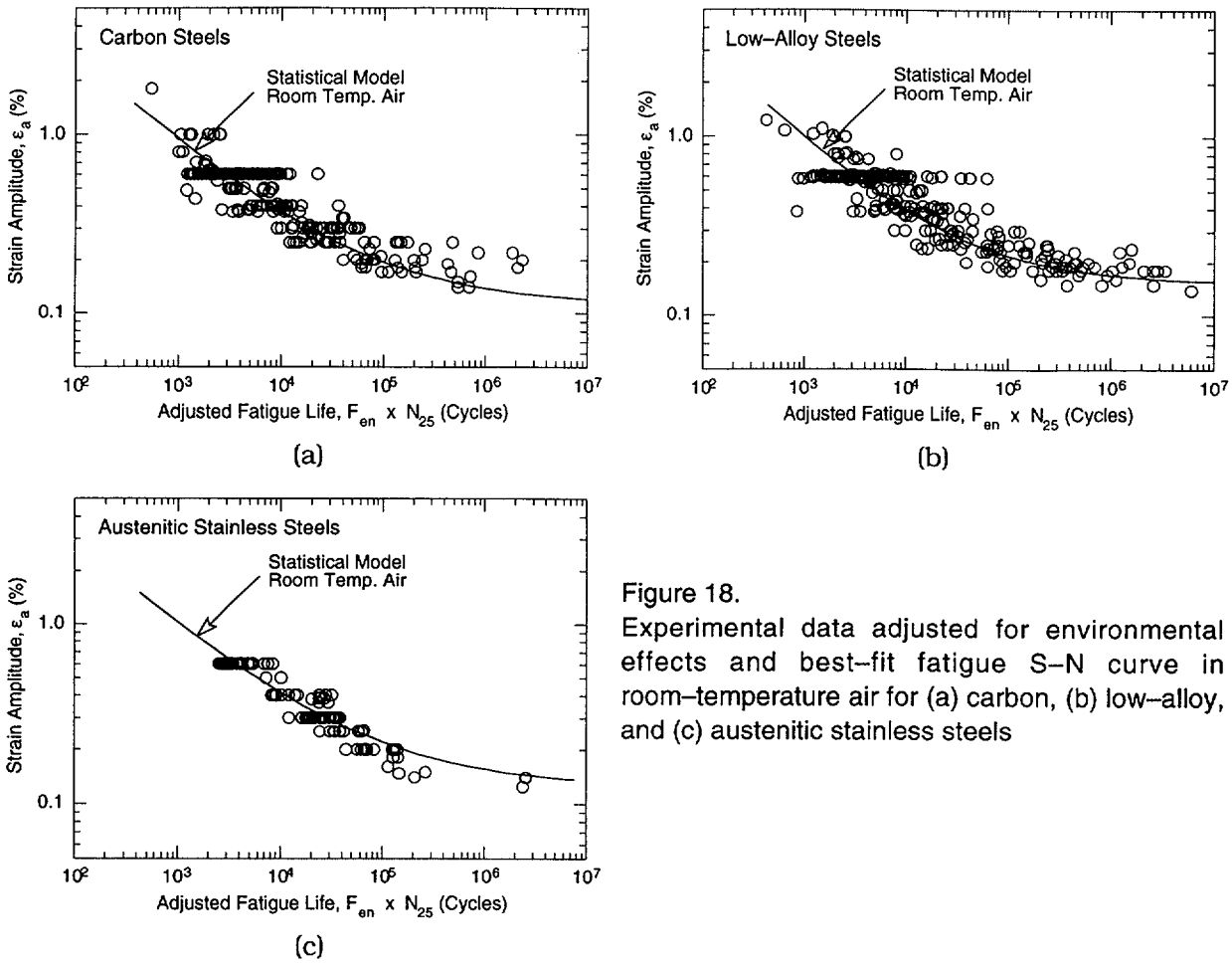

Figure 18.
Experimental data adjusted for environmental effects and best–fit fatigue S–N curve in room–temperature air for (a) carbon, (b) low–alloy, and (c) austenitic stainless steels

A similar approach has been proposed by Mehta and Gosselin;[30,31] however, they defined F_{en} as the ratio of the life in air to that in water, both at service temperature. The F_{en} approach, also known as the EPRI/GE approach, has recently been updated to include the revised statistical models and the PVRC discussions on evaluating environmental fatigue.[72] An "effective" fatigue life correction factor, expressed as $F_{en,eff} = F_{en}/Z$, is defined, where Z is a factor that represents the perceived conservatism in the ASME Code design curves. The $F_{en,eff}$ approach presumes that all uncertainties have been anticipated and accounted for. The possible conservatism in the ASME Code design curves is discussed in Section 6.

5.4 Fracture Mechanics Approach to Estimate Fatigue S–N Curves for Carbon and Low–Alloy Steels

The fatigue S–N behavior of carbon and low–alloy steels in air and LWR environments has been examined from the stand point of fracture mechanics and crack growth data. As discussed in Section 2, fatigue life is considered composed of the growth of MSCs and mechanically small cracks. Studies on crack initiation in smooth fatigue specimens indicate that surface cracks form quite early in life. Smith et al.[73] detected 10–μm–deep surface cracks at temperatures up to 700°C in Waspalloy. Hussain et al.[74] examined the growth of ≈20–μm–deep surface cracks through four or more grains. Tokaji et al.[34,75–77] defined crack initiation as the formation of a 10–μm–deep crack. Gavenda et al.[35] reported that in room–temperature air, 10–μm–deep cracks form early during fatigue life, i.e., <10% of fatigue life. Suh et al.[78,79] reported that a crack is said to have initiated when any cracklike mark grows across a grain boundary, or when the separation of grain boundaries becomes clear. Based on these results, it is reasonable to assume the initial depth of MSCs to be ≈10 μm.

5.4.1 Transition from Microstructurally Small to Mechanically Small Crack

Various criteria may be used to define the crack length for transition from MSC to mechanically small crack; they may be related to the plastic zone size, crack–length–vs.–fatigue–life (a–N) curve, Weibull distribution of the cumulative probability of fracture, stress–range–vs.–crack–length curve, or grain size. The results indicate that the crack length for transition from MSC to mechanically small crack depends on applied stress and microstructure of the material.

Plastic Zone: de los Rios et al.,[80,81] and Lankford[82–84] defined the transition from small to large cracks as the crack length at which the size of the linear elastic fracture mechanics plastic zone exceeds a grain diameter.

Crack–Length–vs.–Fatigue–Life Curve: Obrtlik et al.[36] divided the fatigue–crack–length–vs.–fatigue–life (a–vs.–N) curves into two regimes: MSCs, in which the dependence of crack length on fatigue life can be represented by a straight line; and mechanically small cracks, in which fatigue crack growth is represented by an exponential function fit of the experimental data.

Weibull Distribution of the Cumulative Probability of Fracture: Suh et al.[78,79] used the knee in the Weibull distribution of the cumulative probability of fracture to define the transition from shear crack growth to tensile crack growth. The knee occurred in the range of 3–5 grain diameters.

Stress–Range–vs.–Crack–Length Curve: Kitagawa and Takahashi[85] and Taylor and Knott[86] used the stress–range–vs.–crack–length curve to discriminate a MSC from a mechanically small crack. For crack lengths >500 μm, plots of the threshold stress range for fatigue crack growth ($\Delta\sigma_{th}$) vs. crack length yield a straight line, i.e., the threshold stress intensity factor (ΔK_{th}) is constant. For crack lengths <500 μm, $\Delta\sigma_{th}$ deviates from the linear relationship and approaches a constant value as the crack length becomes smaller. The constant value of $\Delta\sigma_{th}$ is approximately equal to the fatigue limit of a smooth specimen of the material. The crack length at which the $\Delta\sigma_{th}$–vs.–crack–length curve changes from a linear relationship to a constant value is used to define the transition from MSC to mechanically small cracks.

Grain Size: Tokaji et al.[34,75,76] estimated the transition crack length to be approximately eight times the microstructural unit size. Ravichandran[87] reported that large fluctuations in crack shape or aspect ratio occur at crack lengths of approximately a few grain diameters (typically five or fewer grain diameters). Hussain et al.[74] observed that fatigue CGRs decreased systematically at microstructural heterogeneities up to a length of three or four grain diameters. Dowling[88] reported that the J-integral correlation is not valid for surface crack lengths <10 crystallographic grain diameters.

The above studies indicate that the crack length for transition from MSC to mechanically small crack is a function of applied stress and microstucture of the material; actual values may range from 150 to 250 μm. A constant value of ≈200 μm was assumed for convenience, for both carbon and low-alloy steels; it is the initial size for mechanically small cracks.

5.4.2 Fatigue Crack Growth Rates

Air Environment

The growth rates da/dN (mm/cycle) of MSCs, i.e., from 10 to 200 μm, in air can be represented by the Hobson relationship[33,89-91]

$$da/dN = A_1 (\Delta\sigma)^{n_1} (d - a), \quad (23)$$

where a is the length (mm) of the predominant crack, $\Delta\sigma$ is the stress range (MPa), constant A_1 and exponent n_1 are determined from existing fatigue S–N data, and d is the material constant related to grain size. The values of A_1 and n_1 for carbon and low-alloy steels at room temperature and reactor operating temperatures are given in Table 3. A value of 0.3 mm was used for the material constant d. Also, because growth rates increase significantly with decreasing crack length, a constant growth rate was assumed for crack lengths smaller than 0.075 mm. The applied stress range $\Delta\sigma$ is determined from Ramberg–Osgood relationships given by Eqs. B1–B5 of Appendix B; it represents the value at fatigue half-life.

Table 3. Values of the constants A_1 and n_1 in Equation 23

Steel Type	Temperature	A_1	n_1
Carbon	Room	3.33×10^{-41}	13.13
	Operating	9.54×10^{-34}	10.03
Low-Alloy	Room	1.45×10^{-36}	11.10
	Operating	1.07×10^{-43}	13.43

The growth rates of mechanically small cracks in air are estimated from Eq. B8 of Appendix B. A factor of 1.22 enhancement in growth rates was used at reactor operating temperatures.

LWR Environment

A model based on oxide film rupture and anodic dissolution (or slip dissolution/oxidation model) was proposed by Ford et al.,[58] to incorporate the effects of LWR environments on fatigue lives of CSs and LASs. The model considers that a thermodynamically stable protective oxide film forms on the surface to ensure that the crack will propagate with a high aspect ratio without degrading into a blunt pit, and that a strain increment is required to rupture the oxide

film, thereby exposing the underlying matrix to the environment. Once the passive oxide film is ruptured, crack extension is controlled by dissolution of freshly exposed surfaces and by oxidation characteristics. Ford and Andresen[92] proposed that the average crack growth rate da/dt (cm/s) is related to the crack tip strain rate $\dot{\varepsilon}_{ct}$ (s^{-1}) by the relationship

$$da/dt = A_2(\dot{\varepsilon}_{ct})^{n_2}, \tag{24}$$

where the constant A_2 and exponent n_2 depend on the material and environmental conditions at the crack tip. A lower limit of crack propagation rate is associated with blunting when the crack tip cannot keep up with the general corrosion rate of the crack sides or when a critical level of sulfide ions cannot be maintained at the crack tip. The crack propagation rate at which this transition occurs may depend on the DO level, flow rate, etc. Based on these factors, the maximum and minimum environmentally assisted crack propagation rates have been defined by Ford et al.,[58] Ford and Andresen,[92] and Ford.[93] For crack–tip sulfide ion concentrations above the critical level, CGR is expressed as

$$da/dt = 2.25 \times 10^{-4}(\dot{\varepsilon}_{ct})^{0.35}; \tag{25}$$

for crack–tip sulfide ion concentrations below the critical level, it is expressed as

$$da/dt = 1 \times 10^{-2}(\dot{\varepsilon}_{ct})^{1.0}. \tag{26}$$

However, the growth rates predicted by Eqs. 25 and 26 are somewhat higher than those observed experimentally.[35] To be consistent with the experimental data, the constants in Eqs. 25 and 26 were decreased by factors of 3.2 and 2.5, respectively. Assuming that $\dot{\varepsilon}_{ct}$ is approximately the same as the applied strain rate $\dot{\varepsilon}_{app}$, and crack advance due to mechanical fatigue is insignificant during the initial stages of fatigue damage, crack advance per cycle from Eq. 25 for significant environmental effects is given by

$$da/dN = 7.03 \times 10^{-5}(\Delta\varepsilon - \varepsilon_f)(\dot{\varepsilon}_{app})^{-0.65}, \tag{27}$$

and from Eq. 26, for moderate environmental effects, is given by

$$da/dN = 4.00 \times 10^{-3}(\Delta\varepsilon - \varepsilon_f), \tag{28}$$

where $\dot{\varepsilon}_{app}$ is the applied strain rate (s^{-1}) and ε_f is the threshold strain range needed to rupture the oxide film; ε_f was assumed to be 0.0023 and 0.0029, respectively, for CSs and LASs. For strain rates $\geq\approx$0.3%/s, da/dN is lower from Eq. 27 than from Eq. 28. Also, existing fatigue S–N data indicate that strain rate effects on life saturate at ≈0.001%/s.[12] Therefore, Eq. 27 can be applied at rates between 0.003 and 0.00001 s^{-1}; $\dot{\varepsilon}_{app}$ is assumed to be 0.003 s^{-1} for higher values, and 0.00001 s^{-1} for lower values. Equations 27 and 28 assume that the stress–free state for the surface oxide film is at peak compressive stress.

Studies on crack initiation and crack growth in smooth fatigue specimens indicate that the reference fatigue CGR curves (Fig. B1 in Appendix B) for carbon and low–alloy steels in LWR environments are somewhat higher than those determined experimentally from the growth of mechanically small cracks in LWR environments.[35] Furthermore, when reference CGR curves and fracture mechanics analyses are used to examine the fatigue S-N behavior of these steels in LWR environments, the results are conservative. Therefore, the reference

fatigue CGR curves were modified to estimate the growth rates of mechanically small cracks; the modified curves are shown in Fig. 19. The threshold values of ΔK (MPa·m$^{1/2}$) are given by

$$\Delta K_b = 10.11\ \theta^{0.326}, \tag{29}$$

and

$$\Delta K_c = 32.03\ \theta^{0.326}, \tag{30}$$

where rise time θ is in seconds.

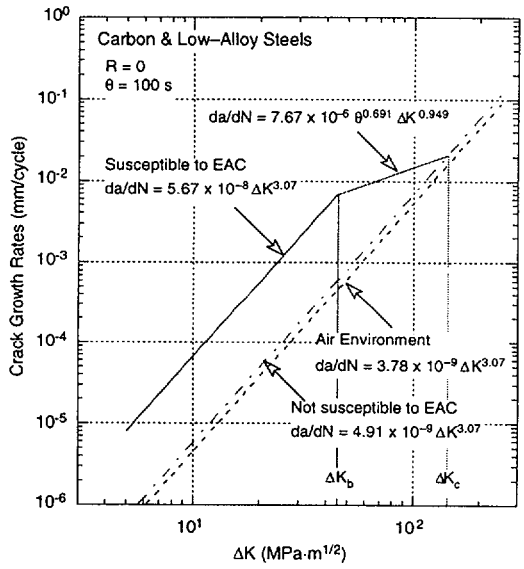

Figure 19.
Modified reference fatigue crack growth rate curves for carbon and low–alloy steels for LWR applications

Environmental effects on fatigue life are moderate when any one of the threshold environmental conditions is not satisfied, e.g., temperature <150°C, DO <0.05 ppm, strain rate >1%/s, or strain range is below the critical value. For moderate environmental effects, the growth rates of mechanically small cracks are represented by the curves for materials not susceptible to environmentally assisted cracking (EAC), and those of MSCs, by either Eq. 28 or 23, whichever yields the higher value. For example, at high strain ranges, growth rates determined from Eq. 23 can be higher than those determined from Eq. 28, i.e., mechanical factors control crack growth and environmental effects are insignificant.

Environmental effects on fatigue life are significant when all of the threshold conditions are satisfied, e.g., temperature ≥150°C, DO ≥0.05 ppm, strain rate <1%/s, and strain range is above the critical value. A minimum threshold S content of 0.005 wt.% was also considered, i.e., S content must also be >0.005 wt.% for significant environmental effects on fatigue life. When all five threshold conditions are satisfied, the growth rates of mechanically small cracks are represented by the curve for materials susceptible to EAC for ΔK values below ΔK_b, by the curve for materials not susceptible to EAC at ΔK values above ΔK_c, and by the transition curve for in–between values of ΔK. The growth rates of MSCs are represented by either Eq. 27 or 23, whichever yields the higher value.

5.4.3 Estimates of Fatigue Life

The existing fatigue S–N data for carbon and low–alloy steels in air and LWR environments were examined with the present model, in which fatigue life consists of the growth of MSCs and mechanically small cracks. The former may be defined as the initiation stage and represents the growth of MSCs from 10 to 200 μm. The growth of mechanically small cracks may be defined as the propagation stage and represents the growth of fatigue cracks from 200 to 3000 μm. During the initiation stage, the growth of MSCs is expressed by a modified Hobson relationship in air (Eq. 23) and by the slip dissolution/oxidation process in water (Eqs. 27 or 28). During the propagation stage, the growth of mechanically small cracks is characterized in terms of the J–integral range ΔJ and CGR data in air and LWR environments (Fig. 19). The correlations for calculating the stress range, stress intensity range ΔK, J–integral range ΔJ, and the CGRs for long cracks in air are given in Appendix B. For the cylindrical fatigue specimens, the stress intensity ranges ΔK were determined from the values of the J–integral range ΔJ. Although ΔJ is often computed only for that portion of the loading cycle during which the crack is open, in the present study, the entire hysteresis loop was used when we estimated ΔJ.[88] The stress intensities associated with conventional cylindrical fatigue specimens were modified according to the correlations developed by O'Donnell and O'Donnell.[94] Typical CGRs and crack growth behavior during fatigue crack initiation in air and simulated PWR and BWR water environments are shown in Figs. 20 and 21.

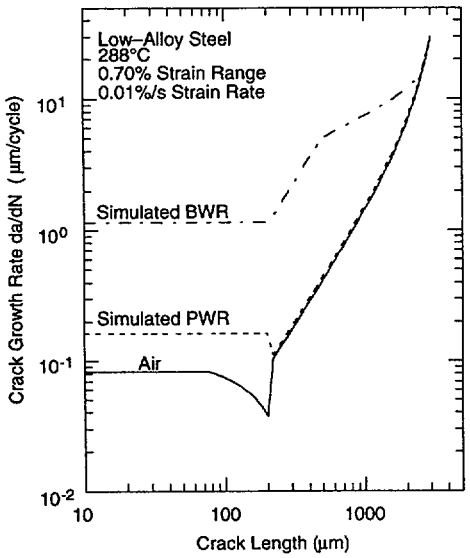

Figure 20.
Crack growth rates during fatigue crack initiation in low–alloy steels in air and simulated PWR and BWR environments

Experimental values of fatigue life and those predicted from the present model in air and low– and high–DO water are plotted in Fig. 22. The predicted fatigue lives in air show excellent agreement with the experimental data; the predicted values in LWR environments, particularly in high–DO water, are slightly lower than the experimental values. The differences in predicted and experimental fatigue lives in LWR environments are most likely due to crack closure effects that are expected to be significant at low strain amplitudes. The fatigue S–N curves developed from the present model and those obtained from the statistical models in air and in PWR and BWR environments are shown in Figs. 23 and 24.

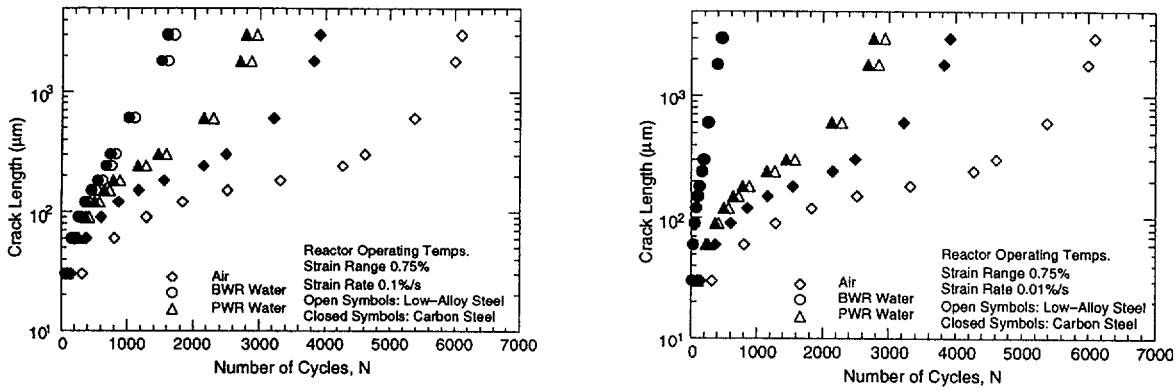

(a) (b)

Figure 21. Crack growth in carbon and low–alloy steels as a function of fatigue cycles at (a) 0.1 and (b) 0.01%/s strain rate

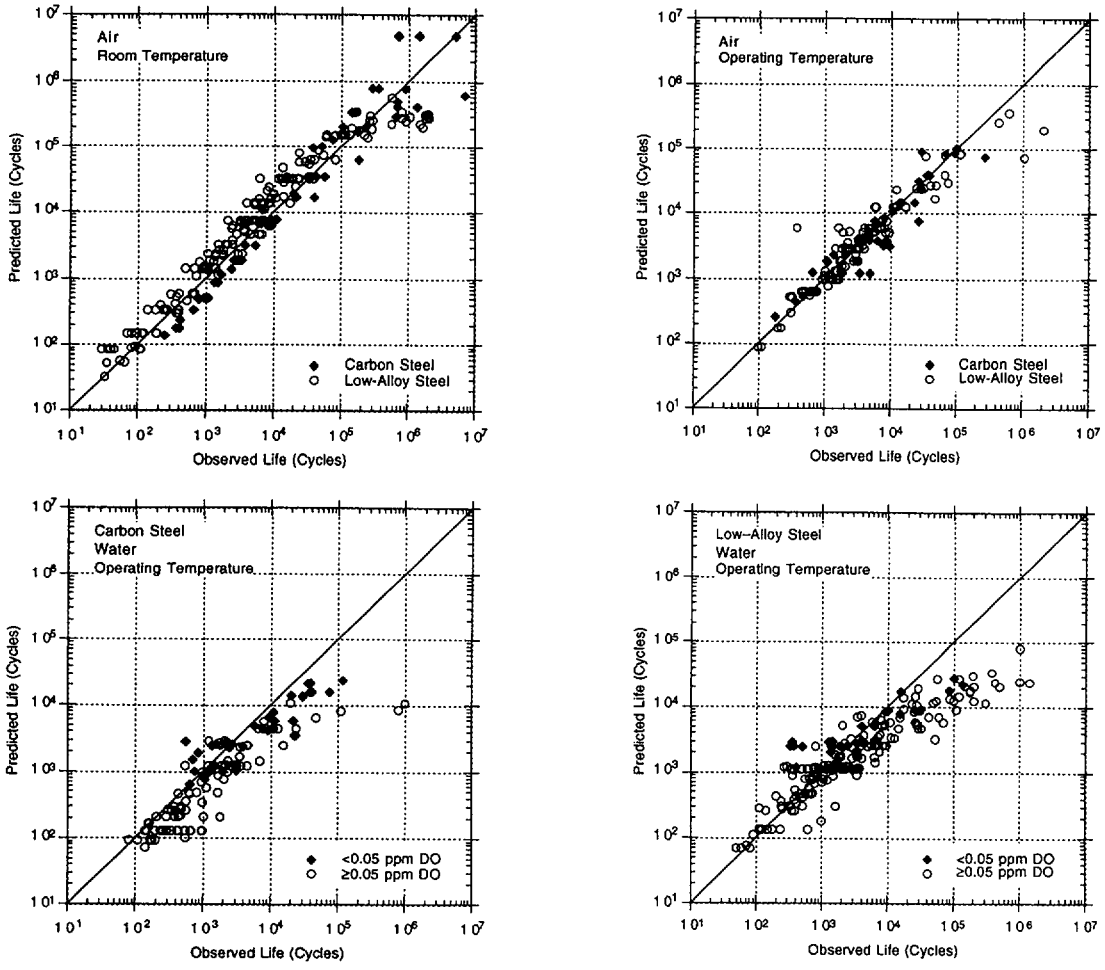

Fig. 22. Experimentally observed values of fatigue life of carbon and low–alloy steels vs. those predicted by the present model in air and water environments

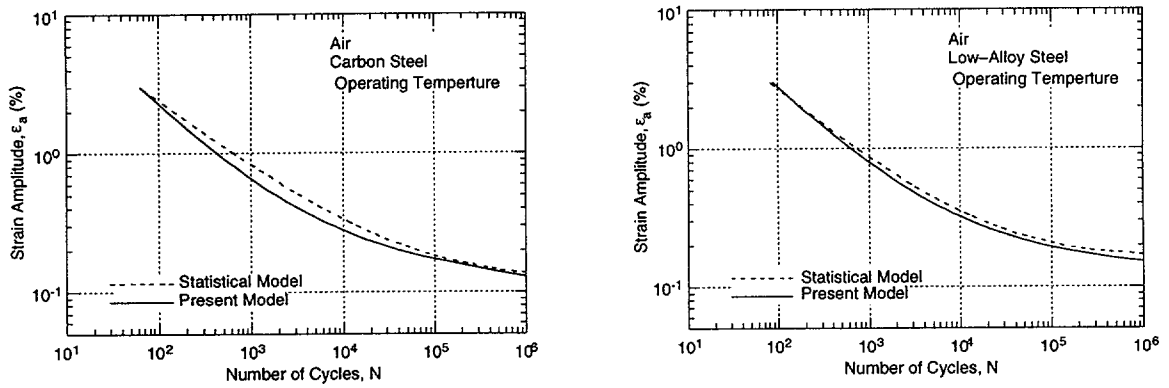

Fig. 23. Fatigue strain–vs.–life curves developed from the present and statistical models for (a) carbon and (b) low–alloy steels in air

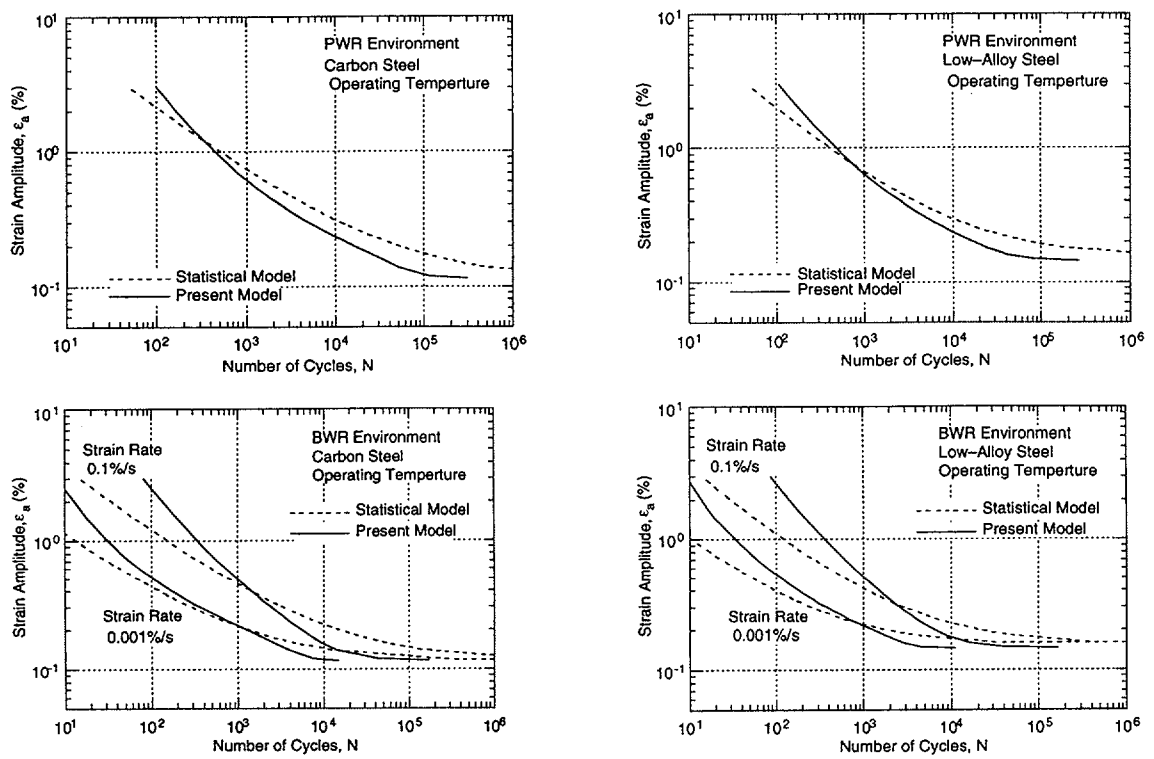

Fig. 24. Fatigue strain–vs.–life curves developed from the present and statistical models for carbon and low–alloy steels in PWR and BWR environments

6 Conservatism in Design Fatigue Curves

A PVRC working group has been compiling and evaluating fatigue S–N data related to the effects of LWR coolant environments on the fatigue lives of pressure boundary materials.[95] One of the tasks in the PVRC activity consisted of defining a set of values for material, loading, and environmental variables that lead to moderate or acceptable effects of environment on fatigue life. A factor of 4 on the ASME mean life was chosen as a working definition of "moderate" or "acceptable" effects of environment, i.e., up to a factor of 4 decrease in fatigue life due to environment is considered acceptable and does not require further fatigue evaluation. The basis for this criterion is that a factor of up to 4 on life constitutes normal data scatter and/or there is at least that much conservatism in the fatigue design curves. The concept of "acceptable" environmental effects has been incorporated in the F_{en} approach for including environmental effects on fatigue life through the."effective" fatigue life correction factor, $F_{en,eff} = F_{en}/Z$, where as noted in Section 5.3, Z is a factor that represents the perceived conservatism in the ASME Code design curves.[72]

The conservatism in the ASME Code fatigue evaluations may arise from the fatigue evaluation procedures and the Code design curves. The overall conservatism in ASME Code fatigue evaluation procedures has been demonstrated in fatigue tests on piping welds and components.[96] In air, the margins on the number of cycles to failure for CS elbows and tees were 118–2500 and 123–1700, respectively. The margins for girth butt welds were significantly lower at 14–128. In these tests, fatigue life was expressed as the number of cycles for the crack to penetrate through the wall, which ranged in thickness from 6 to 18 mm (0.237 to 0.719 in.). The fatigue design curves represent the number of cycles to form a 3-mm-deep crack. Consequently, depending on wall thickness, the actual margins to failure may be lower by a factor of >2.

Deardorff and Smith[97] have discussed the types and extent of conservatisms present in the ASME Section III fatigue evaluation procedures and the effects of LWR environments on fatigue margins. The sources of conservatism include design transients considerably more severe than those experienced in service, grouping of transients, and simplified elastic–plastic analysis. Environmental effects on two components, the BWR feedwater nozzle/safe end and PWR steam generator feedwater nozzle/safe end, which are known to be affected by severe thermal transients, were also investigated in the study. When environmental effects on fatigue life were not considered, they estimated that the ratio of the CUFs for the PWR and BWR nozzles computed with the mean experimental curve for test specimen data to CUFs computed with the Code fatigue design curve were ≈60 and 90, respectively. They estimated the reductions in these margins due to environmental effects to be factors of 5.2 and 4.6 for PWR and BWR nozzles, respectively. Deardorff and Smith argue that after accounting for environmental effects there is a factor of 12 and 20 on life, respectively, for PWR and BWR nozzles, to account for uncertainties due to material variability, surface finish, size, mean stress, and loading history.

As noted previously, to account for the various uncertainties, the mean experimental curve for test specimen data must be adjusted by a factor of 20 on life as well as by a factor of 2 on stress (or strain). Deardorff and Smith[97] have ignored the contributions of the latter to fatigue life. In the high-cycle regime, the factor of 2 on stress would also lead to further decrease in life or fatigue usage factor; it is needed to account for material variability, mean

stress effects, or loading history. The mean experimental curve for test specimen data used by Deardorff and Smith does not include these effects. As discussed below, factors of 2.5 on life and 1.7 on strain provide a 90% confidence for the variations in fatigue life associated with compositional and metallurgical differences, material processing, and experimental scatter.

Much of the margin arises from the calculation of the stresses with the conventional Code procedures which, as discussed by Deardorff and Smith,[97] are quite conservative. Fatigue tests conducted on vessels at Southwest Research Institute for the PVRC[98] show that ≈5-mm-deep cracks can form in carbon and low-alloy steels very close to the values predicted by the ASME Code design curve (Fig. 25). The tests were performed on 0.914-m (36 in.)-diameter vessels with 19-mm (0.75 in.) walls in room-temperature water. These results demonstrate clearly that the Code fatigue design curves do not ensure large margins of safety.

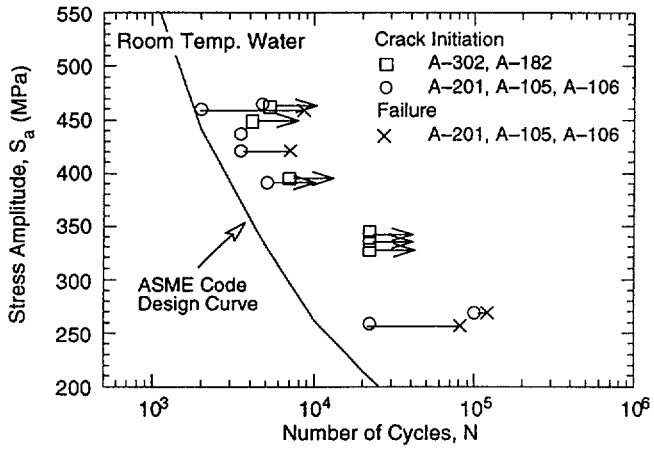

Figure 25.
Fatigue data for carbon and low-alloy steel vessels tested in room-temperature water

The ASME Code design fatigue curves were obtained by first adjusting the best-fit S-N curve for mean stress effects and then lowering the adjusted curve by a factor of 2 on strain and 20 on cycles to account for the differences and uncertainties in relating the fatigue lives of laboratory test specimens to those of actual reactor components. These factors were intended to cover several variables that can influence fatigue life. The actual contribution of these variables is not well documented. Although the factors of 2 and 20 were intended to be somewhat conservative, they should not be considered safety margins. The variables that can affect fatigue life in air and LWR environments can be broadly classified into three groups:

(a) Material
  (i) Composition: S content
  (ii) Metallurgy: grain size, inclusions, orientation within a forging or plate
  (iii) Processing: cold work, heat treatment
  (iv) Size and geometry
  (v) Surface finish: fabrication surface condition
  (vi) Surface preparation: surface work hardening

(b) Loading
  (i) Strain rate: rise time
  (ii) History: linear damage summation or Miner's rule
  (iii) Mean stress
  (iv) Biaxial effects: constraints

(c) Environment
  (i) Water chemistry: DO, lithium hydroxide, boric acid concentrations
  (ii) Temperature
  (iii) Flow rate

The existing fatigue S–N data base covers an adequate range of material parameters (i)–(iii), loading parameter (i), and environment parameters (i) and (ii); therefore, the variability and uncertainty in fatigue life due to these parameters have been incorporated into the model. The results of a rigorous statistical analysis of the fatigue S–N data[27] indicate that relative to the mean curve, the curve that represents a 5% probability of fatigue cracking is a factor of ≈2.5 lower in life and a factor of 1.4–1.7 lower in strain. Therefore, factors of 2.5 on life and 1.7 on strain provide a 90% confidence for the variations in fatigue life associated with compositional and metallurgical differences, material processing, and experimental scatter. The factor of 1.7 on strain has been estimated from the standard deviation on cycles and, therefore may be a conservative value.

Biaxial effects are covered by design procedures and need not be considered in the design fatigue curves. The existing data are conservative with respect to the effects of surface preparation because the fatigue S–N data are obtained for specimens that are free of surface cold work; specimens with surface cold work typically give longer fatigue lives. Fabrication procedures for fatigue test specimens generally follow ASTM guidelines, which require that the final polishing of the specimens avoid surface work hardening. Insufficient data are available to evaluate the contributions of flow rate on fatigue life; most of the tests in water have been conducted at relatively low flow rates. As discussed in Section 3.1, recent results indicate that under the environmental conditions typical of operating BWRs, environmental effects on the fatigue life of carbon and low-alloy steels is a factor of ≈2 lower at high flow rates than those at semistagnant conditions or very low flow rates.

Because the effects of the environment can be included in mean S–N curves for test specimens, only the contributions of size, geometry, surface finish, and loading history (Miner's rule) need to be considered in developing the design fatigue curves that are applicable to components. The effect of specimen size on the fatigue life of CSs and LASs has been investigated for smooth specimens of various diameters in the range of 2–60 mm.[99–102] No intrinsic size effect has been observed for smooth specimens tested in axial loading or plain bending. However, a size effect does occur in specimens tested in rotating bending; the fatigue endurance limit decreases by ≈25% by increasing the specimen size from 2 to 16 mm but does not decrease further with larger sizes.[102] In addition, some effect of size and geometry has been observed on small-scale vessel tests conducted at the Ecole Polytechnique in conjunction with the large-size pressure vessel tests carried out by the Southwest Research Institute.[98] The tests at the Ecole Polytechnique were conducted in room-temperature water on ≈305-mm-inner-diameter, 19-mm-thick shells with nozzles made of machined bar stock. The results indicate that the number of cycles to form a 3-mm-deep crack in a 19-mm-thick shell may be 30–50% lower than those in a small test specimen.[27] Thus, a factor of ≈1.4 on cycles and a factor of ≈1.25 on strain can be used to account for size and geometry.

Fatigue life is sensitive to surface finish; cracks can initiate at surface irregularities that are normal to the stress axis. The height, spacing, shape, and distribution of surface irregularities are important for crack initiation. The most common measure of roughness is average surface roughness R_a, which is a measure of the height of the irregularities.

Investigations of the effects of surface roughness on the low-cycle fatigue of Type 304 SS in air at 593°C indicate that fatigue life decreases as surface roughness increases.[103,104] The effect of roughness on crack initiation $N_i(R)$ is given by

$$N_i(R_q) = 1012\ R_q^{-0.21}, \tag{31}$$

where the RMS value of surface roughness R_q is in micrometers. Typical values of R_a for surfaces finished by various metalworking processes in the automotive industry[105] indicate that an R_a of 3 μm (or an R_q of 4 μm) represents the maximum surface roughness for drawing/extrusion, grinding, honing, and polishing processes and a mean value for the roughness range for milling or turning processes. For carbon or low-alloy steel, an R_q of 4 μm in Eq. 31 (R_q of a smooth polished specimen is ≈0.0075 μm) would decrease fatigue life by a factor of ≈3.[103] No information is available on the effect of surface finish on fatigue limit of carbon and low-alloy steels. A factor of 3 decrease in life corresponds to a factor of ≈1.3 on strain.* A study of the effect of surface finish on fatigue life of CS in room-temperature air showed a factor of 2 decrease in life when R_a is increased from 0.3 to 5.3 μm.[106] These results are consistent with Eq. 31. Fatigue test data on rectangular bars of austenitic SSs under compressive load with differing surface finish indicate a factor of ≈1.6 decrease in stress (or strain) in the high-cycle fatigue regime (i.e., $>10^5$ cycles).[68] In the same study, the effect of grinding on the fatigue limit of welds was very large, e.g., a factor of 3–4 decrease in fatigue limit. Thus, a factor of 2–3 on cycles and 1.6 on strain may be used to account for the effects of surface finish.

The effects of load history during variable amplitude fatigue of smooth specimens is well known.[107–110] The presence of a few cycles at high strain amplitude in a load history causes the fatigue life at a smaller strain amplitude to be significantly lower than that at constant amplitude loading. Furthermore, fatigue damage and crack growth in smooth specimens occur at strain levels below the fatigue limit of the material. The results also indicate that the fatigue limit of medium CSs is lowered even after low-stress high-cycle fatigue; the higher the stress, the greater the decrease in fatigue threshold.[111] In general, the mean fatigue S–N curves are lowered to account for damaging cycles that occur below the constant-amplitude fatigue limit of the material.[112,113] A factor of 1.5–2.5 on cycles and 1.3–1.6 on strain may be used to incorporate the effects of load histories on fatigue life.

The subfactors that may be used to account for the effects of various material, loading, and environmental variables on fatigue life are summarized in Table 4. A factor of at least 10 on cycles is needed to account for the differences and uncertainties in relating the fatigue lives of laboratory test specimens to those of actual reactor components. The factors on strain primarily account for the variation in threshold strain (i.e., fatigue limit of the material) caused by material variability, component size and surface finish, and load history. Because the effects of these parameters are associated with the growth of short cracks (<100 μm), the adjustments on strain to account for the effects of material variability, component size, surface finish, and loading history, are typically not cumulative but rather are controlled by the

*The factor applied on strain (K_S) is obtained from the factor applied on cycles (K_N) by using the relationship $K_S = (K_N)^{0.2326}$.

Table 4. Factors on cycles and on strain to be applied to mean S–N curve

Parameter	Factor on Life	Factor on Strain
Material variability & experimental scatter	2.5	1.4–1.7
Size effect	1.4	1.25
Surface finish	2.0–3.0	1.6
Loading history	1.5–2.5	1.3–1.6
Total adjustment:	10.0–26.0	1.6–1.7

parameter that has the largest effect on life. Thus, a factor of at least 1.6 on strain is needed to account for the differences and uncertainties in relating the fatigue lives of laboratory test specimens to those of actual reactor components. These results suggest that the current ASME Code requirements of a factor of 2 on stress and 20 on cycle to account for differences and uncertainties in fatigue life that are associated with material and loading conditions are quite reasonable.

7 Summary

The work performed at Argonne National Laboratory on fatigue of carbon and low–alloy steels and austenitic SSs in LWR environments is summarized. The existing fatigue S–N data have been evaluated to establish the effects of various material and loading variables such as steel type, strain range, strain rate, temperature, S content in carbon and low–alloy steels, orientation, and DO level in water on the fatigue life of these steels. Statistical models are presented for estimating the fatigue S–N curves as a function of material, loading, and environmental variables. Case studies of fatigue failures in nuclear power plants are presented and the contribution of environmental effects on crack initiation is discussed.

The influence of reactor environments on the mechanism of fatigue crack initiation is discussed. Decreased fatigue lives of carbon and low–alloy steels in high–DO water are caused primarily by the effects of environment on the growth of small cracks <100 μm deep. In LWR environments, the growth of these small fatigue cracks in carbon and low–alloy steels occurs by a slip oxidation/dissolution process. The reduction in fatigue life of austenitic SSs in LWR environments is most likely caused by other mechanisms, such as hydrogen–enhanced crack growth.

A fracture mechanics approach is used to predict the fatigue lives of carbon and low-alloy steels in air and LWR environments. Fatigue life is considered to be composed of the growth of microstructurally and mechanically small cracks. The growth of the former cracks is very sensitive to microstructure and is characterized by decelerating crack growth, that of the latter, which can be predicted by fracture mechanics methodology, is characterized by accelerating crack growth, and has been characterized in terms of the J–integral range ΔJ and CGR data in air and LWR environments. Fatigue lives estimated from the present model show good agreement with the experimental data for carbon and low–alloy steels in air and LWR environments. At low strain amplitudes, i.e., fatigue lives of $>10^4$ cycles, the predicted lives in water are slightly lower than those observed experimentally, most likely because of the effects of crack closure.

The current two methods for incorporating the effects of LWR coolant environments into the ASME Code fatigue evaluations, i.e., the design fatigue curve method and the fatigue life correction factor method, are presented. Both methods are based on statistical models for estimating fatigue lives of carbon and low–alloy steels and austenitic SSs in LWR environments. Although estimates of fatigue lives based on the two methods may differ because of differences between the ASME mean curves used to develop the current design curves and the best–fit curves to the existing data used to develop the environmentally adjusted curves, either of these methods provides an acceptable approach to account for environmental effects.

The environmentally adjusted design fatigue curves provide allowable cycles for fatigue crack initiation in LWR coolant environments. The new design curves maintain the margins of 2 on stress and 20 on life.

In the F_{en} method, environmental effects on life are estimated from the statistical models but the correction is applied to fatigue lives estimated from the current Code design curves. Therefore, estimates of fatigue lives that are based on the two methods may differ because of

differences in the ASME mean curve and the best-fit curve to existing fatigue data. The current Code design curve for CSs is comparable to the statistical-model curve for LASs, whereas it is somewhat conservative at stress levels <500 MPa when compared with the statistical-model curve for CSs. Consequently, usage factors based on the F_{en} method would be comparable to those based on the environmentally adjusted design fatigue curves for LASs and would be somewhat higher for CSs.

For austenitic SSs, the current Code design fatigue curve is nonconservative when compared with the statistical-model curve, i.e., it predicts longer fatigue lives than the best-fit curve to the existing S-N data. Therefore, usage factors that are based on the F_{en} method would be lower than those determined from the environmentally corrected design fatigue curves. The environmentally adjusted design curves account for the effects of both LWR environment and the difference in the mean fatigue curve used to develop the current Code design curve and the best-fit curve of available experimental data.

References

1. C. E. Jaske and W. J. O'Donnell, *Fatigue Design Criteria for Pressure Vessel Alloys*, Trans. ASME J. Pressure Vessel Technol. **99**, 584–592 (1977).

2. O. K. Chopra, *Effects of LWR Coolant Environments on Fatigue Design Curves of Austenitic Stainless Steels*, NUREG/CR–5704, ANL–98/31 (1999).

3. S. Ranganath, J. N. Kass, and J. D. Heald, *Fatigue Behavior of Carbon Steel Components in High–Temperature Water Environments*, BWR Environmental Cracking Margins for Carbon Steel Piping, EPRI NP–2406, Electric Power Research Institute, Palo Alto, CA, Appendix 3 (1982).

4. M. Higuchi and K. Iida, *Fatigue Strength Correction Factors for Carbon and Low–Alloy Steels in Oxygen–Containing High–Temperature Water*, Nucl. Eng. Des. **129**, 293–306 (1991).

5. N. Nagata, S. Sato, and Y. Katada, *Low–Cycle Fatigue Behavior of Pressure Vessel Steels in High–Temperature Pressurized Water*, ISIJ Intl. **31** (1), 106–114 (1991).

6. W. A. Van Der Sluys, *Evaluation of the Available Data on the Effect of the Environment on the Low–Cycle Fatigue Properties in Light Water Reactor Environments*, in Proc. 6th Intl. Symp. on Environmental Degradation of Materials in Nuclear Power Systems – Water Reactors, R. E. Gold and E. P. Simonen, eds., The Metallurgical Society, Warrendale, PA, pp. 1–4 (1993).

7. H. Kanasaki, M. Hayashi, K. Iida, and Y. Asada, *Effects of Temperature Change on Fatigue Life of Carbon Steel in High–Temperature Water*, in Fatigue and Crack Growth: Environmental Effects, Modeling Studies, and Design Considerations, PVP Vol. 306, S. Yukawa, ed., American Society of Mechanical Engineers, New York, pp. 117–122 (1995).

8. G. Nakao, H. Kanasaki, M. Higuchi, K. Iida, and Y. Asada, *Effects of Temperature and Dissolved Oxygen Content on Fatigue Life of Carbon and Low–Alloy Steels in LWR Water Environment*, in Fatigue and Crack Growth: Environmental Effects, Modeling Studies, and Design Considerations, PVP Vol. 306, S. Yukawa, ed., American Society of Mechanical Engineers, New York, pp. 123–128 (1995).

9. M. Higuchi, K. Iida, and Y. Asada, *Effects of Strain Rate Change on Fatigue Life of Carbon Steel in High–Temperature Water*, in Effects of the Environment on the Initiation of Crack Growth, ASTM STP 1298, W. A. Van Der Sluys, R. S. Piascik, and R. Zawierucha, eds., American Society for Testing and Materials, Philadelphia, pp. 216–231 (1997).

10. O. K. Chopra and W. J. Shack, *Evaluation of Effects of LWR Coolant Environments on Fatigue Life of Carbon and Low–Alloy Steels*, in Effects of the Environment on the Initiation of Crack Growth, ASTM STP 1298, W. A. Van Der Sluys, R. S. Piascik, and R. Zawierucha, eds., American Society for Testing and Materials, Philadelphia, pp. 247–266 (1997).

11. O. K. Chopra and W. J. Shack, *Low-Cycle Fatigue of Piping and Pressure Vessel Steels in LWR Environments*, Nucl. Eng. Des. **184**, 49–76 (1998).

12. O. K. Chopra and W. J. Shack, *Effects of LWR Coolant Environments on Fatigue Design Curves of Carbon and Low-Alloy Steels*, NUREG/CR-6583, ANL-97/18 (March 1998).

13. O. K. Chopra and W. J. Shack, *Fatigue Crack Initiation in Carbon and Low-Alloy Steels in Light Water Reactor Environments – Mechanism and Prediction*, in Fatigue, Environmental Factors, and New Materials, PVP Vol. 374, H. S. Mehta, R. W. Swindeman, J. A. Todd, S. Yukawa, M. Zako, W. H. Bamford, M. Higuchi, E. Jones, H. Nickel, and S. Rahman, eds., American Society of Mechanical Engineers, New York, pp. 155–168 (1998).

14. O. K. Chopra and W. J. Shack, *Overview of Fatigue Crack Initiation in Carbon and Low-Alloy Steels in Light Water Reactor Environments*, J. Pressure Vessel Technol. **121**, 49–60 (1999).

15. O. K. Chopra and J. Muscara, *Effects of Light Water Reactor Coolant Environments on Fatigue Crack Initiation in Piping and Pressure Vessel Steels*, in Proc. 8th Intl. Conference on Nuclear Engineering, 2.08 LWR Materials Issue, Paper 8300, American Society of Mechanical Engineers, New York (2000).

16. M. Fujiwara, T. Endo, and H. Kanasaki, *Strain Rate Effects on the Low-Cycle Fatigue Strength of 304 Stainless Steel in High-Temperature Water Environment; Fatigue Life: Analysis and Prediction*, in Proc. Intl. Conf. and Exposition on Fatigue, Corrosion Cracking, Fracture Mechanics, and Failure Analysis, ASM, Metals Park, OH, pp. 309–313 (1986).

17. H. Mimaki, H. Kanasaki, I. Suzuki, M. Koyama, M. Akiyama, T. Okubo, and Y. Mishima, *Material Aging Research Program for PWR Plants*, in Aging Management Through Maintenance Management, PVP Vol. 332, I. T. Kisisel, ed., American Society of Mechanical Engineers, New York, pp. 97–105 (1996).

18. M. Higuchi and K. Iida, *Reduction in Low-Cycle Fatigue Life of Austenitic Stainless Steels in High-Temperature Water*, in Pressure Vessel and Piping Codes and Standards, PVP Vol. 353, D. P. Jones, B. R. Newton, W. J. O'Donnell, R. Vecchio, G. A. Antaki, D. Bhavani, N. G. Cofie, and G. L. Hollinger, eds., American Society of Mechanical Engineers, New York, pp. 79–86 (1997).

19. H. Kanasaki, R. Umehara, H. Mizuta, and T. Suyama, *Fatigue Lives of Stainless Steels in PWR Primary Water*, Trans. 14th Intl. Conf. on Structural Mechanics in Reactor Technology (SMiRT 14), Lyon, France, pp. 473–483 (1997).

20. H. Kanasaki, R. Umehara, H. Mizuta, and T. Suyama, *Effects of Strain Rate and Temperature Change on the Fatigue Life of Stainless Steel in PWR Primary Water*, Trans. 14th Intl. Conf. on Structural Mechanics in Reactor Technology (SMiRT 14), Lyon, France, pp. 485–493 (1997).

21. M. Hayashi, *Thermal Fatigue Strength of Type 304 Stainless Steel in Simulated BWR Environment*, Nucl. Eng. Des. **184**, 135–144 (1998).

22. M. Hayashi, K. Enomoto, T. Saito, and T. Miyagawa, *Development of Thermal Fatigue Testing with BWR Water Environment and Thermal Fatigue Strength of Austenitic Stainless Steels*, Nucl. Eng. Des. **184**, 113–122 (1998).

23. O. K. Chopra and D. J. Gavenda, *Effects of LWR Coolant Environments on Fatigue Lives of Austenitic Stainless Steels*, in Pressure Vessel and Piping Codes and Standards, PVP Vol. 353, D. P. Jones, B. R. Newton, W. J. O'Donnell, R. Vecchio, G. A. Antaki, D. Bhavani, N. G. Cofie, and G. L. Hollinger, eds., American Society of Mechanical Engineers, New York, pp. 87–97 (1997).

24. O. K. Chopra and D. J. Gavenda, *Effects of LWR Coolant Environments on Fatigue Lives of Austenitic Stainless Steels*, J. Pressure Vessel Technol. **120**, 116–121 (1998).

25. O. K. Chopra and J. L. Smith, *Estimation of Fatigue Strain–Life Curves for Austenitic Stainless Steels in Light Water Reactor Environments*, in Fatigue, Environmental Factors, and New Materials, PVP Vol. 374, H. S. Mehta, R. W. Swindeman, J. A. Todd, S. Yukawa, M. Zako, W. H. Bamford, M. Higuchi, E. Jones, H. Nickel, and S. Rahman, eds., American Society of Mechanical Engineers, New York, pp. 249–259 (1998).

26. S. Majumdar, O. K. Chopra, and W. J. Shack, *Interim Fatigue Design Curves for Carbon, Low–Alloy, and Austenitic Stainless Steels in LWR Environments*, NUREG/CR–5999, ANL–93/3 (1993).

27. J. Keisler, O. K. Chopra, and W. J. Shack, *Fatigue Strain–Life Behavior of Carbon and Low–Alloy Steels, Austenitic Stainless Steels, and Alloy 600 in LWR Environments*, NUREG/CR–6335, ANL–95/15 (1995).

28. J. Keisler, O. K. Chopra, and W. J. Shack, *Fatigue Strain–Life Behavior of Carbon and Low–Alloy Steels, Austenitic Stainless Steels, and Alloy 600 in LWR Environments*, Nucl. Eng. Des. **167**, 129–154 (1996).

29. A. G. Ware, D. K. Morton, and M. E. Nitzel, *Application of NUREG/CR–5999 Interim Design Curves to Selected Nuclear Power Plant Components*, NUREG/CR–6260, INEL–95/0045 (1995).

30. H. S. Mehta and S. R. Gosselin, *An Environmental Factor Approach to Account for Reactor Water Effects in Light Water Reactor Pressure Vessel and Piping Fatigue Evaluations, Fatigue and Fracture Volume 1*, PVP Vol. 323, H. S. Mehta, ed., American Society of Mechanical Engineers, New York, pp. 171–185 (1996).

31. H. S. Mehta and S. R. Gosselin, *Environmental Factor Approach to Account for Water Effects in Pressure Vessel and Piping Fatigue Evaluations*, Nucl. Eng. Des. **181**, 175–197 (1998).

32. M. Higuchi, *Difference ofEnvironment Effects Between Japanese EFD and ANL Approaches*, presented at Working Group Meeting on S–N Data Analysis, the Pressure Vessel Research Council, Orlando, FL (May 1996).

33. K. J Miller, *Initiation and Growth Rates of Short Fatigue Cracks*, Fundamentals of Deformation and Fracture, Eshelby Memorial Symposium, Cambridge University Press, Cambridge, U.K., pp. 477–500 (1985).

34. K. Tokaji, T. Ogawa, and S. Osaka, *The Growth of Microstructurally Small Fatigue Cracks in a Ferrite–Pearlite Steel*, Fatigue Fract. Eng. Mater. Struct. **11**, 311–342 (1988).

35. D. J. Gavenda, P. R. Luebbers, and O. K. Chopra, *Crack Initiation and Crack Growth Behavior of Carbon and Low-Alloy Steels*, Fatigue and Fracture 1, Vol. 350, S. Rahman, K. K. Yoon, S. Bhandari, R. Warke, and J. M. Bloom, eds., American Society of Mechanical Engineers, New York, pp. 243–255 (1997).

36. K. Obrtlik, J. Polák, M. Hájek, and A. Vasek, *Short Fatigue Crack Behaviour in 316L Stainless Steel*, Intl. J. Fatigue **19**, 471–475 (1997).

37. S. G. Sundara Raman, D. Argence, and A. Pineau, *High Temperature Short Fatigue Crack Behaviour in a Stainless Steel*, Fatigue Fract. Eng. Mater. Struct. **20**, 1015–1031 (1997).

38. K. J. Miller, *Damage in Fatigue: A New Outlook*, International Pressure Vessels and Piping Codes and Standards: Volume 1 – Current Applications, PVP Vol. 313–1, K. R. Rao and Y. Asada, eds., American Society of Mechanical Engineers, New York, pp. 191–192 (1995).

39. F. P. Ford, *Overview of Collaborative Research into the Mechanisms of Environmentally Controlled Cracking in the Low Alloy Pressure Vessel Steel/Water System*, Proc. 2nd Int. Atomic Energy Agency Specialists' Meeting on Subcritical Crack Growth, NUREG/CP–0067, MEA–2090, Vol. 2, pp. 3–71 (1986).

40. H. Hänninen, K. Törrönen, and W. H. Cullen, *Comparison of Proposed Cyclic Crack Growth Mechanisms of Low Alloy Steels in LWR Environments*, Proc. 2nd Int. Atomic Energy Agency Specialists' Meeting on Subcritical Crack Growth, NUREG/CP–0067, MEA–2090, Vol. 2, pp. 73–97 (1986).

41. J. L. Smith, and O. K. Chopra, *Crack Initiation in Smooth Fatigue Specimens of Austenitic Stainless Steel in Light Water Reactor Environments*, Operations, Applications, and Components – 1999, PVP Vol. 395, I. T. Kisisel, ed., American Society of Mechanical Engineers, New York, pp. 235–242 (1999).

42. Y. Katada, N. Nagata, and S. Sato, *Effect of Dissolved Oxygen Concentration on Fatigue Crack Growth Behavior of A533 B Steel in High-Temperature Water*, ISIJ Intl. **33** (8), 877–883 (1993).

43. M. Higuchi, *Fatigue Properties of Carbon Steel Weldments in Oxygenated High-Temperature Water – Evaluation of Effects of Tensile Strength and Sulfur Content*, presented at Working Group Meeting on S–N Data Analysis, the Pressure Vessel Research Council, June, Milwaukee (June 1995).

44. A. Hirano, M. Yamamoto, K. Sakaguchi, K. Iida, and T. Shoji, *Effects of Water Flow Rate on Fatigue Life of Carbon Steel in High Temperature Pure Water Environment*, in Assessment Methodologies for Predicting Failure: Service Experience and Environmental Considerations, PVP Vol. 410-2, R. Mohan, ed., American Society of Mechanical Engineers, New York, pp. 13-18 (2000).

45. E. Lenz, N. Wieling, and H. Muenster, *Influence of Variation of Flow Rates and Temperature on the Cyclic Crack Growth Rate under BWR Conditions*, in Environmental Degradation of Materials in Nuclear Power Systems - Water Reactors, The Metallurgical Society, Warrendale, PA (1988).

46. S. Yukawa, *Meeting of the Steering Committee for Cyclic Life and Environmental Effects (CLEE)*, the Pressure Vessel Research Council, Columbus, OH (June 1999).

47. K. Kussmaul, R. Rintamaa, J. Jansky, M. Kemppainen, and K. Törrönen, *On the Mechanism of Environmental Cracking Introduced by Cyclic Thermal Loading*, in IAEA Specialists Meeting Corrosion and Stress Corrosion of Steel Pressure Boundary Components and Steam Turbines, VTT Symp. 43, Espoo, Finland, pp. 195-243 (1983).

48. K. Iida, *A Review of Fatigue Failures in LWR Plants in Japan*, Nucl. Eng. Des. **138**, 297-312 (1992).

49. NRC Bulletin No. 88-11, *Pressurizer Surge Line Thermal Stratification*, U.S. Nuclear Regulatory Commission, Washington, DC (Dec. 20, 1988).

50. NRC IE Bulletin No. 79-13, *Cracking in Feedwater System Piping*, U.S. Nuclear Regulatory Commission, Washington, DC (June 25, 1979).

51. NRC Information Notice 93-20, *Thermal Fatigue Cracking of Feedwater Piping to Steam Generators*, U.S. Nuclear Regulatory Commission, Washington, DC (March 24, 1993).

52. R. B. Dooley, and R. S. Pathania, *Corrosion Fatigue of Water Touched Pressure Retaining Components in Power Plants*, EPRI TR-106696, Electric Power Research Institute, Palo Alto, CA (1997).

53. K. Kussmaul, D. Blind, and J. Jansky, *Formation and Growth of Cracking in Feed Water Pipes and RPV Nozzles*, *Nucl. Eng. Des.* **81**, 105-119 (1984).

54. H. Watanabe, *Boiling Water Reactor Feedwater Nozzle/Sparger, Final Report*, NEDO-21821-A, General Electric Co., San Jose, CA, (1980).

55. B. M. Gordon, D. E. Delwiche, and G. M. Gordon, *Service Experience of BWR Pressure Vessels*, in Performance and Evaluation of Light Water Reactor Pressure Vessels, PVP Vol.-119, American Society of Mechanical Engineers, New York, pp. 9-17 (1987).

56. E. Lenz, B. Stellwag, and N. Wieling, *The Influence of Strain-Induced Corrosion Cracking on the Crack Initiation in Low-Alloy Steels in HT-Water - A Relation Between Monotonic and Cyclic Crack Initiation Behavior*, in IAEA Specialists Meeting Corrosion and Stress Corrosion of Steel Pressure Boundary Components and Steam Turbines, VTT Symp. 43, Espoo, Finland, pp. 243-267 (1983).

57. J. Hickling and D. Blind, *Strain-Induced Corrosion Cracking of Low-Alloy Steels in LWR Systems – Case Histories and Identification of Conditions Leading to Susceptibility*, Nucl. Eng. Des. **91**, 305–330 (1986).

58. F. P. Ford, S. Ranganath, and D. Weinstein, *Environmentally Assisted Fatigue Crack Initiation in Low-Alloy Steels – A Review of the Literature and the ASME Code Requirements*, EPRI TR-102765, Electric Power Research Institute, Palo Alto, CA (1993).

59. J.-M. Stephan and J. C. Masson, *Auxiliary Feedwater Line Stratification and Coufast Simulation*, Int. Conf. on Fatigue of Reactor Components, Napa CA, July 31–August 2, 2000.

60. J. F. Enrietto, W. H. Bamford, and D. F. White, *Preliminary Investigation of PWR Feedwater Nozzle Cracking*, Intl. J. Pressure Vessels and Piping, 9, pp. 421–443 (1981).

61. G. Katzenmeier, K. Kussmaul, E. Roos, and H. Diem, *Component Testing at the HDR-Facility for Validating the Calculation Procedures and the Transferability of the Test Results from Specimen to Component*, Nucl. Eng. Des. **119**, 317-327 (1990).

62. W. J. Foley, R. S. Dean, and A. Hennick, *Closeout of IE Bulletin 79–13: Cracking in Feedwater System Piping*, NUREG/CR-5258, U.S. Nuclear Regulatory Commission, Washington, DC (1991).

63. W. H. Bamford, G. V. Rao, and J. L. Houtman, *Investigation of Service-Induced Degradation of Steam Generator Shell*, in Proc. 5th Intl. Symp. on Environmental Degradation of Materials in Nuclear Power Systems – Water Reactors, American Nuclear Society, La Grange Park, IL (1982).

64. NRC Information Notice 88-01, *Safety Injection Pipe Failure*, U.S. Nuclear Regulatory Commission, Washington, DC (Jan. 27, 1988).

65. NRC Bulletin No. 88-08, *Thermal Stresses in Piping Connected to Reactor Coolant Systems*, U.S. Nuclear Regulatory Commission, Washington, DC (June 22; Suppl. 1, June 24; Suppl. 2, Aug. 4, 1988; Suppl. 3, April 1989).

66. V. N. Shah, M. B. Sattison, C. L. Atwood, A. G. Ware, G. M. Grant, and R. S. Hartley, *Assessment of Pressurized Water Reactor Primary System Leaks*, NUREG/CR-6582, INEEL/EXT-97-01068 (Dec. 1998).

67. T. Sakai, *Leakage from CVCS Pipe of Regenerative Heat Exchanger Induced by High-Cycle Thermal Fatigue at Tsuruga Nuclear Power Station Unit 2*, Int. Conf. on Fatigue of Reactor Components, Napa, CA, July 31–August 2, 2000.

68. C. Faidy, T. Le Courtois, E. de Fraguier, J-A Leduff, A. Lefrancois, and J. Dechelotte, *Thermal Fatigue in French RHR System*, Int. Conf. on Fatigue of Reactor Components, Napa, CA, July 31–August 2, 2000.

69. E. Lenz, A. Liebert, and N. Wieling, *Thermal Stratification Tests to Confirm the Applicability of Laboratory Data on Strain-Induced Corrosion Cracking to Component Behavior*, in 3rd IAEA Specialists Meeting on Sub-Critical Crack Growth, Moscow, pp. 67–91 (1990).

70. M. J. Manjoine, and R. L. Johnson, *Fatigue Design Curves for Carbon and Low Alloy Steels up to 700°F (371°C)*, in Pressure Vessel and Piping Conference, 88–PVP–6, American Society of Mechanical Engineers, New York (1988).

71. M. J. Manjoine, and R. L. Johnson, *Fatigue Design Curves for Carbon and Low Alloy Steels up to 700°F (371°C)*, in Material Durability/Life Prediction Modeling: Materials for the 21st Century, PVP–Vol. 290, American Society of Mechanical Engineers, New York (1994).

72. H. S. Mehta, *An Update on the EPRI/GE Environmental Fatigue Evaluation Methodology and its Applications*, Probabilistic and Environmental Aspects of Fracture and Fatigues, PVP Vol. 386, S. Rahman, ed., American Society of Mechanical Engineers, New York, pp. 183–193 (1999).

73. R. A. Smith, Y. Liu, and L. Garbowski, *Short Fatigue Crack Growth Behavior in Waspaloy at Room and Elevated Temperature*, Fatigue Fract. Eng. Mater. Struct. **19**, 1505-1514 (1996).

74. K. Hussain, A. Tauqir, S. M. Hashmi, and A. Q. Khan, *Short Fatigue Crack Growth Behavior in Ferrite-Bainitic Steel*, Metall. Trans. A **25A**, 2421-2425 (1994).

75. K. Tokaji and T. Ogawa, *The Growth Behavior of Microstructurally Small Fatigue Cracks in Metals*, Short Fatigue Cracks, ESIS 13, Mechanical Engineering Pub., pp. 85-99 (1992).

76. K. Tokaji, T. Ogawa, and Y. Harada, *The Growth of Small Fatigue Cracks in a Low–Carbon Steel; The Effect of Microstructure and Limitation of Linear Elastic Fracture Mechanics*, Fatigue Fract. Eng. Mater. Struct. **9**, 205-217 (1986).

77. K. Tokaji, T. Ogawa, Y. Harada, and Z. Ando, *Limitation of Linear Elastic Fracture Mechanics in Respect of Small Fatigue Cracks and Microstructure*, Fatigue Fract. Eng. Mater. Struct. **9**, 1-14 (1986).

78. C. M. Suh, J. J. Lee, and Y. G. Kang, *Fatigue Microcracks in Type 304 Stainless Steel at Elevated Temperature*, Fatigue Fract. Eng. Mater. Struct. **13**, 487-496 (1990).

79. C. M. Suh, R. Yuuki, and H. Kitagawa, *Fatigue Microcracks in a Low Carbon Steel*, Fatigue Fract. Eng. Mater. Struct. **8**, 193-203 (1985).

80. E. R. de los Rios, A. Navarro, and K. Hussain, *Microstructural Variations in Short Fatigue Crack Propagation of a C-Mn Steel*, Short Fatigue Cracks, ESIS 13, Mechanical Engineering Pub., pp. 115-132 (1992).

81. E. R. de los Rios., X. D. Wu, and K. J. Miller, *A Micro-Mechanics Model of Corrosion-Fatigue Crack Growth in Steels*, Fatigue Fract. Eng. Mater. Struct. **19**, 1383-1400 (1996).

82. J. Lankford, *Initiation and Early Growth of Fatigue Cracks in High Strength Steels*, Eng. Fract. Mech. **9**, 617-624 (1977).

83. J. Lankford, *The Growth of Small Fatigue Cracks in 7075-T6 Aluminum*, Fatigue Fract. Eng. Mater. Struct. **5**, 233-248 (1982).

84. J. Lankford, *The Influence of Microstructure on the Growth of Small Fatigue Cracks*, Fatigue Fract. Eng. Mater. Struct. **8**, 161-175 (1985).

85. H. Kitagawa and S. Takahashi, *Applicability of Fracture Mechanics to Very Small Cracks of the Cracks in the Early Stage*, in Proc. 2nd Int. Conf. on Mechanical Behavior of Materials, ASM, Metals Park, OH, pp. 627-631 (1976).

86. D. Taylor and J. F. Knott, *Fatigue Crack Propagation Behavior of Short Cracks; The Effect of Microstructure*, Fatigue Fract. Eng. Mater. Struct. **4**, 147-155 (1981).

87. K. S. Ravichandran, *Effects of Crack Aspect Ratio on the Behavior of Small Surface Cracks in Fatigue; Part II. Experiments on a Titanium (Ti-8Al) Alloy*, Metall. Trans. A **28A**, 157-167 (1997).

88. N. E. Dowling, *Crack Growth During Low-Cycle Fatigue of Smooth Axial Specimens*, ASTM STP 637, pp. 97-121 (1977).

89. P. D. Hobson, *The Formulation of a Crack Growth Equation for Short Cracks*, Fatigue Fract. Eng. Mater. Struct. **5**, 323-327 (1982).

90. M. W. Brown, *Interface Between Short, Long and Non-Propagating Cracks*, Mechanical Engineering Pub., pp. 423-439 (1986).

91. E. P. Carbonell and M. W. Brown, *A Study of Short Crack Growth in Torsional Low-Cycle Fatigue for a Medium Carbon Steel*, Fatigue Fract. Eng. Mater. Struct. **9**, 15-33 (1986).

92. F. P. Ford and P. L. Andresen, *Corrosion in Nuclear Systems: Environmentally Assisted Cracking in Light Water Reactors*, Marcel Dekker Inc., pp. 501-546 (1995).

93. F. P. Ford, *Quantitative Prediction of Environmentally Assisted Cracking*, Corrosion **52**, 375-395 (1996).

94. T. P. O'Donnell and W. J. O'Donnell, *Stress Intensity Values in Conventional S-N Fatigue Specimens*, in Int Pressure Vessels and Piping Codes and Standards Volume 1, Current Applications, PVP 313-1, K. R. Rao and Y. Asada, eds., American Society of Mechanical Engineers, New York, pp. 195-197 (1995).

95. W. A. Van Der Sluys and S. Yukawa, *Status of PVRC Evaluation of LWR Coolant Environmental Effects on the S–N Fatigue Properties of Pressure Boundary Materials*, in Fatigue and Crack Growth: Environmental Effects, Modeling Studies, and Design Considerations, PVP Vol. 306, S. Yukawa, ed., American Society of Mechanical Engineers, New York, pp. 47–58 (1995).

96. M. E. Mayfield, E. C. Rodabaugh, and R. J. Eiber, *A Comparison of Fatigue Test Data on Piping with the ASME Code Fatigue Evaluation Procedure*, ASME paper 79–PVP–92, American Society of Mechanical Engineers, New York (1979).

97. A. F. Deardorff and J. K. Smith, *Evaluation of Conservatisms and Environmental Effects in ASME Code, Section III, Class 1 Fatigue Analysis*, SAND94–0187, prepared by Structural Integrity Associates, San Jose, CA, under contract to Sandia National Laboratories, Albuquerque, NM (1994).

98. L. F. Kooistra, E. A. Lange, and A. G. Pickett, *Full–Size Pressure Vessel Testing and Its Application to Design*, J. Eng. Power **86**, 419–428 (1964).

99. R. E. Peterson, *Fatigue Tests of Small Specimens with Particular Reference to Size Effect*, Trans. Amer. Soc. Steel Testing **18**, 1041–1053 (1930).

100. D. Morkovin and H. F. Moore, *Third Progress Report on the Effect of Size of Specimen on Fatigue Strength of Three Types of Steel*, Proc. Amer. Soc. Test. Mater. **44**, 137–158 (1944).

101. C. E. Philips and R. B. Heywood, *The Size Effect in Fatigue of Plain and Notched Steel Specimens Loaded Under Reversed Direct Stress*, Proc. Inst. Mech. Eng. **165**, 113–124 (1951).

102. C. Massonnet, *The Effect of Size, Shape, and Grain Size on the Fatigue Strength of Medium Carbon steel*, Proc. Amer. Soc. Test. Mater. **56**, 954–978 (1956).

103. P. S. Maiya and D. E. Busch, *Effect of Surface Roughness on Low–Cycle Fatigue Behavior of Type 304 Stainless Steel*, Met. Trans. **6A**, 1761–1766 (1975).

104. P. S. Maiya, *Effect of Surface Roughness and Strain Range on Low–Cycle Fatigue Behavior of Type 304 Stainless Steel*, Scripta Metall. **9**, 1277–1282 (1975).

105. K. J. Stout, *Surface Roughness – Measurement, Interpretation, and Significance of Data*, Mater. Eng. **2**, 287–295 (1981).

106. K. Iida, *A Study of Surface Finish Effect Factor in ASME B & PV Code Section III*, in Pressure Vessel Technology, Vol. 2, L. Cengdian and R. W. Nichols, eds., Pergamon Press, New York, pp. 727–734 (1989).

107. M. A. Pompetzki, T. H. Topper, and D. L. DuQuesnay, *The Effect of Compressive Underloads and Tensile Overloads on Fatigue Damage Accumulation in SAE 1045 Steel*, Int. J. Fatigue **12** (3), 207–213 (1990).

108. A. Conle and T. H. Topper, *Evaluation of Small Cycle Omission Criteria for Shortening of Fatigue Service Histories*, Int. J. Fatigue **1**, 23–28 (1979).

109. A. Conle and T. H. Topper, *Overstrain Effects During Variable Amplitude Service History Testing*, Int. J. Fatigue **2**, 130–136 (1980).

110. Li Nian and Du Bai–Ping, *Effect of Monotonic and Cyclic Prestrain on the Fatigue Threshold in Medium–Carbon steels*, Int. J. Fatigue **14** (1), 41–44 (1992).

111. Li Nian and Du Bai–Ping, *The Effect of Low–Stress High–Cycle Fatigue on the Microstructure and Fatigue Threshold of a 40Cr Steel*, Int. J. Fatigue **17** (1), 43–48 (1995).

112. E. Haibach and D. Schutz, *Fatigue Life Evaluation with Particular Attention to Local Strain and Stress Time Histories*, Proc. Inst. Mech. Eng., 1974.

113. D. J. Dowdell, H. H. E. Leipholz, and T. H. Topper, *The Modified Life Law Applied to SAE–1045 Steel*, Int. J. Fract. **31**, 29–36 (1986).

Appendix A: Fatigue Test Results

Table A1. Fatigue test results for A106–Gr B carbon steel at 288°C

Test Number	Specimen Number	Environ -ment[a]	Dissolved Oxygen[b] (ppb)	pH at RT	Conduc- tivity (μS/cm)	ECP[b] Pt mV (SHE)	ECP[b] Steel mV (SHE)	Tensile Rate (%/s)	Compres- sive Rate (%/s)	Stress Range (MPa)	Strain Range (%)	Life N_{25} (Cycles)
1498	J7-02	Air	–	–	–	–	–	0.4	0.4	1001.4	1.00	1,048
1546	J7-05	Air	–	–	–	–	–	0.4	0.4	975.7	0.92	1,365
1553	J7-12	Air	–	–	–	–	–	0.4	0.4	921.1	0.76	3,253
1554	J7-13	Air	–	–	–	–	–	0.4	0.4	896.8	0.73	3,753
1674[c]	J7–41	Air	–	–	–	–	–	0.4	0.4	1003.6	0.76	6,275
1686[c]	J7–58	Air	–	–	–	–	–	0.4	0.4	1017.2	0.80	2,592
1731	J7–74	Air	–	–	–	–	–	0.4	0.004	1005.5	0.76	3,485
1615	J7-19	Air	–	–	–	–	–	0.04	0.4	959.8	0.76	3,873
1609	J7-09	Air	–	–	–	–	–	0.004	0.4	1026.0	0.76	3,721
1612	J7-17	Air	–	–	–	–	–	0.004	0.4	1008.2	0.78	3,424
1673	J7–40	Air	–	–	–	–	–	0.004	0.4	1003.6	0.76	6,275
1548	J7-07	Air	–	–	–	–	–	0.4	0.4	831.9	0.55	10,632
1543	J7-03	Air	–	–	–	–	–	0.4	0.4	818.2	0.50	14,525
1619	J7-21	Air	–	–	–	–	–	0.4	0.4	741.7	0.40	37,142
1636[d]	J7-29	Air	–	–	–	–	–	0.4	0.4	749.6	0.40	34,829
1621	J7-24	Air	–	–	–	–	–	0.01	0.4	787.1	0.40	38,128
1550	J7-08	Air	–	–	–	–	–	0.4	0.4	681.7	0.35	66,768
1552	J7-11	Air	–	–	–	–	–	0.4	0.4	680.6	0.35	93,322
1555	J7-18	Air	–	–	–	–	–	0.4	0.4	676.3	0.34	98,456
1644	J7-37	Air	–	–	–	–	–	0.004	0.4	702.0	0.36	>94,657
1744[d]	J7–81	DI	<1	6.5	0.082	-452	-597	0.4	0.4	760.5	0.41	19,860
1738[d]	J7–76	DI	1	6.5	0.092	-441	-592	0.004	0.4	976.2	0.78	1,350
1547	J7-04	PWR	8	6.7	23.260	-676	-761	0.4	0.4	1010.9	0.99	692
1564	J7-14	PWR	12	6.6	21.740	-630	-720	0.4	0.4	942.0	0.77	1,525
1676	J7–36	PWR	2	6.5	20.830	-703	-667	0.4	0.4	926.7	0.74	2,230
1679	J7–44	PWR	3	6.5	20.410	-687	-694	0.004	0.4	1005.8	0.76	2,141
1681	J7–53	PWR	1	6.5	20.000	-705	-714	0.0004	0.4	1015.7	0.76	2,672
1549	J7-06	PWR	8	6.7	25.640	-681	-725	0.4	0.4	827.0	0.53	9,396
1560	J7-20	PWR	12	6.6	23.730	-645	-721	0.4	0.4	701.3	0.36	35,190
1556	J7-10	PWR	8	6.6	22.730	-605	-711	0.4	0.4	710.9	0.36	38,632
1632	J7-27	Hi DO	800	5.8	0.110	230	193	0.4	0.4	913.3	0.74	2,077
1705	J7–68	Hi DO	650	5.9	0.150	195	178	0.4	0.4	947.9	0.77	1,756
1680[c]	J7–45	Hi DO	700	6.0	0.080	183	175	0.4	0.4	999.6	0.82	1,007
1690[c]	J7–60	Hi DO	700	6.0	0.080	185	165	0.4	0.4	1002.2	0.82	1,092
1687[e]	J7–55	Hi DO	700	6.0	0.100	207	186	0.4	0.4	1020.0	0.81	840
1757	J7–85	Hi DO	670	5.9	0.072	264	156	0.4	0.0	942.2	0.74	1,195
1693	J7–57	Hi DO	650	6.0	0.100	210	193	0.04	0.4	920.0	0.74	1,125
1694[f]	J7–61	Hi DO	650	6.0	0.080	183	175	0.04	0.4	935.7	0.75	980
1614	J7-16	Hi DO	400	5.9	0.110	155	80	0.004	0.4	930.4	0.79	303
1682	J7–54	Hi DO	700	6.0	0.090	190	181	0.004	0.4	921.1	0.75	469
1725	J7–72	DI	20	5.8	0.150	-235	54	0.004	0.4	926.3	0.74	548
1733	J7–75	DI	2	6.4	0.106	-388	-573	0.004	0.4	1020.7	0.80	2,415
1836	J7–97	Hi DO	880	6.0	0.061	232	197	0.004	0.4	903.1	0.77	470
1696[f]	J7–62	Hi DO	610	5.9	0.070	185	186	0.004	0.4	923.3	0.75	363
1623	J7-25	Hi DO	800	5.9	0.080	209	156	0.004	0.004	943.8	0.79	338
1616	J7-22	Hi DO	800	5.8	0.080	195	155	0.0004	0.4	912.8	0.80	153
1620	J7-23	Hi DO	900	5.9	0.110	225	160	0.00004	0.004	943.1	0.79	161
1706	J7–69	Hi DO	600	5.9	0.070	212	197	0.4	0.4	825.2	0.53	7,858
1634	J7-28	Hi DO	800	5.8	0.160	232	197	0.4	0.4	733.2	0.40	19,318
1624	J7-26	Hi DO	800	5.9	0.100	210	185	0.004	0.4	775.7	0.46	2,276
1639	J7-32	Hi DO	800	5.9	0.090	230	210	0.004	0.4	751.6	0.42	2,951
1643	J7-33	Hi DO	800	6.0	0.110	195	177	0.004	0.4	698.5	0.36	>65,000

[a]DI = Deionized water and PWR = simulated PWR water with 2 ppm lithium and 1000 ppm boron.
[b]Represent DO levels and ECP values in effluent water.
[c]Tested with 5–min hold period at peak tensile strain.
[d]Specimen preoxidized in water with 600 ppb DO for 100 h at 288°C.
[e]Tested with 30–min hold period at peak tensile strain.
[f]Tested with sine waveform.

Table A2. Fatigue test results for A533–Gr B low–alloy steel at 288°C

Test Number	Specimen Number	Environ –ment[a]	Dissolved Oxygen[b] (ppb)	pH at RT	Conduc- tivity (μS/cm)	ECP[b] Pt mV (SHE)	ECP[b] Steel mV (SHE)	Tensile Rate (%/s)	Compres- sive Rate (%/s)	Stress Range (MPa)	Strain Range (%)	Life N_{25} (Cycles)
1508	44-02	Air	–	–	–	–	–	0.4	0.4	910.9	1.002	3,305
1524	44-09	Air	–	–	–	–	–	0.4	0.4	892.3	0.950	3,714
1523	44-08	Air	–	–	–	–	–	0.4	0.4	898.6	0.917	2,206
1521	44-06	Air	–	–	–	–	–	0.4	0.4	889.4	0.910	3,219
1522	44-07	Air	–	–	–	–	–	0.4	0.4	905.4	0.899	3,398
1515	44-03	Air	–	–	–	–	–	0.4	0.4	866.1	0.752	6,792
1749[c]	44-61	Air	–	–	–	–	–	0.4	0.4	–	–	6,372
1717	44-51	Air	–	–	–	–	–	0.4	0.004	884.6	0.758	6,217
1625	44-25	Air	–	–	–	–	–	0.004	0.4	887.7	0.757	4,592
1865	44-82	Air	–	–	–	–	–	0.0004	0.4	907.5	0.749	5,930
1629[d]	44-28	Air	–	–	–	–	–	0.4	0.4	782.9	0.503	31,243
1590	44-24	Air	–	–	–	–	–	0.4	0.004	821.1	0.503	24,471
1576	44-19	Air	–	–	–	–	–	0.004	0.4	805.8	0.503	28,129
1505	44-01	Air	–	–	–	–	–	0.4	0.4	767.6	0.501	31,200
1525	44-10	Air	–	–	–	–	–	0.4	0.4	743.6	0.452	65,758
1640	44-29	Air	–	–	–	–	–	0.4	0.4	710.9	0.402	65,880
1798	44-73	Air	–	–	–	–	–	0.4	0.4	715.6	0.399	115,119
1538	44-17	Air	–	–	–	–	–	0.4	0.4	708.0	0.387	>1,000,000
1517	44-05	Air	–	–	–	–	–	0.4	0.4	692.5	0.353	2,053,295
1659	44-46	Air	–	–	–	–	–	0.004	0.4	656.2	0.343	>114,294
1526	44-11	DI	–	–	–	–	–	0.4	0.4	876.4	0.873	3,332
1527	44-12	DI	–	6.0	–	–	–	0.4	0.4	752.8	0.493	10,292
1528	44-13	DI	5	5.8	–	–	–	0.4	0.4	744.1	0.488	25,815
1743[e]	44-59	DI	<1	6.5	0.08	-405	-465	0.4	0.4	712.6	0.386	84,700
1530	44-15	PWR	3	6.9	41.67	-716	-730	0.4	0.4	885.5	0.894	1,355
1545	44-21	PWR	8	6.9	22.73	-684	-729	0.4	0.4	889.7	0.886	3,273
1533	44-16	PWR	4	6.9	45.45	-722	-764	0.004	0.4	916.0	0.774	3,416
1529	44-14	PWR	3	6.9	45.45	-718	-737	0.4	0.4	743.4	0.484	31,676
1605	44-22	PWR	9	6.5	23.81	-678	-689	0.4	0.004	785.2	0.460	>57,443
1588	44-23	PWR	6	6.5	23.26	-675	-668	0.004	0.4	828.7	0.514	15,321
1539	44-18	PWR	6	6.8	38.46	-645	-670	0.4	0.4	690.9	0.373	136,570
1542	44-20	PWR	6	6.6	27.03	-700	-740	0.4	0.4	631.8	0.354	>1,154,892
1645	44-31	Hi DO	800	6.1	0.07	-697	-697	0.4	0.4	831.1	0.721	2,736
1768	44-63	Hi DO	600	6.0	0.07	248	206	0.4	0.004	907.3	0.755	1,350
1626	44-26	Hi DO	900	5.9	0.13	225	200	0.004	0.4	910.1	0.788	247
1715	44-41	Hi DO	600	5.9	0.08	198	182	0.004	0.4	904.1	0.813	381
1864	44-81	Hi DO	630	6.5	0.083	343	202	0.004	0.4	895.8	0.746	340
1866	44-83	Hi DO	730	6.3	0.063	361	263	0.0004	0.4	889.9	0.748	137
1867	44-84	Hi DO	780	6.5	0.061	337	229	0.00004	0.4	897.0	0.738	123
1718	44-47	Hi DO	240	6.1	0.390	124	127	0.004	0.4	904.3	0.807	346
1720	44-52	Hi DO	45	5.8	0.095	-58	116	0.004	0.4	905.9	0.806	330
1735	44-56	Hi DO	25	6.1	0.188	25	212	0.004	0.4	909.7	0.812	502
1723	44-53	Hi DO	20	5.9	0.080	-249	82	0.004	0.4	907.2	0.807	371
1730	44-55	Hi DO	5	6.6	0.088	-368	-551	0.004	0.4	911.7	0.803	1,900
1736	44-58	Hi DO	1	6.1	0.073	-381	-151	0.004	0.4	934.2	0.810	1,447
1711	44-45	Hi DO	630	5.8	0.31	234	220	0.4	0.4	772.1	0.542	5,850
1707	44-42	Hi DO	650	5.9	0.08	155	140	0.4	0.004	803.0	0.488	3,942
1709	44-44	Hi DO	650	5.9	0.11	195	180	0.4	0.004	805.1	0.501	3,510
1627	44-27	Hi DO	800	5.9	0.10	229	210	0.004	0.4	826.8	0.534	769
1641	44-30	Hi DO	800	5.9	0.09	176	160	0.4	0.4	693.0	0.385	17,367
1665	44-38	Hi DO	800	6.1	0.08	200	189	0.004	0.4	717.0	0.376	3,455
1666	44-40	Hi DO	750	6.1	0.09	195	187	0.0004	0.4	729.6	0.376	>7,380
1647	44-32	Hi DO	800	6.1	0.09	215	201	0.4	0.4	688.0	0.380	26,165
1660	44-37	Hi DO	750	6.1	0.11	200	185	0.004	0.4	689.6	0.360	>83,024
1649	44-33	Hi DO	700	6.3	0.08	208	196	0.4	0.4	673.4	0.352	28,710
1652	44-34	Hi DO	700	6.1	0.09	214	202	0.4	0.4	638.1	0.328	56,923
1655	44-36	Hi DO	750	6.1	0.10	191	179	0.4	0.4	567.6	0.289	>1,673,954

[a]DI = Deionized water and PWR = simulated PWR water with 2 ppm lithium and 1000 ppm boron.
[b]Represent DO levels and ECP values in effluent water.
[c]Tested with 5–min hold period at peak tensile strain.
[d]Specimen preoxidized in water with 600 ppb DO for 100 h at 288°C.
[e]Specimen preoxidized in water with 600 ppb DO for 30 h at 288°C.

Table A3. Fatigue test results for A106–Gr B and A533–Gr B steels at room temperature

Test Number	Specimen Number	Environ -ment[a]	Dissolved Oxygen[b] (ppb)	pH at RT	Conduc- tivity (μS/cm)	ECP[b] Pt mV (SHE)	ECP[b] Steel mV (SHE)	Tensile Rate (%/s)	Compres- sive Rate (%/s)	Stress Range (MPa)	Strain Range (%)	Life N_{25} (Cycles)
A106 Gr B												
1700	J7–67	Air	–	–	–	–	–	0.4	0.4	715.2	0.76	6,574
1766	J7–86	Air	–	–	–	–	–	0.4	0.4	719.7	0.76	7,120
1770	J7–92	Air	–	–	–	–	–	0.4	0.4	608.5	0.40	37,379
1699	J7–66	Hi DO	850	6.0	0.070	–	–	0.4	0.4	728.7	0.75	4,794
1772	J7–89	Hi DO	745	6.2	0.074	–	–	0.4	0.4	618.7	0.40	23,300
A533 Gr B												
1727	44–54	Air	–	–	–	–	–	0.4	0.4	766.7	0.76	9,145
1785	44–68	Air	–	–	–	–	–	0.4	0.4	763.7	0.76	8,840
1779	44–67	Air	–	–	–	–	–	0.004	0.4	759.8	0.76	5,960
1729	44–57	Air	–	–	–	–	–	0.4	0.4	677.5	0.41	77,759
1786	44–71	Air	–	–	–	–	–	0.4	0.4	687.7	0.40	61,100
1795	44–54	Air	–	–	–	–	–	0.4	0.4	694.6	0.40	82,050
1759	44–60	Hi DO	610	6.1	0.068	–	–	0.4	0.4	774.7	0.75	6,250
1761	44–62	Hi DO	770	6.1	0.080	–	–	0.4	0.4	694.5	0.40	46,500

[a]DI = Deionized water and PWR = simulated PWR water with 2 ppm lithium and 1000 ppm boron.
[b]Represent DO levels and ECP values in effluent water.

Table A4. Fatigue test results for A302–Gr B low–alloy steel at 288°C

Test Number	Specimen Number[a]	Environ -ment[b]	Dissolved Oxygen[c] (ppb)	pH at RT	Conduc- tivity (μS/cm)	ECP[c] Pt mV (SHE)	ECP[c] Steel mV (SHE)	Tensile Rate (%/s)	Compres- sive Rate (%/s)	Stress Range (MPa)	Strain Range (%)	Life N_{25} (Cycles)
1697	214–C01	Air	–	–	–	–	–	0.4	0.4	944.5	0.76	8,070
1780	214–R03	Air	–	–	–	–	–	0.4	0.4	908.6	0.76	1,598
1809	214–A03	Air	–	–	–	–	–	0.4	0.4	938.8	0.76	7,220
1701	214–C02	Air	–	–	–	–	–	0.004	0.4	1021.4	0.76	4,936
1828	214–C15	Air	–	–	–	–	–	0.004	0.4	1019.5	0.76	3,945
1781	214–R04	Air	–	–	–	–	–	0.004	0.4	952.4	0.76	375
1830	214–A08	Air	–	–	–	–	–	0.004	0.4	1014.2	0.76	4,650
1712[d]	214–C07	Air	–	–	–	–	–	0.0004	0.4	1041.9	0.76	5,350
1789	214–C09	Air	–	–	–	–	–	0.4	0.4	859.5	0.51	46,405
1783	214–C08	Air	–	–	–	–	–	0.4	0.4	796.1	0.41	1,044,000
1782	214–R05	Air	–	–	–	–	–	0.4	0.4	752.8	0.40	33,650
1811	214–A04	Air	–	–	–	–	–	0.4	0.4	770.1	0.40	1,300,000
1787	214–R07	Air	–	–	–	–	–	0.4	0.4	667.5	0.34	431,150
1702	214–C03	PWR	3	6.5	20.0	-682	-700	0.4	0.4	921.2	0.74	6,212
1776	214–R02	PWR	1	6.4	18.4	-707	-625	0.4	0.4	887.1	0.77	1,244
1777	214–A02	PWR	1	6.4	19.2	-701	-735	0.4	0.4	913.8	0.77	4,366
1704	214–C04	PWR	3	6.5	19.2	-695	-710	0.004	0.4	1022.6	0.75	3,860
1774	214–R01	PWR	2	6.4	19.4	-747	-774	0.004	0.4	949.7	0.76	348
1775	214–A01	PWR	1	6.5	19.4	-722	-752	0.004	0.4	995.6	0.75	1,458
1837	214–A09	PWR	3	6.5	18.2	-654	-644	0.004	0.4	1005.7	0.75	4,070
1716[d]	214–C05	PWR	5	6.5	19.2	-693	-717	0.0004	0.4	1042.3	0.74	3,718
1833	214–C12	Hi DO	345	6.4	0.06	–	–	0.004	0.4	959.8	0.75	330
1788	214–C06	Hi DO	650	5.9	0.10	-97	197	0.004	0.4	957.0	0.75	317
1784	214–R06	Hi DO	510	6.0	0.07	257	214	0.004	0.4	937.6	0.75	111
1813	214–A05	Hi DO	880	6.0	0.12	250	209	0.004	0.4	963.4	0.76	238
1822	214–C10	Hi DO	600	5.9	0.07	207	192	0.004	0.4	848.6	0.49	550
1820	214–R08	Hi DO	660	6.0	0.07	240	196	0.004	0.4	847.3	0.48	360
1819	214–A06	Hi DO	700	6.0	0.08	259	178	0.004	0.4	868.0	0.48	755

[a]Specimen ID numbers with C = rolling direction, R = radial direction, and A = transverse direction.
[b]DI = Deionized water and PWR = simulated PWR water with 2 ppm lithium and 1000 ppm boron.
[c]Represent DO levels and ECP values in effluent water.
[d]Slow strain rate applied only during 1/8 cycle near peak tensile strain.

Table A5. Fatigue test results for Type 316NG austenitic stainless steel

Test Number	Specimen Number	Environ -ment[a]	Dissolved Oxygen[b] (ppb)	pH at RT	Conduc- tivity[c] (μS/cm)	ECP[b] Pt mV (SHE)	ECP[b] Steel mV (SHE)	Tensile Rate (%/s)	Compres- sive Rate (%/s)	Stress Range (MPa)	Strain Range (%)	Life N_{25} (Cycles)
25°C												
1394	S-12	Air	–	–	–	–	–	0.99	0.99	694.7	1.51	4,649
1391	S-08	Air	–	–	–	–	–	0.66	0.66	554.8	1.00	13,561
1390	S-01	Air	–	–	–	–	–	0.50	0.50	518.1	0.75	25,736
1396	S-07	Air	–	–	–	–	–	0.50	0.50	506.7	0.76	30,000
1420	S-30	Air	–	–	–	–	–	0.49	0.49	495.3	0.49	54,249
1392	S-09	Air	–	–	–	–	–	0.33	0.33	475.9	0.51	60,741
1393	S-10	Air	–	–	–	–	–	0.27	0.27	464.7	0.41	127,386
1395	S-13	Air	–	–	–	–	–	0.23	0.23	456.7	0.35	183,979
1397	S-21	Air	–	–	–	–	–	0.20	0.20	446.0	0.30	347,991
1398	S-15	Air	–	–	–	–	–	0.18	0.18	436.7	0.27	666,000
1399	S-16	Air	–	–	–	–	–	0.17	0.17	431.8	0.25	>1,900,000
1400	S-17	Air	–	–	–	–	–	0.17	0.17	427.4	0.25	1,775,000
288°C												
1408	S-22	Air	–	–	–	–	–	0.50	0.50	416.6	0.76	21,548
1790	S-46	Air	–	–	–	–	–	0.005	0.50	452.8	0.75	16,765
1409	S-23	Air	–	–	–	–	–	0.50	0.50	377.2	0.50	53,144
1410	S-25	Air	–	–	–	–	–	0.50	0.50	377.6	0.50	51,194
1792	S-49	Air				-20.3	-20.3	0.005	0.50	413.4	0.51	35,710
1407	S-24	Air	–	–	–	–	–	0.27	0.27	364.4	0.40	82,691
1430	S-36	Air	–	–	–	–	–	0.20	0.20	348.3	0.30	168,852
1435	S-38	Air	–	–	–	–	–	0.17	0.17	342.0	0.25	314,352
1480	S-40	Air	–	–	–	–	–	0.16	0.16	340.1	0.25	319,308
1485	S-41	Air	–	–	–	–	–	0.17	0.17	340.4	0.25	369,206
320°C												
1405	S-19	Air	–	–	–	–	–	0.50	0.50	426.0	0.75	20,425
1404	S-18	Air	–	–	–	–	–	0.50	0.50	387.4	0.50	47,011
1406	S-20	Air	–	–	–	–	–	0.50	0.50	371.6	0.40	82,691
288°C												
1796	S-47	PWR	5	6.40	20.202	-681	-677	0.50	0.50	403.6	0.80	12,500
1812	S-45	PWR	2	6.48	20.000	-693	-690	0.05	0.50	413.9	0.80	6,375
1791	S-51	PWR	4	6.45	19.230	-701	-701	0.005	0.50	441.9	0.77	3,040
1793	S-50	PWR	4	6.41	19.230	-703	-704	0.005	0.50	434.3	0.80	3,020
1794	S-48	PWR	4	6.40	20.000	-694	-693	0.005	0.50	390.9	0.50	7,370
1814	S-44	PWR	1	6.50	20.000	-698	-695	0.05	0.50	348.7	0.29	33,200
1426	S-32	Hi DO	>200	–	–	-8	-18	0.80	0.80	405.1	0.80	12,069
1427	S-33	Hi DO	>200	–	–	-8	–	0.08	0.08	421.7	0.82	6,679
1428	S-34	Hi DO	>200	–	–	-4	-18	0.007	0.007	441.4	0.74	5,897
1797	S-43	Hi DO	750	5.90	0.076	195	60	0.005	0.50	437.3	0.78	4,520
1414	S-26	Hi DO	>200	–	–	–	–	0.50	0.50	375.3	0.50	26,230
1418	S-28	Hi DO	>200	–	–	–	–	0.50	0.50	375.5	0.50	25,714
1423	S-29	Hi DO	>200	–	–	-63	25	0.05	0.05	378.8	0.50	17,812
1425	S-31	Hi DO	>200	–	–	-37	-15	0.00	0.00	393.2	0.49	13,684
1431	S-35	Hi DO	>200	–	–	-26	-22	0.29	0.29	356.5	0.29	116,754
1434	S-37	Hi DO	>200	–	–	-5	-18	0.03	0.03	350.0	0.29	40,643
1436	S-39	Hi DO	>200	–	–	-5	-13	0.25	0.25	354.0	0.25	>1,719,851
1512	S-42	Hi DO	>200	–	–	35	90	0.24	0.24	361.2	0.24	2,633,954

[a]DI = Deionized water and PWR = simulated PWR water with 2 ppm lithium and 1000 ppm boron. Specimens tested in high DO water were soaked only for 24 h, the ECP values had not stabilized at the start of the test.

[b]Represent DO levels and ECP values in effluent water.

[c]Conductivity of water measured in feedwater supply tank.

Table A6. Fatigue test results for Type 304 austenitic stainless steel at 288°C

Test Number	Specimen Number	Environ -ment[a]	Dissolved Oxygen[b] (ppb)	pH at RT	Conduc-tivity[c] (μS/cm)	ECP[b] Pt mV (SHE)	ECP[b] Steel mV (SHE)	Tensile Rate (%/s)	Compres-sive Rate (%/s)	Stress Range (MPa)	Strain Range (%)	Life N_{25} (Cycles)
1801	309-01	Air	-	-	-	-	-	0.4	0.4	419.2	0.76	24,500
1805	309-03	Air	-	-	-	-	-	0.004	0.4	467.9	0.76	14,410
1804	309-02	Air	-	-	-	-	-	0.4	0.4	382.8	0.51	61,680
1817	309-12	Air	-	-	-	-	-	0.004	0.4	421.7	0.51	42,180
1825	309-08	Air	-	-	-	-	-	0.04	0.4	394.4	0.30	>625,860[d]
1846	309-16	Air	-	-	-	-	-	0.04	0.4	396.4	0.32	>316,000
1806	309-04	PWR	4	6.0	18.867	-682	-679	0.4	0.4	428.9	0.73	11,500
1810	309-07	PWR	5	6.4	18.887	-688	-685	0.04	0.4	447.6	0.77	5,800
1808	309-06	PWR	4	6.4	18.868	-693	-690	0.004	0.4	468.3	0.77	2,850
1821	309-09	PWR	2	6.5	22.222	-700	-697	0.004	0.4	474.3	0.76	2,420
1859	309-28	PWR	2	6.5	18.692	-699	-696	0.004	0.4	471.7	0.77	2,420
1861	309-36	DI	1	6.2	0.059	-601	-614	0.004	0.4	463.0	0.79	2,620
1862	309-27	DI	2	6.2	0.058	-608	-607	0.004	0.4	466.1	0.78	2,450
1863	309-31	DI	1	6.3	0.061	-446	-540	0.004	0.4	476.5	0.77	2,250
1829	309-15	PWR	2	6.5	18.182	-705	-705	0.0004	0.4	493.6	0.73	1,560
1834	309-19	PWR	2	6.5	18.182	-711	-712	0.0001	0.4	535.9	0.69	1,415
1807	309-05	PWR	4	6.5	18.868	-685	-682	0.4	0.4	374.6	0.51	25,900
1823	309-10	PWR	3	6.6	23.055	-701	-699	0.004	0.4	408.2	0.51	6,900
1826	309-13	PWR	2	6.5	18.762	-711	-710	0.01	0.4	375.8	0.29	>89,860[e]
1847	309-17	PWR	5	6.5	18.868	-700	-696	0.01	0.4	388.9	0.32	>165,300[f]
1827[g]	309-14	Hi DO	850	6.0	0.086	254	76	0.004	0.4	475.8	0.75	3,650
1860[g]	309-29	Hi DO	810	6.1	0.560	273	125	0.004	0.4	468.3	0.77	3,050
1852	309-18	Hi DO	790	6.1	0.061	235	149	0.4	0.4	429.1	0.74	10,800
1853	309-22	Hi DO	880	6.1	0.059	248	155	0.004	0.4	466.5	0.76	12,300
1855	309-23	Hi DO	890	6.0	0.115	275	150	0.004	0.4	464.4	0.77	8,080
1856	309-24	Hi DO	870	6.2	0.074	272	163	0.004	0.4	473.6	0.75	10,450
1857	309-30	Hi DO	790	6.1	0.420	254	143	0.004	0.4	461.9	0.78	5,300
1845	309-21	Hi DO	870	6.0	0.063	270	181	0.0004	0.4	488.7	0.71	>7,310
1869	309-33	Hi DO	720	6.1	0.059	253	201	0.4	0.4	375.0	0.51	24,100
1868	309-32	Hi DO	760	6.1	0.059	261	126	0.004	0.4	419.4	0.50	33,900

[a]DI = Deionized water and PWR = simulated PWR water with 2 ppm lithium and 1000 ppm boron. Specimens tested in high DO water were soaked for ≈120 h for the ECP values to stabilize.

[b]Represent DO levels and ECP values in effluent water.

[c]Conductivity of water measured in feedwater supply tank.

[d]Specimen failed after additional 331,300 cycles at 0.322% strain range.

[e]Specimen failed after additional 41,240 cycles at 0.315% strain range.

[f]Specimen failed after additional 50,700 cycles at 0.343% strain range.

[g]Specimens were soaked only for 24 h, the ECP values had not stabilized at the start of the test.

Table A7. Fatigue test results for CF–8M cast stainless steels at 288°C

Test Number	Specimen Number	Environ -ment[a]	Dissolved Oxygen[b] (ppb)	pH at RT	Conduc- tivity[c] (μS/cm)	ECP[b] Pt mV (SHE)	ECP[b] Steel mV (SHE)	Tensile Rate (%/s)	Compres- sive Rate (%/s)	Stress Range (MPa)	Strain Range (%)	Life N_{25} (Cycles)
Unaged Heat #74												
1831	U74–01	Air	–	–	–	–	–	0.4	0.4	429.7	0.76	26,500
1832	U74–05	Air	–	–	–	–	–	0.004	0.4	534.0	0.76	9,050
1848	U74–06	Air	–	–	–	–	–	0.004	0.4	440.7	0.76	17,900
1850	U74–02	PWR	5	6.5	17.241	-695	-693	0.004	0.4	419.5	0.76	10,700
1854	U74–03	PWR	2	6.5	18.692	-699	-695	0.004	0.4	448.4	0.75	4,720
Aged Heat #74												
1839	A74–01	Air	–	–	–	–	–	0.4	0.4	474.2	0.76	15,293
1840	A74–05	Air	–	–	–	–	–	0.004	0.4	534.8	0.75	19,800
1851	A74–04	PWR	4	6.5	18.182	-700	-699	0.4	0.4	482.1	0.75	6,420
1844	A74–03	PWR	2	6.5	18.182	-671	-690	0.004	0.4	527.7	0.72	2,180
1842	A74–02	BWR	820	6.1	0.063	267	141	0.004	0.4	508.5	0.75	1,375
Aged Heat #75												
1835	A75–01	Air	–	–	–	–	–	0.004	0.4	631.2	0.76	7,200
1843	A75–03	PWR	2	6.5	18.182	-572	-580	0.004	0.4	625.3	0.80	1,464
1838	A75–02	BWR	870	6.5	0.061	257	109	0.004	0.4	636.1	0.78	1,320

[a]DI = Deionized water and PWR = simulated PWR water with 2 ppm lithium and 1000 ppm boron.
[b]Represent DO levels and ECP values in effluent water.
[c]Conductivity of water measured in feedwater supply tank.

Appendix B:
Correlation for Calculating Stress Range, Stress Intensity Range, and Crack Growth Rates

Cyclic Stress Range

The cyclic stress–strain response of carbon and low-alloy steels varies with steel type, temperature, and strain rate. In general, these steels exhibit initial cyclic hardening, followed by cyclic softening or a saturation stage. The CSs, with a pearlite and ferrite structure and low yield stress, show significant initial hardening. The LASs, which consist of tempered ferrite and a bainite structure, exhibit a relatively high yield stress, and show little or no initial hardening, may exhibit cyclic softening at high strain ranges. At 200–370°C, these steels exhibit dynamic strain aging, which leads to enhanced cyclic hardening, a secondary hardening stage, and negative strain rate sensitivity. Under the conditions of dynamic strain aging, cyclic stress increases with decreases in strain rate.

The relationship of cyclic stress range vs. strain range is expressed by the modified Ramberg–Osgood relationship given by

$$\Delta\varepsilon = (\Delta\sigma/E) + (\Delta\sigma/A_3)^{n_3}, \tag{B1}$$

where E is Young's modulus, constant A_3 and exponent n_3 are determined from the experimental data, and cyclic stress range corresponds to the value at half-life. At room temperature, the relationship of cyclic stress range $\Delta\sigma$ (MPa) to strain range $\Delta\varepsilon$ (%) for CSs may be represented by

$$\Delta\varepsilon = (\Delta\sigma/2010) + (\Delta\sigma/766.1)^{(1/0.207)}, \tag{B2}$$

and for LASs, by

$$\Delta\varepsilon = (\Delta\sigma/2010) + (\Delta\sigma/847.4)^{(1/0.173)}. \tag{B3}$$

The effect of strain rate on the cyclic stress–strain curve is not considered at room temperature. At 288°C, the cyclic stress–strain curves may be represented by the correlations developed by Chopra and Shack.[B1] For CSs, the curve is given by the relationship

$$\Delta\varepsilon = (\Delta\sigma/1965) + (\Delta\sigma/\mathrm{Asig})^{(1/0.129)}, \tag{B4a}$$

where Asig varies with the strain rate $\dot{\varepsilon}$ (%/s) expressed as

$$\mathrm{Asig} = 1079.7 - 50.9 \log(\dot{\varepsilon}). \tag{B4b}$$

For LASs, the curve is given by the relationship

$$\Delta\varepsilon = (\Delta\sigma/1965) + (\Delta\sigma/\mathrm{Bsig})^{(1/0.110)}, \tag{B5a}$$

where Bsig is expressed as

$$\mathrm{Bsig} = 961.8 - 30.3 \log(\dot{\varepsilon}). \tag{B5b}$$

Stress Intensity Factor Range

For cylindrical fatigue specimens, the range of stress intensity factor ΔK was determined from the value of the J–integral range ΔJ, which, for a small semicircular surface crack, is given by Dowling[B2] as

$$\Delta J = 3.2\ (\Delta\sigma^2/2E)\ a + 5\ [\Delta\sigma\ \Delta\varepsilon_p/(S + 1)]\ a, \tag{B6a}$$

where $\Delta\varepsilon_p$ is the plastic strain range (%) (second term in the Ramberg Osgood relationship) and S is the reciprocal of the strain hardening exponent n in Eq. B1. The stress intensity factor range ΔK is obtained from

$$\Delta K = (E\ \Delta J)^{1/2}, \tag{B6b}$$

where E is the elastic modulus. Equation B6a incorporates a combined surface and flaw shape correction factor F_S of 0.714, which is derived from equivalent linear elastic solutions; Eq. B6a is valid as long as the crack size is very small when compared with the specimen diameter. For conventional fatigue tests, life is defined as the number of cycles for the tensile stress to decrease 25% from the peak or steady–state value, i.e., the crack–depth–to–specimen–diameter ratio can be as high as 0.4. Therefore, the geometrical correction factor F_s for a small semicircular surface crack was modified according to the correlation developed by O'Donnell and O'Donnell:[B3]

$$F_s = 0.6911 + 1.2685\ (a/D) - 5.6638\ (a/D)^2 + 21.511\ (a/D)^3, \tag{B7}$$

where D is specimen diameter. For conventional fatigue tests on cylindrical specimens, F_s may increase up to 1.7.

The J–integral range ΔJ is calculated from the ranges of cyclic stress and plastic strain, determined from stable hysteresis loops, i.e., at fatigue half–life. In general, ΔJ is computed only for that portion of the loading cycle during which the crack is open. For fully reversed cyclic loading, the crack opening point can be identified as the point where the curvature of the load–vs.–displacement line changed before the peak compressive load. In the present study, evidence of a crack opening point was observed for cracks that had grown relatively large, i.e., near the end of fatigue life. Therefore, as recommended by Dowling,[B2] the entire hysteresis loop was used in estimating ΔJ.

Crack Growth Rate

The fatigue CGRs da/dN of structural materials are characterized in terms of the range of applied stress intensity factor ΔK and are given in Article A–4300 of Section XI of the ASME Boiler and Pressure Vessel Code. For a stress ratio R in the range of $-2 < R < 0$, the reference fatigue CGRs da/dN (mm/cycle) of carbon and low–alloys steels exposed to air environments are given by

$$da/dN = 3.78 \times 10^{-9}\ (\Delta K)^{3.07}, \tag{B8}$$

where $\Delta K = K_{max}$, the maximum stress intensity factor ($MPa \cdot m^{1/2}$). However, the effect of temperature is not considered in Eq. B8; Logsdon and Liaw[B4] have shown that CGRs are

generally higher at 288°C than at room temperature. The results of Logsdon and Liaw indicate that for both CSs and LASs, CGRs are ≈22% higher at 288°C than at room temperature.

Section XI of the ASME Code also includes CGR curves for these steels exposed to LWR environments. The growth rates are represented by two curves for low and high values of ΔK. However, the curves do not consider the effects of loading rate. Recent experimental results have shown the importance of key variables of material, environment, and loading rate on CGRs in LWR environments. Fatigue CGR correlations have been developed to explicitly consider the effects of loading rate, stress ratio R, ΔK, and sulfur content in the steel.[B5] The new correlations, shown in Fig. B1, are divided into two categories: (a) for materials not susceptible to environmental effects, e.g., when S content in the steel is low, CGRs are a factor of 2.8 higher than those in air; and (b) for materials susceptible to environmental effects, e.g., when S content in the steel is high, CGRs are defined in terms of rise time θ, stress ratio R, and ΔK.

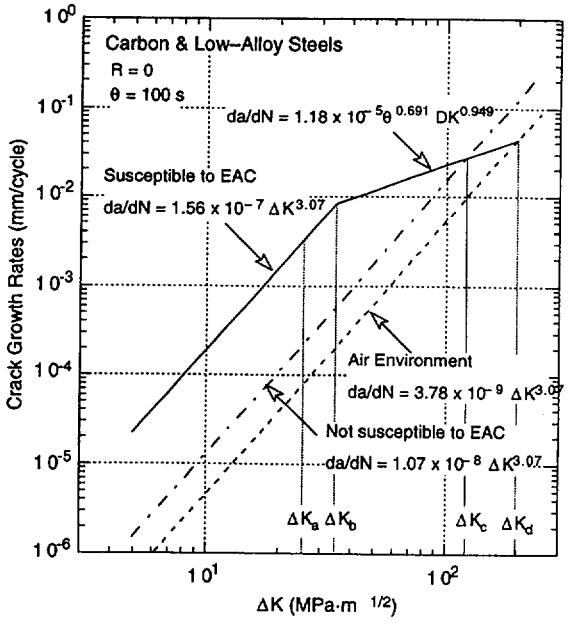

Figure B1.
Proposed reference fatigue crack growth rate curves for carbon and low–alloy steels in LWR environments for a rise time of 100 s and R = –1

The correlations in Fig. B1 correspond to a rise time of 100 s and K_{min} <0, e.g., fully reversed cyclic loading; R is set to zero. The various threshold values of ΔK (MPa·m$^{1/2}$) are given by

$$\Delta K_a = 14.156\ \theta^{0.125}, \quad \text{(B9a)}$$

$$\Delta K_b = 7.691\ \theta^{0.326}, \quad \text{(B9b)}$$

$$\Delta K_c = 27.186\ \theta^{0.326}, \quad \text{(B9c)}$$

$$\Delta K_d = 44.308\ \theta^{0.326}, \quad \text{(B9d)}$$

where rise time θ is in seconds.

References

B1. O. K. Chopra and W. J. Shack, *Effects of LWR Coolant Environments on Fatigue Design Curves of Carbon and Low-Alloy Steels*, NUREG/CR-6583, ANL-97/18 (March 1998).

B2. N. E. Dowling, *Crack Growth During Low-Cycle Fatigue of Smooth Axial Specimens*, ASTM STP 637, pp. 97-121 (1977).

B3. T. P. O'Donnell and W. J. O'Donnell, *Stress Intensity Values in Conventional S-N Fatigue Specimens*, in International Pressure Vessels and Piping Codes and Standards, PVP 313, pp. 195-197 (1995).

B4 W. A. Logsdon and P. K. Liaw, *Fatigue Crack Growth Rate Properties of SA508 and SA533 Pressure Vessel Steels and Submerged Arc Weldments in Room and Elevated Temperature Air Environments*, Eng. Frac. Mech. **22**, 509-526 (1985).

B5 E. D. Eason, E. E. Nelson, and J. D. Gilman, *Modeling of Fatigue Crack Growth Rate for Ferritic Steels in Light Water Reactor Environments*, Changing Priorities of Code and Standards, PVP 286, ASME, New York, pp. 131-142 (1994).

NRC FORM 335 (2–89) NRCM 1102, 3201, 3202

U. S. NUCLEAR REGULATORY COMMISSION

BIBLIOGRAPHIC DATA SHEET

(See instructions on the reverse)

1. REPORT NUMBER *(Assigned by NRC. Add Vol., Supp., Rev., and Addendum Numbers, if any.)*

NUREG/CR- 6717
ANL-00/27

2. TITLE AND SUBTITLE

Environmental Effects on Fatigue Crack Initiation in Piping and Pressure Vessel Steels

3. DATE REPORT PUBLISHED

MONTH	YEAR
May	2001

4. FIN OR GRANT NUMBER

W6610

5. AUTHOR(S)

O. K. Chopra and W. J. Shack

6. TYPE OF REPORT

Technical

7. PERIOD COVERED *(Inclusive Dates)*

8. PERFORMING ORGANIZATION – NAME AND ADDRESS *(If NRC, provide Division, Office or Region, U.S. Nuclear Regulatory Commission, and mailing address; if contractor, provide name and mailing address.)*

Argonne National Laboratory
9700 South Cass Avenue
Argonne, IL 60439

9. SPONSORING ORGANIZATION – NAME AND ADDRESS *(If NRC, type "Same as above": if contractor, provide NRC Division, Office or Region, U.S. Nuclear Regulatory Commission, and mailing address.)*

Division of Engineering Technology
Office of Nuclear Regulatory Research
U.S. Nuclear Regulatory Commission
Washington, DC 20555–0001

10. SUPPLEMENTARY NOTES

J. Muscara, NRC Task Manager

11. ABSTRACT (200 words or less)

The ASME Boiler and Pressure Vessel Code provides rules for the construction of nuclear power plant components. Appendix I to Section III of the Code specifies fatigue design curves for structural materials. However, the effects of light water reactor (LWR) coolant environments are not explicitly addressed by the Code design curves. Test data illustrate potentially significant effects of LWR environments on the fatigue resistance of carbon and low-alloy steels and austenitic stainless steels. This paper summarizes the work performed at Argonne National Laboratory on the fatigue of piping and pressure vessel steels in LWR coolant environments. The existing fatigue S–N data have been evaluated to establish the effects of various material and loading variables, such as steel type, strain range, strain rate, temperature, and dissolved-oxygen level in water, on the fatigue lives of these steels. Statistical models are presented for estimating the fatigue S–N curves for carbon and low-alloy steels and austenitic stainless steels as a function of material, loading, and environmental variables. The influence of reactor environments on the mechanism of fatigue crack initiation are discussed. Decreased fatigue lives of carbon and low-alloy steels and austenitic stainless steels in water are caused primarily by the effects of environment on the growth of short cracks. The results suggest that for carbon and low-alloy steels, the growth of these small cracks in high-purity oxygenated water occurs by a slip oxidation/dissolution process. A fracture mechanics approach has been used to evaluate the effects of environment on fatigue crack initiation in carbon and low-alloy steels. Environmentally assisted reduction in fatigue life of austenitic stainless steels is most likely caused by other mechanisms such as hydrogen-enhanced crack growth. Two methods for incorporating environmental effects into the ASME Code fatigue evaluations are discussed. Differences between the methods and their impact on the design fatigue curves are also discussed.

12. KEY WORDS/DESCRIPTORS *(List words or phrases that will assist researchers in locating this report.)*

Fatigue Strain-Life Curves
Fatigue Design Curves
Fatigue Crack Initiation
LWR Environment
Carbon Steels
Low-Alloy Steels
Austenitic Stainless Steels
Cast Austenitic Stainless Steels

13. AVAILABILITY STATEMENT

Unlimited

14. SECURITY CLASSIFICATION

(This Page)

Unclassified

(This Report)

Unclassified

15. NUMBER OF PAGES

16. PRICE

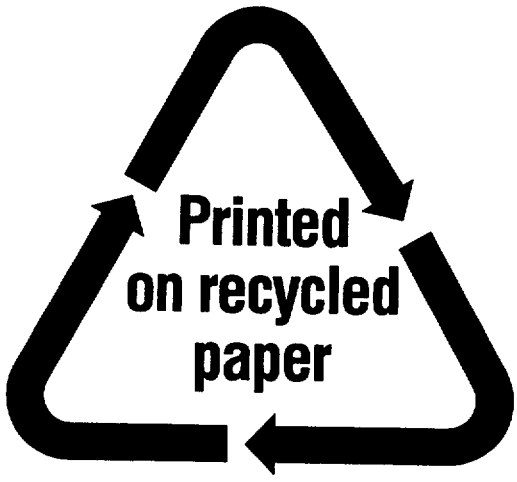

Federal Recycling Program